Eindhoven University of Technology

MASTER

Development of an Automated Emergency Braking System for a Renault Twizy

van Hoek, Daniël E.A.W.

Award date:
2022

Link to publication

Disclaimer
This document contains a student thesis (bachelor's or master's), as authored by a student at Eindhoven University of Technology. Student theses are made available in the TU/e repository upon obtaining the required degree. The grade received is not published on the document as presented in the repository. The required complexity or quality of research of student theses may vary by program, and the required minimum study period may vary in duration.

General rights
Copyright and moral rights for the publications made accessible in the public portal are retained by the authors and/or other copyright owners and it is a condition of accessing publications that users recognise and abide by the legal requirements associated with these rights.

- Users may download and print one copy of any publication from the public portal for the purpose of private study or research.
- You may not further distribute the material or use it for any profit-making activity or commercial gain

Department of Mechanical Engineering
Dynamics and Control group
Automotive Technology

Development of an Automated Emergency Braking System for a Renault Twizy

Master Thesis

D.E.A.W. (Daniël) van Hoek
0960958

DC 2022.020

Supervisors:
dr.ir. P.W.A. Zegelaar
dr.ir. T.P.J. van der Sande
prof.dr. H. Nijmeijer

Eindhoven, March 25, 2022

TU/e EINDHOVEN UNIVERSITY OF TECHNOLOGY

Declaration concerning the TU/e Code of Scientific Conduct for the Master's thesis

I have read the TU/e Code of Scientific Conduct[i].

I hereby declare that my Master's thesis has been carried out in accordance with the rules of the TU/e Code of Scientific Conduct

Date

24-3-2022

Name

Daniël van Hoek

ID-number

0960958

Signature

Submit the signed declaration to the student administration of your department.

[i] See: https://www.tue.nl/en/our-university/about-the-university/organization/integrity/scientific-integrity/
The Netherlands Code of Conduct for Scientific Integrity, endorsed by 6 umbrella organizations, including the VSNU, can be found here also. More information about scientific integrity is published on the websites of TU/e and VSNU

February 21, 2020

Abstract

In this research an Automated Emergency Braking (AEB) system is developed for the Renault Twizy used in the i-CAVE research program. The AEB system should be able to avoid a collision or at least minimize the impact velocity in case a collision threat is detected. The AEB system is implemented in a simulation environment, which includes a model of the modified brake system of the Renault Twizy. The performance of the AEB system is evaluated via simulations for different driving scenarios.

The absolute motion of a detected object is required to determine if the object is relevant for the AEB system and present in the driving path of the host vehicle, and to determine the threat level of the current traffic situation. The absolute motion of the object is estimated from the available sensor measurements using a linear discrete-time Kalman filter. The motion model used in the Kalman filter is the constant acceleration model, which normally describes the relative motion between the object and the host vehicle. However, in this research, the motion model is slightly adapted, since the absolute motion of the object is required. As the radar sensor on the host vehicle has a lower sampling rate than the AEB controller, the state estimates are only updated in case a new measurement becomes available.

To determine if a detected object is relevant for the AEB system, first the paths of both the host vehicle and the object are predicted. The position of the object is predicted by making a n-step a-priori prediction using the last available state estimates from the Kalman filter, and the position of the host vehicle is predicted directly from the available sensor measurements. A new method is proposed where uncertainty ellipses around the predicted positions of both the host vehicle and the object are used to determine if the object is present in the driving path of the host vehicle and relevant for the AEB system.

After determining if a detected object is relevant and present in the driving path of the host vehicle, the AEB controller uses a risk metric called the Brake-Threat-Number (BTN) to determine if a brake intervention is required, which is a measure of the threat level and indicates the effort that is required to avoid a collision with the object. The BTN is defined as the required host acceleration to avoid a collision divided by the minimal achievable host acceleration. To compensate for the response delay of the brake system, the threat level is determined using the predicted future motions of the host vehicle and the object. When activated, the AEB system can operate in four different operating modes, being Forward Collision Warning (FCW), pre-charging of the brakes, partial braking and full braking.

Acknowledgments

Before diving into the contents of this research, I would like to express my gratitude to all people who have guided and supported me during my graduation project, which has been performed at the Eindhoven University of Technology within the Dynamics and Control group of Mechanical Engineering. First of all, I would like to thank my supervisors dr.ir. Peter Zegelaar and dr.ir. Tom van der Sande for providing me with this challenging and interesting graduation project. Furthermore, I would like to thank them for their guidance during the graduation project, the insightful discussions during the weekly meetings, and their continuous support and patience throughout difficult periods. Tom, thank you for your critical view on my work, it really helped me to improve the graduation project and I learned to critically reflect on my own work. Peter, thank you for patiently explaining all concepts concerning Automated Emergency Braking (AEB) systems, which was very interesting and contributed significantly to a successful completion of this project. Secondly, I would like to thank prof.dr. Henk Nijmeijer for the interesting discussions and his critical inputs during the progress meetings.

Next, I would like to thank my friends and fellow graduates Bram Kersten and Dylan Frijters for the useful discussions and suggestions, and for the provided feedback. I really enjoyed the time we spent together in the AES lab, which boosted my progress and provided me with extra motivation. Finally, I would like to thank my parents and my family for their unconditional love, continuous support, patience and encouragement throughout my entire study, and in particular during the months I worked from home due to the Corona pandemic.

Contents

List of abbreviations

ABS	Anti-lock Brake System
ADAS	Advanced Driver Assistance Systems
AEB	Automated Emergency Braking
BTN	Brake-Threat-Number
CCRb	Car-to-Car Rear braking scenario
CCRm	Car-to-Car Rear moving scenario
CM	center of mass
EHB	Electronic Hydraulic Brake
EKF	Extended Kalman Filter
ESC	Electronic Stability Control
FCW	Forward Collision Warning
FoV	field of view
i-CAVE	Integrated Cooperative Automated Vehicles
IMU	Inertial Measurement Unit
PF	Particle Filter
RMS	root-mean-square
SD	standard deviation
TTB	time to brake
TTC	time to collision
TTS	time to steer
TTV	time to vehicle
UKF	Unscented Kalman Filter
VRU	Vulnerable Road User
WC	worst-case

List of symbols

Symbol	Description	Unit
α	Road slope angle	rad
α_f	Side slip angle front axle	rad
α_r	Side slip angle rear axle	rad
δ_c	Camshaft angle of the cam-follower mechanism	rad
$\delta_{c,err}$	Error on the camshaft angle	rad
δ_{cmin}	Camshaft angle needed to achieve minimum acceleration	rad
$\delta_{c,req}$	Required camshaft angle	rad
δ_{rw}	Road wheel angle	rad
δ_{sw}	Steering wheel angle	rad
$\eta_y(t)$	Measurement noise of measurement signal $y(t)$	-
θ	Heading angle with respect to the $\vec{e}_x^G$ direction	rad
μ	Tire-road friction coefficient	-
ρ_{air}	Air density	kg/m^3
σ	Standard deviation	-
τ_b	Response delay of the brake system	s
ω_z	Yaw rate	rad/s
a	Radius major axis of the uncertainty ellipse	m
a_b	Actual brake acceleration	m/s^2
$a_{b,req}$	Required brake acceleration	m/s^2
a_{min}^h	Minimal achievable host acceleration	m/s^2
$a_{partial}$	Acceleration for partial braking	m/s^2
$a_{pre-charge}$	Acceleration for pre-charging	m/s^2
a_{req}^h	Required host acceleration needed to avoid a collision	m/s^2
a_x	Longitudinal acceleration	m/s^2
a_y	Lateral acceleration	m/s^2
A_f	Frontal area vehicle	m^2
$\mathbf{A}$	System matrix	-
b	Radius minor axis of the uncertainty ellipse	m
$\mathbf{B}$	Input matrix	-
$\text{BTN}_{\text{deactivate}}$	BTN threshold for deactivation	-
BTN_{FCW}	BTN threshold for FCW activation	-
BTN_{full}	BTN threshold for full braking activation	-
$\text{BTN}_{\text{partial}}$	BTN threshold for partial braking activation	-
$\text{BTN}_{\text{pre-charge}}$	BTN threshold for pre-charging activation	-
C	Cost function used to tune the process noise values	-
C_d	Drag coefficient	-
C_f	Cornering stiffness front axle	kN/rad
C_r	Cornering stiffness rear axle	kN/rad

$\mathbf{C}$	Observation matrix	-
d_{safe}	Safety distance	m
d_{stop}	Stopping distance	m
d_{full}	Distance at which full braking is initiated	m
d_x	Longitudinal distance	m
d_y	Lateral distance	m
$\mathbf{D}$	Observed input matrix	-
$\underline{\vec{e}}^G$	Cartesian global fixed frame	-
$\underline{\vec{e}}^h$	Cartesian body-fixed frame of the host vehicle	-
$\underline{\vec{e}}^i$	Cartesian body-fixed frame of vehicle i	-
f_r	Rolling resistance coefficient	-
F_d	Air drag force	N
F_g	Gravitational force due to road grade influences	N
F_r	Rolling resistance force	N
F_{res}	Total longitudinal resistant force	N
F_v	Viscous friction force	N
F_x	Total longitudinal force	N
$F_{x,f}$	Total longitudinal force front axle	N
$F_{x,r}$	Total longitudinal force rear axle	N
F_y	Total lateral force	N
$F_{y,f}$	Total lateral force front axle	N
$F_{y,r}$	Total lateral force rear axle	N
g	Gravitational acceleration	m/s^2
$\mathbf{G}$	Process noise matrix	-
i_{bm}	Motor gear ratio	-
i_{st}	Steering ratio	-
I_{zz}	Vehicle mass moment of inertia	kg m^2
J_{bm}	Brake motor moment of inertia	kg m^2
J_c	Camshaft moment of inertia	kg m^2
k_c	Cubic spring stiffness	Nm/rad
k_l	Linear spring stiffness	Nm/rad
k_{lin}	Linear viscous friction term	Ns/m
K	Total number of samples	-
$\mathbf{K}_k$	Kalman gain	-
l_a	Distance between the front axle and the center of mass	m
l_b	Distance between the rear axle and the center of mass	m
l_f	Distance between the center of mass and the radar sensor	m
m	Vehicle mass	kg
m_{eff}	Effective vehicle mass	kg
n	Prediction horizon in samples	-
n_b	Response delay of the brake system in samples	-
N	Total number of states	-
p_b	Brake pressure	bar
$p_{b,req}$	Required brake pressure	bar
P_x	Parameter used to vary the longitudinal jerk	-
P_y	Parameter used to vary the lateral jerk	-
$\mathbf{P}_{k\|k-1}$	a-priori state estimation covariance at time k	-
$\mathbf{P}_{k\|k}$	a-posteriori state estimation covariance at time k	-
$\mathbf{q}$	Noise variance matrix	-
$\mathbf{Q}$	Process noise covariance matrix	-

r_w	Effective rolling radius of a wheel	m
$\mathbf{R}(\theta)$	Rotation matrix	-
$\mathbf{R}$	Measurement noise covariance matrix	-
s	Scale of the uncertainty ellipse	-
$\mathbf{S}_k$	Innovation covariance matrix	-
t	Time	s
t_{pre}	Prediction time	s
t_{stop}	Stopping time	s
t_{TTT}	Time-to-Touch	s
T_b	Brake torque	Nm
$T_{b,req}$	Required brake torque	Nm
T_{bm}	Brake motor torque	Nm
$T_{bm,ff}$	Feedforward part brake motor torque	Nm
$T_{bm,PID}$	PID part brake motor torque	Nm
T_c	Coulomb friction torque	Nm
T_s	Sample time	s
$\underline{\mathrm{u}}_k$	Input vector at time k	-
v_{wind}	Wind velocity	m/s
v_x	Longitudinal velocity	m/s
v_y	Lateral velocity	m/s
$\underline{\mathrm{v}}_k$	Measurement noise vector at time k	-
w	Host vehicle width	m
w_{j_x}	Noise on the longitudinal jerk	$\mathrm{m/s^3}$
w_{j_y}	Noise on the lateral jerk	$\mathrm{m/s^3}$
$\underline{\mathrm{w}}_k$	Process noise vector at time k	-
$\underline{\mathrm{x}}_k$	State vector at time k	-
$\underline{\hat{\mathrm{x}}}_{k\|k-1}$	a-priori state estimate at time k	-
$\underline{\hat{\mathrm{x}}}_{k\|k}$	a-posteriori state estimate at time k	-
$y(t)$	Measurement signal at time t	-
$y_{gt}(t)$	Ground truth of measurement signal $y(t)$	-
$\underline{\mathrm{y}}_k$	Measurement vector at time k	-

List of subscripts

Subscript	Description
X^{gt}	Ground truth value
X^{h}	Host vehicle
$X^{h,F}$	Front of the host vehicle
X^{r}	Relative
X^{t}	Object (target vehicle)
X_0	Initial value
X_k	Current value
X_{k+1}	Next value
X_{k-1}	Previous value
X_x	Longitudinal direction
X_y	Lateral direction
$\hat{X}_0$	Initial estimate
$\hat{X}_{k\|k}$	Current a-posteriori estimate
$\hat{X}_{k\|k-1}$	Current a-priori estimate
$\hat{X}_{k-1\|k-1}$	Previous a-posteriori estimate
$\hat{X}^{*}_{k-1\|k-1}$	Corrected previous a-posteriori estimate
$\hat{X}_{k+n\|k}$	Predicted a-priori estimate over a prediction horizon of n samples
$\hat{X}_{k+n_b\|k}$	Predicted a-priori estimate over a prediction horizon of n_b samples
$\hat{X}_{k+n}$	Predicted estimate over a prediction horizon of n samples
$\hat{X}_{k+n_b}$	Predicted estimate over a prediction horizon of n_b samples

Chapter 1

Introduction

According to the World Health Organization road traffic accidents are currently estimated to be the 8th leading cause of death globally for all age groups [1]. Every year approximately 1.3 million people die from road traffic accidents, and between 20 and 50 million people suffer non-fatal injuries. Furthermore, more than half of those killed are vulnerable road users, which include pedestrians, cyclists and motorcyclists. The main cause of road traffic accidents is human error, which accounts for approximately 95% of all road traffic accidents [2]. Examples of human error are distracted driving, driving under the influence of alcohol or other psychoactive substances, speeding, and non-use of seat-belts, child restraints and motorcycle helmets [1]. Using Advanced Driver Assistance Systems (ADAS) on vehicles improves road safety and reduces the number of accidents significantly [3]. According to the European Transport Safety Council, the number of road deaths in the European Union has decreased by 36% between 2010 and 2020, which is partially caused by the improvement of safety features and the application of ADAS on vehicles [4]. To further increase the EU's road safety, the European Parliament and the Council of the EU have decided to make several ADAS mandatory in new models from June 2022 and in all new vehicles from June 2024. Among these mandatory systems are Intelligent Speed Assistance (ISA) and Automated Emergency Braking (AEB) [3]. Every ADAS contributes to the driving automation of a vehicle on a different level. The Society of Automotive Engineers (SAE) has defined six levels of driving automation, ranging from no automation (level 0) to full automation (level 5), where the automation levels 0-2 are classified as driver support features and the automation levels 3-5 are classified as automated driving features [5].

A large number of road traffic accidents are rear-end collisions, which are collisions between two vehicles driving in the same direction [6]. These kind of accidents are often caused by driver inattention or distraction, which could for example happen when a leading vehicle suddenly brakes and the distracted driver of the following vehicle fails to react in time to avoid a collision. One type of ADAS, which can significantly reduce the number of rear-end collisions or at least mitigate their severity, is an Automated Emergency Braking (AEB) system. Research shows a reduction of at least 38% in rear-end collisions for vehicles equipped with an AEB system compared to similar vehicles without an AEB system [7][8]. An AEB system is defined by UNECE regulation No. 131 [9] as "a system which can automatically detect a potential forward collision and activate the vehicle braking system to decelerate the vehicle with the purpose of avoiding or mitigating a collision". Since an AEB system only provides momentary assistance to the driver in case of an emergency, this type of ADAS belongs to level 0 of driving automation [5]. The European New Car Assessment Programme (Euro NCAP), which is a European non-profit car safety performance assessment program, distinguishes between AEB Car-to-Car systems and AEB Vulnerable Road User (VRU) systems [10]. Especially for AEB VRU systems, determining if a road user is present in the driving path of the vehicle is important, since a brake intervention by the AEB system should only be initiated if a possible collision is detected [11].

To address automated driving, the i-CAVE (Integrated Cooperative Automated Vehicles) research program has been set up, which is a collaboration of multiple universities and automotive companies in the Netherlands that is designing and researching a Cooperative Dual Mode Automated Transport (C-DMAT) system [12]. This system consists of dual mode vehicles, which can be driven both autonomously and manually to improve user acceptance and flexibility. The i-CAVE research program consists of multiple project groups, where each group has a different specialization. This project is part of the second project group, which has as goal to develop controllers for cooperative and automated vehicles [13]. The vehicle used in the i-CAVE research program is a Renault Twizy, which has very limited safety features. The vehicle is not equipped with any active safety systems and is only equipped with passive safety systems such as a frontal airbag and a seat belt for the driver. Therefore, when testing developed controllers and systems on the Renault Twizy, the risks for both the driver and the test environment are high. The goal of this graduation project is to develop an Automated Emergency Braking (AEB) system, which functions for both AEB Car-to-Car and AEB Vulnerable Road User scenarios, and that can eventually be implemented on the Renault Twizy to improve its safety. In this research, the Renault Twizy will be called the host vehicle and the vehicle or vulnerable road user present in front of the host vehicle will be called the object (or target vehicle).

1.1 Research objectives

The main objective of this research is defined as follows:

Develop an Automated Emergency Braking (AEB) system for the Renault Twizy used in the i-CAVE research program.

To achieve the main-objective of this research, the following sub-objectives are defined:

1. Develop a state estimator to estimate the motion of a detected object from radar sensor measurements and measurements of the Renault Twizy's own motion.
2. Determine if a detected object is relevant for the AEB system and present in the driving path of the Renault Twizy. To this end, the paths of both the Renault Twizy and the object need to be predicted, where the uncertainty of the predicted motion resulting from sensor noise and model uncertainty needs to be taken into account.
3. Estimate the threat level of the current traffic situation, which indicates the probability of a collision with an object in front of the Renault Twizy. Furthermore, develop a controller in the form of a finite state machine, which uses the estimated threat level to determine which system response should be initiated.

1.2 Report outline

First, in Chapter 2, a literature review on the various components of an AEB system will be given. Thereafter, in Chapter 3, the host vehicle will be described, as well as the simulation framework, the driving scenarios and the simulation parameters used throughout this research. In Chapter 4, the state estimator is discussed, which is used to estimate the motion of a detected object from radar sensor measurements and measurements of the host vehicle's own motion. Furthermore, this chapter discusses the methods used to predict the paths of the detected object and the host vehicle. Next, in Chapter 5, the method used to determine if a detected object is relevant for the AEB system will be explained. Thereafter, the method used to predict the future motion of the host vehicle and the object will be explained together with the measure used to describe the threat level of the current traffic situation. Besides, the developed controller in the form of a finite state machine will be discussed. In Chapter 6, the AEB system will be tested for different driving scenarios to evaluate the performance of the system. Finally, the conclusions and recommendations will be given in Chapter 7.

Chapter 2

Literature review

An AEB system enables the host vehicle to brake autonomously, once a collision threat is detected, or will provide emergency braking assistance if the driver does not brake sufficiently to avoid a collision. To explain the workings of an AEB system, the standard architecture of an Advanced Driver Assistance System (ADAS) as given in Figure 2.1 is used [6].

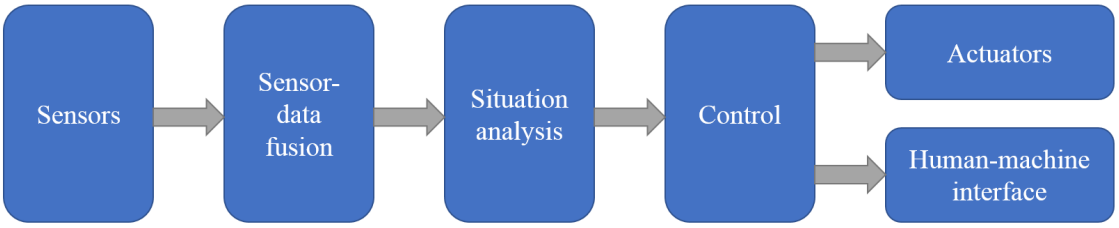

Figure 2.1: Standard architecture of an Advanced Driver Assistance System (ADAS) [6].

The first layer is the sensor layer, which for an AEB system includes sensors measuring the host vehicle's own motion as well as environmental sensors used to detect and measure the motion of objects in front of the host vehicle. The environmental sensors frequently used by AEB systems are radar sensors, mono and stereo cameras, and lidar sensors. Often multiple environmental sensors are combined, which results in more accurate measurements, since the strengths of the individual sensors complement each other. Furthermore, it improves the reliability of the AEB system, since erroneous measurements of a sensor can be detected, and undesired responses of the AEB system can be prevented. It is, however, also possible to realize an AEB system using a single environmental sensor [6].

Then, in the second layer, which is the sensor-data fusion layer, the measurements of all sensors are combined to create a model of the host vehicle's surroundings. The environmental sensors measure the relative motion between an object and the host vehicle. However, an AEB system requires the absolute motion of an object. By combining the measurements of the environmental sensors together with the measurements of the host vehicle's own motion, the absolute motion of an object can be estimated. This is often done using a state estimator, such as a Kalman filter. Furthermore, depending on the available sensors, also the size and type of an object can be obtained, which can be used to evaluate the threat level of the traffic situation [6]. Crossing pedestrians or bicyclists are often assumed to move with a constant velocity, whereas the target vehicle in Car-to-Car scenarios is often assumed to move with a constant acceleration [14][15].

Next, in the third layer being the situation analysis layer, the motion of both the host vehicle and the object are predicted into the future, which involves making assumptions. Since the prediction horizons required for AEB systems are short, the prediction errors are relatively small.

The predicted future motions are used to estimate the threat level of the current traffic situation, which indicates the probability of a collision with an object in front of the host vehicle. Different measures exist to describe the threat level [6]. Moreover, determining if an object is relevant for the AEB system is important, since a brake intervention should only be initiated if the object is present in the driving path of the host vehicle.

In the fourth layer, which is the control layer, the estimated threat level is used to determine an appropriate action. AEB systems often use a finite state machine as a controller, which compares the estimated threat level with thresholds to determine which system response should be initiated. Furthermore, conditions are checked by the controller to determine if the driver is active and not distracted, in which case a response of the AEB system is not allowed. If the driver fails to react properly, the controller runs through a cascade of system responses. Typical system responses in AEB systems are a Forward Collision Warning (FCW) to alert the driver of a possible collision, pre-charging the brakes such that a subsequent brake intervention can be carried out quicker, partial braking to slightly reduce the velocity of the host vehicle, and full braking to avoid a collision or at least minimize the impact velocity [6].

Finally, depending on the current system response, the corresponding actuators and human-machine interface are activated. For AEB systems the brake system of the host vehicle is relevant to allow automated braking as well as the motor control unit to release the throttle once a brake intervention is initiated.

The focus of this research is defined by the research objectives given in Section 1.1. Before being able to reach these objectives, a literature review on the various components of an AEB system will be given in this chapter. First, the different possible state estimation methods used to estimate the motion of a detected object from the available sensor measurements will be discussed. Thereafter, the methods often used to predict the paths of the host vehicle and the object will be discussed, as well as the methods used to determine if an object is relevant. Then, the available methods used to estimate the threat level of the current traffic situation will be given. Next, the state of the art on AEB system will be described. Finally, the performance rating for an AEB system will be discussed.

2.1 State estimation

An AEB system requires the absolute motion of an object, which can be estimated from the available sensor measurements using a state estimator. Various types of state estimators exist, of which the Kalman filter is the most widely used state estimator in object tracking applications [16]. Given a linear model of the system dynamics and the measurements, a (discrete-time) Kalman filter can be used to estimate the states described by the state vector $\underline{x}_k$ using the available noisy measurements included in the measurement vector $\underline{y}_k$, when assuming that both the process noise and measurement noise are zero-mean, white and uncorrelated noise processes with covariance matrices $\mathbf{Q}_k$ and $\mathbf{R}_k$ respectively. A Kalman filter is a recursive filter, since the estimated states are only based on the last estimate and the last set of measurements. In general, a Kalman filter has two phases, namely a prediction phase and a measurement update phase. In the prediction phase, the states are estimated using the last state estimates together with a linear model of the system dynamics. Then, in the measurement update phase, the predicted state estimates are updated with the measurements $\underline{y}_k$ using a linear measurement model. For linear systems with Gaussian noise, the Kalman filter is the optimal state estimator [17].

A Kalman filter uses a linear model of the system dynamics. However, in reality the motion of an object is often nonlinear due to its turning behaviour as described by the yaw rate. Therefore, in reality, the system dynamics and/or the measurement model is frequently nonlinear, and using a Kalman filter could result in erroneous state estimates. For nonlinear systems, the Extended

Kalman Filter (EKF) or the Unscented Kalman Filter (UKF) can be used [18]. The EKF is the most widely used state estimator for nonlinear systems. Similar to the Kalman filter, the EKF has two phases, being the prediction phase and the measurement update phase. However, when using an EKF, the system dynamics and the measurement model are linearized by evaluating the Jacobians of the system dynamics model and the measurement model around the Kalman filter estimate [17]. In contrast to the Kalman filter, the EKF is not an optimal state estimator and there is no guarantee that the EKF works properly [16]. Furthermore, tuning of the EKF can be difficult and when considering a highly nonlinear system, the EKF will give unreliable state estimates [17].

Compared with the EKF, an Unscented Kalman Filter (UKF) can improve the estimation performance for nonlinear systems, while having similar computational cost as an EKF [19]. An UKF is an extension of the Kalman filter, which reduces the linearization errors of the EKF. As mentioned before, an EKF requires the computation of Jacobians, whereas an UKF does not use Jacobians. For some systems, it is numerically difficult to compute Jacobians. The UKF uses a deterministic sampling technique, called the unscented transformation, to select a minimal set of points around the mean, which are called sigma points. Compared to the EKF, the UKF has one additional phase, being the calculation of these sigma points [17].

For linear systems with Gaussian noise, the Kalman filter is the optimal state estimator. However, for nonlinear systems with non-Gaussian noise, another state estimator might outperform the Kalman filter. One option is the Particle Filter (PF), which is a probability-based and completely nonlinear state estimator. Despite its high performance, a large disadvantage of using a PF is an increased level of computational effort [17]. A PF determines an approximate solution to the sequential estimation, where the required posterior density function is given by a set of weighted random samples (also called particles). The magnitudes of weights associated with each particle is used to estimate the states [18]. For nonlinear systems, the UKF can provide a balance between the high performance of a PF and the low computational cost of a Kalman filter [17].

2.2 Path prediction and object relevance

A state estimator is always based on a model describing the dynamics. In case of object tracking applications this is a motion model describing how the motion of the object and/or the host vehicle is expected to evolve over time [20]. An advantage of using motion models is the ability to predict the future position of the object and/or the host vehicle, which can be used to predict their paths [21]. Once the predicted paths are known, a possible collision between the host vehicle and the object can be found and a brake intervention by the AEB system can be initiated if necessary. When using a discrete-time Kalman filter as a state estimator, the future position can be obtained by making a n-step a-priori prediction, which basically comes down to iterating the prediction phase of the Kalman filter n times to obtain the predicted position ahead of the available measurements [17][22]. Here, n is the prediction horizon in samples. The larger the prediction horizon n, the larger the uncertainty of the predicted position will be. Since the prediction horizon n is fixed, this type of prediction is also called a fixed-lead prediction. Other types of prediction are a fixed-point prediction and a fixed-interval prediction [16].

Different motion models exist for tracking applications, which are distinguished from each other by having different levels of complexity. The motion models range from simple kinematic models, where the object is assumed to be a freely moving point mass, to more sophisticated models like a single-track vehicle model. The most suitable motion model depends on the scenario to be considered and the assumptions that are made [21]. However, most motion models used for object tracking are simple kinematic models [20]. Often it is not possible to measure the states of the object required by complex motion models with the sensors available on the host vehicle, such as the lateral acceleration or the yaw rate of the object [21].

The kinematic motion models can be subdivided into linear motion models and curvilinear (nonlinear) motion models. In linear motion models, the object is assumed to move straight and rotations around the vehicle's z-axis are not taken into account. Two commonly used linear motion models are the constant velocity model and the constant acceleration model [21]. When using these motion models, the movement of an object is assumed to be uncoupled across the different coordinate directions [20]. On the other side, curvilinear motion models also take rotations around the z-axis into account. Two commonly used curvilinear motion models are the Constant Turn Rate and Velocity model and the Constant Turn Rate and Acceleration model [21]. In both of these curvilinear motion models, it is assumed that there is no relation between the velocity and the yaw rate of the vehicle. However, when this relation and the nonholonomic constraints to which a vehicle is subjected need to be considered, a single-track vehicle model can be used [23]. To track the motion of crossing pedestrians or bicyclists often the constant velocity model is used, whereas for the target vehicle in Car-to-Car scenarios the constant acceleration model is used more frequently [14][15].

When using a recursive filter like a Kalman filter, the future position of the object and/or the host vehicle can be predicted by making a n-step a-priori prediction based on a chosen motion model. The predicted position is uncertain due to the model uncertainty of the chosen motion model and the measurement uncertainty of the available sensor measurements. When using a Kalman filter, the level of uncertainty on the predicted position can be estimated from the predicted state estimation covariance. In [24], the levels of uncertainty on the predicted positions of both the host vehicle and the object are used to draw uncertainty ellipses around the predicted positions. Here, an elliptic shape is chosen due to the probabilistic uncertainty model. A collision between the host vehicle and the object is found if their corresponding uncertainty ellipses intersect for a certain prediction horizon n.

One issue when predicting a path by solely using a motion model is the model uncertainty, since it is not exactly known how the object/host vehicle will move in the future [6]. In literature several other methods are proposed for path prediction, which are suitable for short term prediction, long term prediction or both. In [25], a path prediction method is proposed which uses a Constant Turn Rate and Acceleration motion model in combination with maneuver recognition. The proposed Maneuver Recognition Module is able to select the current maneuver from a predefined set of maneuvers by comparing a local curvilinear model of the path of the vehicle with the center lines of the road's lanes. The predicted path based on the motion model is very accurate in the short term, whereas the predicted path based on the maneuver recognition is more accurate for larger prediction horizons. Similarly, in [26], an interactive multiple model trajectory prediction (IMMTP) method is proposed that combines a physics-based path prediction method with a maneuver-based path prediction method. Again, the physics-based path prediction method is very accurate for short term predictions, whereas the maneuver-based prediction approach improves accuracy of the predicted path in the long term. In [27], a set of paths is predefined for different maneuvers and a Hidden Markov Model is used to determine the most probable path of an object in the short term based on the current measurements. In [28], an efficient vehicle path prediction framework is proposed based on recurrent neural network called long short-term memory (LSTM) that analyzes the temporal behaviour and predicts the future positions of surrounding vehicles. Then, in [29], several recursive Bayesian filters for pedestrian path prediction at short time horizons are compared. These include EKFs based on a single motion model and Interacting Multiple Models (IMM) where multiple motion models are combined. Finally, in [30], a novel approach for path prediction is proposed which is able to predict the vehicle's path several seconds in advance. Here, a joint probability distribution is inferred as motion model, which uses previously observed motion patterns. The distribution is then used to predict the path by calculating the probability for the future motion, while taking into account the previously observed motion patterns. The uncertainty of the predicted path can be examined by evaluating the variance and can be depicted by covariance ellipses around the predicted positions.

2.3 Threat assessment

After determining if an object is relevant and present in the driving path of the host vehicle, the threat level of the current traffic situation needs to be estimated, which is used to decide if a brake intervention by the AEB system is required. The threat level is a measure, which indicates the probability of a collision with an object in front of the host vehicle. The estimated threat level is compared with predefined thresholds by the AEB controller to determine which system response should be initiated. Different measures exist to describe the threat level and they are often related to an estimation of time. One possible measure is the time to steer (TTS), which is the remaining time till the last possible moment at which the driver can still avoid a collision by performing a steering maneuver [6]. Another option is the time to brake (TTB) defined as the remaining time the driver has to still avoid a collision by performing a braking maneuver [31]. The threat becomes more critical, when the TTS and TTB become smaller [6].

Another measure often used in AEB systems is the time to collision (TTC), which is defined as the time needed for two vehicles (or objects) to collide if they continue at their present speed and on the same path. The larger the TTC, the lower the risk of a collision. In literature, the TTC has proven to be an effective measure to describe the threat level of the current traffic situation [32]. The calculation of the TTC depends on the chosen motion model, which describes how the motion of the object and the host vehicle is expected to evolve over time. In [15], the TTC is calculated using either the constant velocity model or the constant acceleration model. For AEB systems designed for AEB Vulnerable Road User scenarios, the TTC can be combined with the time to vehicle (TTV). The TTV is the time needed by a crossing vulnerable road user to reach the driving path of the host vehicle and therefore depends on the lateral velocity the vulnerable road user [14].

Some AEB systems use a measure to describe the threat level related to the acceleration required to avoid a collision. An example of such a measure is the Brake Threat Number (BTN), which is defined as the required acceleration of the host vehicle needed to avoid a collision divided by the minimal achievable host vehicle acceleration [33]. In practice, the BTN ranges from 0 to 1, since a BTN larger than 1 indicates a collision with the object cannot be avoided by braking the vehicle due to the physical limitations of the brake system. In [33], a threat assessment algorithm is proposed which uses both the time to brake (TTB) and the Brake Threat Number (BTN) based on an enhanced model including road information to predict the braking behavior of the target vehicle. The resulting algorithm is called the Consistent Threat Assessment for Longitudinal Motion Algorithm (CTALMA), and the obtained results show a good and consistent assessment of the threat level for several test examples.

2.4 State of the art on AEB systems

In conventional AEB systems, it is assumed that the host vehicle is driving on a flat road surface with a constant tire-road friction coefficient. Furthermore, these AEB systems do not monitor the driver's intention before initiating a warning or a brake intervention. In literature several extensions are proposed to improve conventional AEB systems. In [34], an AEB system adaptive to the tire-road friction is proposed, which could be useful when for example driving on a snowy road. On snowy roads this adaptive AEB system starts to brake earlier compared to a conventional AEB system. It was proven that in conditions of reduced friction, drivers feel safer and have more trust in the adaptive AEB system than the conventional one. Furthermore, an AEB system adaptive to the tire-road friction could significantly improve collision prevention in winter conditions compared to conventional AEB systems. In [35], an AEB control algorithm is proposed which also takes into account the effects of road friction and in addition the road gradient. Depending on the current road conditions and the corresponding maximum deceleration, their AEB activation control determines the minimal required braking distance with margin parameters. Then, the

deceleration controller with a feedforward term makes sure a collision is avoided by controlling the acceleration of the vehicle. The proposed AEB system turns out to be very effective on a sloped low friction road and avoids collisions, whereas under similar circumstances using the conventional AEB system resulted in a collision in several cases. In [36], a driver intention detection algorithm for AEB systems is developed. Conventional AEB systems warn the driver and take over the vehicle control when a frontal collision risk is detected. However, by monitoring the driver's intention before initiating an automated brake intervention, driver's annoyance can be avoided and the number of warnings can be reduced when the driver is aware of its surroundings. This could especially be beneficial for AEB systems designed for AEB Vulnerable Road User scenarios in urban environments, where pedestrians enter the path of the host vehicle frequently.

2.5 AEB system performance rating

The decisions made by an AEB system are based on the estimated states, the predicted paths and the estimated threat level of the current traffic situation. All of them are associated with some uncertainty, which means the AEB system bases its decisions on uncertain parameters. Therefore, the challenge in designing an AEB system is to find a balance between the effectiveness of avoiding collisions and the risk of false alarms [37]. A trade-off needs to be made between reducing the number of false positives or the number of false negatives. A false positive means an unnecessary brake intervention or warning is initiated by the AEB system. On the other hand, a false negative means a brake intervention or a warning should be initiated by the AEB system, but the system does not react [34]. If there is a low tolerance for false alarms, then the number of false positives should be minimized. This is the case when it is desired to prevent driver's annoyance and consequently a possible deactivation of the AEB system. However, if it is desired to maximize safety and a collision should be avoided at all times even if there is only a slight collision risk, then the number of false negatives should be minimized [37]. Currently, all AEB systems in production are tuned such that the number of false positives is minimized [34]. False negatives are not prioritized since an AEB system is considered to be a driver assistance system, which means the driver remains responsible for paying attention to the road and keeping a safe distance to other road users. For all AEB systems the number of true positives and true negatives should be as large as possible. A true positive means a brake intervention or warning is initiated by the AEB system and the decision is correct. A true negative means no brake intervention or warning is initiated by the AEB system and the decision is correct. An overview of the performance rating for an AEB system is given in Figure 2.2.

	Positive	**Negative**
True	Brake intervention/warning Decision correct	No brake intervention/warning Decision correct
False	Brake intervention/warning Decision not correct	No brake intervention/warning Decision not correct

Figure 2.2: Performance rating for an AEB system.

2.6 Summary

In this chapter a literature review is given on the various components of an AEB system. In general, an Advanced Driver Assistance System (ADAS), such as an AEB system, consists of five layers. These layers are the sensor layer, the sensor-data fusion layer, the situation analysis layer, the control layer and the layer including the actuators and the human-machine interface.

Different state estimation methods can be used to estimate the motion of a detected object from the available sensor measurements. For linear systems with Gaussian noise, the Kalman filter is the optimal state estimator. For nonlinear systems, the Extended Kalman Filter (EKF) or the Unscented Kalma! Filter (UKF) can be used. However, in contrast to the Kalman filter, the EKF and the UKF are not optimal and there is no guarantee that they work properly.

A brake intervention by the AEB system should only be initiated if the object is present in the driving path of the host vehicle. The paths of both the host vehicle and the object can be predicted using a motion model. Two commonly used linear motion models are the constant velocity model and the constant acceleration model. Two commonly used curvilinear motion models are the Constant Turn Rate and Velocity model and the Constant Turn Rate and Acceleration model. When using a recursive filter like a discrete-time Kalman filter, the future position of the object and/or the host vehicle can be predicted by making a n-step a-priori prediction based on a chosen motion model. One issue when predicting a path by solely using a motion model is the model uncertainty, since it is not exactly known how the object/host vehicle will move in the future. Therefore, for long term path prediction, a motion model is often combined with maneuver recognition.

Several methods exist to estimate the treat level of the current traffic situation. The threat level is a measure, which indicates the probability of a collision with an object in front of the host vehicle. Often these measures are related to an estimation of time, such as the time to steer (TTS), the time to brake (TTB), the time to collision (TTC), and the time to vehicle (TTV). Some AEB systems use a measure to describe the threat level related to the acceleration required to avoid a collision. An example of such a measure is the Brake Threat Number (BTN), which is defined as the required acceleration of the host vehicle needed to avoid a collision divided by the minimal achievable host vehicle acceleration.

In conventional AEB systems, it is assumed that the host vehicle is driving on a flat road surface with a constant tire-road friction coefficient. Furthermore, these AEB systems do not monitor the driver's intention before initiating a warning or a brake intervention. In literature, several extensions are proposed to improve conventional AEB systems. For example, an AEB system adaptive to the tire-road friction or an AEB system adaptive to the road gradient. Furthermore, it is also possible to monitor the driver's intention before initiating an automated brake intervention, to reduce the number of warnings and to avoid driver's annoyance.

The challenge in designing an AEB system is to find a balance between the effectiveness of avoiding collisions and the risk of false alarms. A trade-off needs to be made between reducing the number of false positives or the number of false negatives. A false positive means an unnecessary brake intervention or warning is initiated by the AEB system. On the other hand, a false negative means a brake intervention or a warning should be initiated by the AEB system, but the system does not react. Currently, all AEB systems in production are tuned such that the number of false positives is minimized.

Chapter 3

Host vehicle description and simulation framework

In this research an AEB system will be developed for the Renault Twizy used in the i-CAVE research program. The AEB system will be implemented in a simulation environment and the performance of the AEB system will be evaluated via simulations. To draw conclusions from the simulation results, it is important that the simulation model gives a good representation of the actual system. By testing the AEB system in the simulation environment instead of testing on the actual vehicle, time can be saved and more tests can be performed for various driving scenarios. Furthermore, in this way the potential risk of an accident due to system failure can be overcome. Another benefit is the availability of the ground-truth signals, which can be used to analyze the performance of the AEB system.

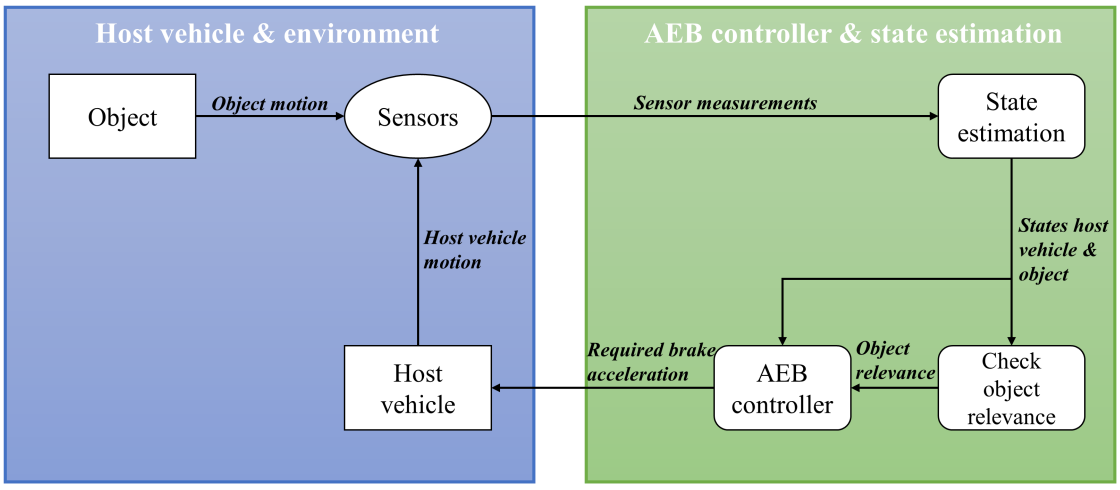

Figure 3.1: High-level architecture of the AEB system.

The high-level architecture of the AEB system developed in this research is shown in Figure 3.1. Here, it can be seen that the AEB system consists of two main parts, being:

1. Host vehicle & environment, which includes the vehicle models of the host vehicle and the object together with the sensor models of the sensors equipped on the host vehicle.

2. AEB controller & state estimation, which includes the state estimator used to estimate the motion of the object and the method used to determine if the object is relevant for the AEB

system and present in the driving path of the host vehicle. Furthermore, it includes the AEB controller, which uses the states of the host vehicle and the object to determine the required brake acceleration needed to avoid a collision with the object.

In this chapter, first the host vehicle will be described. Thereafter, the sensors equipped on the host vehicle and used by the AEB system will be discussed together with the way they are modelled in the simulation environment. Then, the modified brake system of the host vehicle together with the brake sytem model will be described. Next, the single-track vehicle model used to model the motion of the host vehicle and the object will be discussed. Finally, this chapter is concluded by describing a set of driving scenarios and giving the simulation parameters. All simulation results presented in this research are based on the simulation framework and driving scenarios discussed in this chapter.

3.1 Host vehicle description

The vehicle used in the i-CAVE research program is a Renault Twizy, which is a two-seated all-electric city vehicle [13]. Originally, the vehicle is not equipped with any driver assistance systems. However, the vehicle used in the i-CAVE research program is equipped with additional sensors and actuators, which makes the vehicle suitable for the implementation of both autonomous and cooperative driving functionalities such as an AEB system. The vehicle considered as the host vehicle is shown in Figure 3.2.

Figure 3.2: The modified Renault Twizy used in the i-CAVE research program.

3.2 Sensors

In this research only the sensors on the host vehicle are used. Table 3.1 gives an overview of the available sensors used by the AEB system with their operating frequencies. Similar to the operating frequencies of the Inertial Measurement Unit (IMU) and the odometer, the real-time operating system of the Renault Twizy also runs at a base frequency of 100 Hz [38]. For all sensors, the noise levels of the corresponding measurement signals are listed in Table 3.2 and are

expressed in standard deviations. Next, the sensors used by the AEB system will be discussed in more detail together with the way they are modelled in the simulation environment.

Table 3.1: Operating frequencies of the available sensors [38][39]

Sensor	Operating frequency
Radar	16.7 Hz
IMU	100 Hz
Odometer	100 Hz

Table 3.2: Overview of the noise levels of the measurement signals considered in this research and expressed in standard deviations (SD)

Parameter	Noise level (SD)	Measurement signal	Sensor
$\sigma_{d_x^r}$	0.12 m	Longitudinal relative distance	Radar [39]
$\sigma_{v_x^r}$	0.11 m/s	Longitudinal relative velocity	Radar [39]
$\sigma_{d_y^r}$	0.12 m	Lateral relative distance	Radar [39]
$\sigma_{v_y^r}$	0.11 m/s	Lateral relative velocity	Radar [39]
$\sigma_{v_x^h}$	0.10 m/s	Longitudinal velocity host vehicle	Odometer [40]
$\sigma_{a_x^h}$	0.098 m/s^2	Longitudinal acceleration host vehicle	IMU [41]
$\sigma_{w_z^h}$	0.0017 rad/s	Yaw rate host vehicle	IMU [41]

3.2.1 Radar sensor

The radar sensor used on the Renault Twizy is a Bosch MMRevo14 radar sensor, which is a front facing mid-range radar sensor that is able to identify, track, and classify objects. As shown in Figure 3.2, the radar sensor is located behind the front bumper at the center of the vehicle. In this research, only a single object is considered at the same time, which is detected and tracked by the front facing radar sensor. The raw radar measurements are processed by the object tracking algorithm present on the radar sensor. Therefore, it is assumed that the radar sensor provides the longitudinal relative distance d_x^r and velocity v_x^r, as well as the lateral relative distance d_y^r and velocity v_y^r of a detected object [40].

The radar sensor has a range of approximately 160 m and uses digital beam forming and four independent receiving channels. Figure 3.3 shows the field of view (FoV) of the radar sensor. Here, objects located at a long distance from the host vehicle are detected using the three narrow beams of the main antenna. They have cones of respectively 6°, 9° and 10° with a range of respectively 160 m, 100 m and 60 m. Objects closer to the host vehicle are detected using the two wider beams of the close-range elevation antenna. They have cones of respectively 25° and 42° with a range of respectively 36 m and 12 m. The elevation antenna is also able to measure the vertical position and height of objects [39].

The radar sensor is able to track up to 32 objects simultaneously and classifies them in different object types, which are unknown, pedestrian, construction element, motorcycle or car. Furthermore, the sample time of the radar sensor is approximately 60 ms [39]. The noise levels of the radar measurement signals given in Table 3.2 are obtained from the product data sheet of the Bosch MMRevo14 radar sensor [39]. Here, the noise levels of the longitudinal and lateral relative distance are set equal to the noise level of the range, and the noise levels of the longitudinal and lateral relative velocity are set equal to the noise level of the range rate.

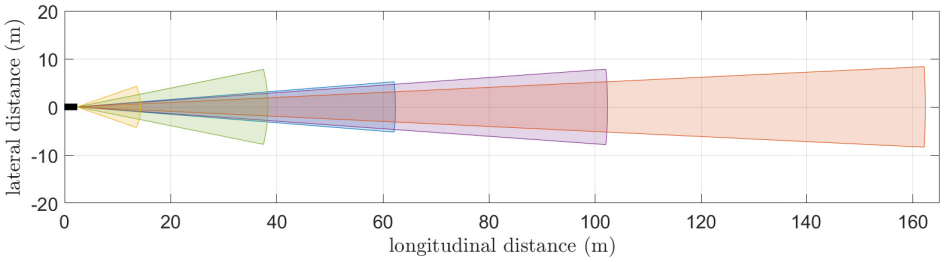

Figure 3.3: Field of view of the Bosch MMRevo14 radar sensor [39].

3.2.2 IMU

The inertial signals of the host vehicle are measured with an Inertial Measurement Unit (IMU), which is installed near the center of mass of the vehicle. The IMU used on the Renault Twizy is a Bosch MM5.10 sensor, which measures the longitudinal, lateral and vertical acceleration as well as the yaw rate and roll rate [41]. Furthermore, all measured signals are low-pass filtered at a cut-off frequency of 15 Hz [40]. The noise levels of the IMU measurement signals as given in Table 3.2 are obtained from the product data sheet of the Bosch MM5.10 sensor [41].

3.2.3 Odometer

The odometer measures the motor speed of the host vehicle, which by using a fixed gear ratio is translated to the rotational speed of the rear axle. Now, by using the effective rolling radius of the Renault Twizy, the longitudinal velocity can be determined from the rotational speed of the rear axle [38]. Here, it is assumed that the wheels on the rear axle have no wheel slip. Usually, the longitudinal velocity signal obtained from the odometer is larger than the actual longitudinal velocity of the vehicle, and therefore needs to be calibrated first. However, it is assumed that the longitudinal velocity signal from the odometer is equal to the actual longitudinal velocity. Furthermore, the estimation of the longitudinal velocity in the presence of wheel slip is considered as future work.

3.2.4 Sensor models

The radar sensor, IMU and odometer are modelled in the simulation environment. Here, the radar measurements used by the AEB system are the longitudinal relative distance d_x^r and velocity v_x^r, as well as the lateral relative distance d_y^r and velocity v_y^r. Furthermore, the measurements from the IMU used by the AEB system are the longitudinal acceleration of the host vehicle a_x^h and the yaw rate of the host vehicle ω_z^h. Finally, the longitudinal velocity of the host vehicle v_x^h measured by the odometer is also used by the AEB system. In the simulation environment, the virtual sensor measurements provided by the sensors used by the AEB system are modelled by adding zero-mean Gaussian white measurement noise to the ground truth signals from the vehicle models. At time t a certain virtual measurement signal y is modelled as follows

$$y(t) = y_{gt}(t) + \eta_y(t), \tag{3.1}$$

where $y_{gt}(t)$ is the ground truth value and $\eta_y(t)$ is the measurement noise of measurement signal y. The noise levels of the measurement signals are listed in Table 3.2. Furthermore, sensor biases are ignored, and sensor delay is assumed to be neglectable compared to the response delay of the brake system. In the simulation environment, the sensors provide virtual measurements at their respective operating frequency as given in Table 3.1. Finally, the virtual measurements of the radar sensor are only available if the object is present in the FoV as shown in Figure 3.3.

3.3 Brake system model

The conventional brake system of the Renault Twizy used in the i-CAVE research program consists of disc brakes at the front and the rear of the vehicle. The Renault Twizy is not equipped with an Electronic Hydraulic Brake (EHB) system or an Electronic Stability Control (ESC) system, which can be used to control the brake system. Therefore, some modifications of the conventional brake system are required to control the brake system of the Renault Twizy and enable autonomous braking by the AEB system. In previous research [40] the brake system of the Renault Twizy has been modified as is shown in Figure 3.4. Here, a brake cam actuator is added to the brake master cylinder of the vehicle, which keeps the conventional brake system intact. The brake cam actuator consists of an electric motor (with controller), which via a gearbox is connected to a cam-follower mechanism. As the brake cam actuator is not directly coupled to the brake pedal system, the added actuator can only apply pressure on the brake master cylinder and not pull the brake master cylinder. This allows the driver to apply more pressure on the brake master cylinder by operating the brake pedal system if required [40].

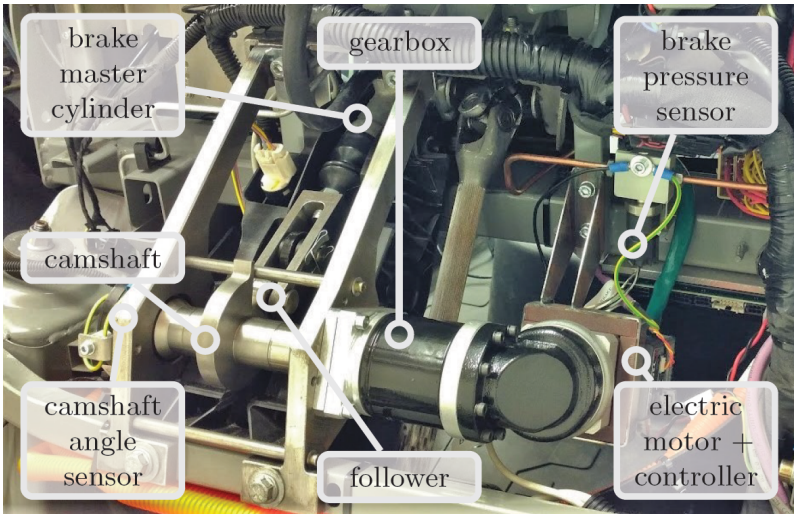

Figure 3.4: Overview of the modified brake system [40].

The brake system model of the modified brake system, as shown in Figure 3.5, consists of two main parts, namely the brake cam actuator controller followed by the modelled brake cam actuator dynamics. Eventually, only the brake cam actuator controller should be implemented on the host vehicle and the brake cam actuator dynamics part is only used to model the behaviour of the brake cam actuator. The input signal to the brake system model is the required brake acceleration $a_{b,req}$, which is determined by the AEB controller. Furthermore, to control the brake system, the camshaft angle δ_c of the cam-follower mechanism is required, which is measured by the camshaft angle sensor [40].

3.3.1 Brake cam actuator dynamics

In previous research [40], a model of the brake system dynamics has been created, where the cam-follower mechanism and gearbox are modelled as a lumped mass and have an inertia J_c, the brake motor torque T_{bm} is modelled on the inertia of the brake motor J_{bm} and the resistance resulting from the brake hydraulics is represented by a damper and nonlinear spring, which is modelled as a combination of a cubic spring and a linear spring. Here, the electrical dynamics of the brake cam actuator are ignored, as it is assumed that the time constant of the electrical dynamics is significantly smaller than the time constant of the mechanical system. The resulting equation of

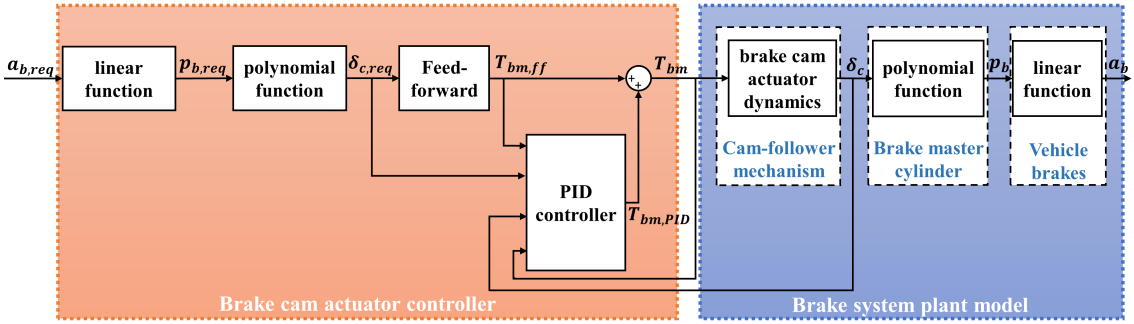

Figure 3.5: Model of the modified brake system consisting of the brake cam actuator controller and the brake cam actuator dynamics.

motion of the brake system describes the relation between the brake motor torque T_{bm} and the camshaft angle δ_c and is given by [40]

$$\left(J_\mathrm{c} + J_\mathrm{bm} i_\mathrm{bm}^2\right) \ddot{\delta}_\mathrm{c} = T_\mathrm{bm} i_\mathrm{bm} - k_l \delta_\mathrm{c} - k_c \delta_\mathrm{c}^3 - T_\mathrm{c} \dot{\delta}_\mathrm{c}, \tag{3.2}$$

where i_bm is the gear ratio of the brake motor, k_l is the stiffness of the linear spring, k_c is the stiffness of the cubic spring and T_c is the Coulomb friction torque [40]. The parameters used in the equation of motion of the brake system are given in Table 3.3.

Table 3.3: Parameters brake system model [40][42]

Parameter	Value	Description	Unit
i_{bm}	20	Motor gear ratio	-
J_{bm}	0.26e-4	Brake motor moment of inertia	kg m^2
J_c	0.0393	Camshaft moment of inertia	kg m^2
k_c	0.0604	Cubic spring stiffness	Nm/rad
k_l	0.1291	Linear spring stiffness	Nm/rad
T_c	2.5340	Coulomb friction torque	Nm

Next, the resulting camshaft angle δ_c from the brake cam actuator is converted into a brake pressure p_b via the brake master cylinder, as is shown in Figure 3.5. Here, based on a simplified model of the brake system dynamics presented by Gerdes *et al.* [43] an assumption is made that the dynamics of the brake master cylinder can be ignored and a static polynomial input/output relation can be used instead. However, neglecting the dynamics of the brake master cylinder introduces some model uncertainty. Gerdes *et al.* [43] presents multiple reduced-order models of brake system dynamics. A single state model with only one hydraulic state is presented, which can be used to design vehicle control systems. This model assumes a single brake line connects the brake master cylinder to the vehicle brakes. The single state model results in a cubic polynomial relation between the brake pressure p_b and the volume of the brake master cylinder. As the camshaft angle δ_c is directly proportional to the volume of the brake master cylinder, also a cubic polynomial relation can be used to model the relation between the brake pressure p_b and the camshaft angle δ_c. To obtain this relation, a dynamic test was performed in previous research [40], where the camshaft angle δ_c is used as the input and the resulting brake pressure p_b is measured. A polynomial model fit of the resulting measurement data is used to define the cubic polynomial relation between the camshaft angle δ_c and the brake pressure p_b, which is given by

$$\delta_c = -0.0509(\sqrt[3]{p_b})^2 + 1.1703\sqrt[3]{p_b}. \tag{3.3}$$

In the simulation environment, the inverse of this relation is used to determine the actual brake pressure p_b from the actual camshaft angle δ_c. Finally, the brake pressure p_b applied on the vehicle

brakes by the brake master cylinder results in a brake torque T_b, which eventually results in an acceleration of the vehicle. Since the host vehicle is not equipped with an Anti-lock Brake System (ABS), the rear brakes are equipped with a brake pressure limiter to prevent wheel lock-up of the rear wheels. In previous research [42], the brake torque has been measured by the dynamometer for various applied brake pressures. Figure 3.6 shows the resulting fit of the brake torque of a front wheel and a rear wheel as a function of the brake pressure. Here, the effect of the brake pressure limiter is clearly visible as the brake torque for a rear wheel shows a decreasing slope for brake pressures above 25 bar.

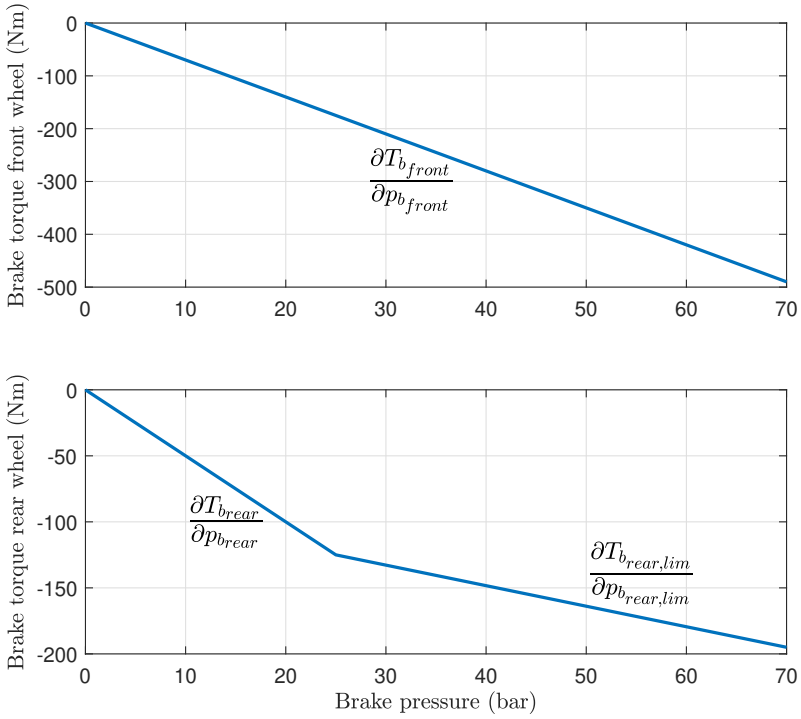

Figure 3.6: Single wheel brake torque as a function of the brake pressure.

To determine the brake torque T_b from the brake pressure p_b, the brake pressure limiter needs to be taken into account, which is activated above a brake pressure of 25 bar, as is shown in Figure 3.6. If the brake pressure limiter is inactive, the total brake torque T_b is determined by

$$T_b = 2\left(\frac{\partial T_{b_{front}}}{\partial p_{b_{front}}} + \frac{\partial T_{b_{rear}}}{\partial p_{b_{rear}}}\right) p_b, \text{ for } p_b \leq 25\,\text{bar}, \tag{3.4}$$

where $\frac{\partial T_{b_{front}}}{\partial p_{b_{front}}}$ and $\frac{\partial T_{b_{rear}}}{\partial p_{b_{rear}}}$ are the gradients of the relation between the brake torque and the brake pressure for respectively a single front wheel and rear wheel as shown in Figure 3.6. However, if the brake pressure limiter is active, the total brake torque T_b is obtained as follows

$$T_b = 2\left(\left(\frac{\partial T_{b_{front}}}{\partial p_{b_{front}}} + \frac{\partial T_{b_{rear,lim}}}{\partial p_{b_{rear,lim}}}\right) p_b + T_{b,0}\right), \text{ for } p_b > 25\,\text{bar}, \tag{3.5}$$

where $\frac{\partial T_{b_{rear,lim}}}{\partial p_{b_{rear,lim}}}$ is the gradient of the relation between the brake torque and the brake pressure for a single rear wheel if the brake pressure limiter is active and $T_{b,0}$ is the corresponding theoretical

value of the brake torque for a single rear wheel at a brake pressure of 0 bar. Here, it is assumed again that the dynamics of the brake hydraulics and brakes can be ignored and a static linear input/output relation can be used to model the relation between the brake pressure p_b and the brake torque T_b. This assumption is supported by the work presented by Gerdes *et al.* [43], where the single state model also results in a linear relation between the brake pressure p_b and the brake torque T_b. However, neglecting the dynamics of the brake hydraulics and brakes again introduces some additional model uncertainty.

Using the total brake torque T_b, the actual brake acceleration a_b can be obtained as follows

$$a_b = \frac{T_b}{m_{eff} r_w}, \tag{3.6}$$

where m_{eff} is the effective vehicle mass being the sum of the vehicle mass and the rotational inertias, which is equal to 755 kg [42]. Furthermore, r_w is the effective rolling radius of a wheel, which is equal to 0.2778 m [42].

3.3.2 Brake cam actuator controller

The brake cam actuator controller, which is the part of the brake system model that should be implemented on the host vehicle, uses the required brake acceleration $a_{b,req}$ determined by the AEB controller as an input. As shown in Figure 3.5, the brake cam actuator controller first determines the required brake pressure $p_{b,req}$ from the required brake acceleration $a_{b,req}$. This can be done by first calculating the total required brake torque $T_{b,req}$ using the same relation as given in (3.6).

Next, the required brake pressure $p_{b,req}$ can be determined by taking into account the brake pressure limiter, which is active for brake pressures above 25 bar. As shown in Figure 3.6, at a brake pressure of 25 bar the total brake torque of a single front wheel and a single rear wheel is equal to -300 Nm. If the brake pressure limiter is inactive, meaning $0 \geq T_{b,req} \geq -600\,\text{Nm}$, the required brake pressure $p_{b,req}$ can be obtained using the same relation as given in (3.4). However, if the brake pressure limiter is active, meaning $T_{b,req} < -600\,\text{Nm}$, the required brake pressure $p_{b,req}$ can be obtained using the same relation as given in (3.5). Here, the required brake pressure $p_{b,req}$ is limited to values between 0 bar and 100 bar [40].

From the required brake pressure $p_{b,req}$, the required camshaft angle $\delta_{c,req}$ of the cam-follower mechanism can be determined using the same polynomial model fit as given in (3.3). Here, the required camshaft angle $\delta_{c,req}$ is limited to values between 0 rad and 5 rad [40].

Then, a position controller is used to control the brake motor torque T_{bm} given a required camshaft angle $\delta_{c,req}$. The position controller, which is developed in previous research [40], consists of a feedforward part and a PID controller. The feedforward part takes into account an amount of friction and a deadzone on the input signal, which is the required camshaft angle $\delta_{c,req}$. Again, a polynomial model fit of acquired measurement data is used to define the relation between the required camshaft angle $\delta_{c,req}$ and the brake motor torque from the feedforward part $T_{bm,ff}$ [40], which is given by

$$T_{bm,ff} = 0.0178\delta_{c,req}^2 - 0.0195\delta_{c,req}. \tag{3.7}$$

The brake motor torque T_{bm} is determined by adding the brake motor torque from the feedforward part $T_{bm,ff}$ to the brake motor torque from the PID controller $T_{bm,PID}$. The discrete-time PID controller can either operate in control mode or in tracking mode. The gains of the PID controller can be found in Appendix A.1. The input of the PID controller is the error on the camshaft angle $\delta_{c,err}$, which is given by

$$\delta_{c,err} = \delta_{c,req} - \delta_c. \tag{3.8}$$

However, in tracking mode, which is used when no input signal is provided by the AEB controller, the PID controller tracks the error of the brake motor torque, which is determined by subtracting the brake motor torque from the feedforward part $T_{bm,ff}$ from the actual brake motor torque T_{bm}. The resulting brake motor torque T_{bm} from the position controller is limited to values between -1.35 Nm and 1.35 Nm [40].

3.3.3 Response delay of the brake system model

When a brake intervention is initiated by the AEB controller and the brake system receives the required brake acceleration needed to avoid a collision, a certain amount of time will pass before the vehicle actually brakes with this desired acceleration. This amount of time is defined as the response delay of the brake system and is indicated by τ_b. It is assumed that the response delay of the brake system is equal to the response delay of the modelled brake cam actuator dynamics.

The response delay of the modelled brake cam actuator dynamics is not a fixed delay, but depends on the current camshaft angle δ_c, which is measured by the camshaft angle sensor on the host vehicle. This response delay is defined as the time that is required to reach 95% of the camshaft angle needed to achieve minimum acceleration δ_{cmin} starting from the current camshaft angle δ_c. Here, 95% is chosen since this is commonly used to determine the rise time of a response and using a larger percentage would overestimate the response delay since the camshaft angle needed to achieve minimum acceleration δ_{cmin} is approached slowly [44]. To determine the response delay of the brake system τ_b as a function of the current camshaft angle δ_c, first the camshaft angle needed to achieve minimum acceleration δ_{cmin} needs to be defined. The minimal achievable host vehicle acceleration a^h_{min} depends on the tire-road friction coefficient μ [45]. It is assumed that the host vehicle is driving on a dry road surface with a tire-road friction coefficient μ of 0.9. Furthermore, the vehicle body pitch and vertical acceleration are assumed to be zero and the tire-road friction coefficient μ is assumed to be independent of the vertical forces acting on the vehicle. As the Renault Twizy is not equipped with an ABS system, a safety margin is added to the minimal achievable host vehicle acceleration a^h_{min} to prevent the wheels from blocking when braking the vehicle, which could cause stability and steerability issues. Therefore, a^h_{min} is chosen to be -7 m/s^2 and the corresponding camshaft angle needed to achieve minimum acceleration δ_{cmin} is equal to 4.03 rad.

Figure 3.7 shows the response delay of the brake system τ_b as a function of the current camshaft angle δ_c, which is obtained by performing simulations. To obtain this figure, multiple step inputs are used for the required brake accelerations $a_{b,req}$, where the final value of every step input is set to the minimal achievable host vehicle acceleration a^h_{min}. For every step input, both the response delay τ_b and the camshaft angle δ_c are determined, and the results are shown in Figure 3.7. Here, it can be seen that the response delay of the brake system τ_b decreases non-linearly for increasing camshaft angles δ_c. Furthermore, it can be seen that the response delay is equal to 0 s for camshaft angles δ_c equal to or larger than 95% of the camshaft angle needed to achieve minimum acceleration δ_{cmin}.

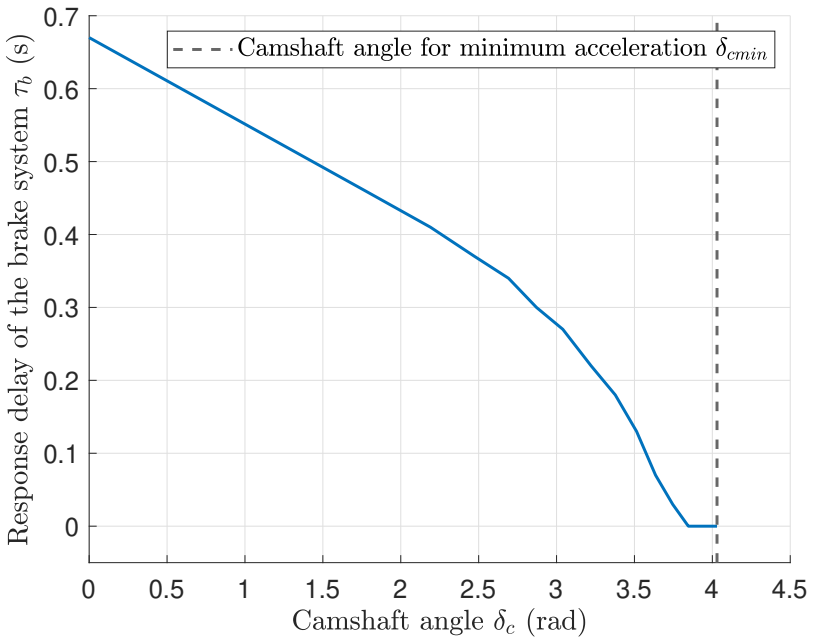

Figure 3.7: Response delay of the brake system as a function of the current camshaft angle.

3.4 Single-track vehicle model

The motion of both the host vehicle and the object are modelled using a single-track vehicle model as shown in Figure 3.8, which has three degrees of freedom: the longitudinal, lateral and yaw motion. A single-track vehicle model is used since the desired inputs to the vehicle model are the steering angle and the longitudinal tyre forces, which are used to accelerate and brake the vehicle. Furthermore, it is a simple model that is a good representation of a vehicle and includes its cornering behaviour. When using this vehicle model, several assumptions are made [45], which are:

- For both the front and rear axle, the left and right tyre are lumped into a single tyre and the forces act along the center line of the front and rear axle.
- The vehicle has no longitudinal and lateral load transfer, so no body pitch and body roll.
- The vehicle is driving on a flat road surface without any slopes, so the motion of the vehicle is restricted to the X,Y-plane.
- The vehicle is considered as a rigid body.
- The vehicle has centre point steering.
- The side slip angles α_f and α_r, and the road wheel angle δ_{rw} are small.

In Figure 3.8, the Cartesian global fixed frame $\underline{\vec{e}}^G$ is given by

$$\underline{\vec{e}}^G = [\vec{e}_x^G \quad \vec{e}_y^G]^T, \tag{3.9}$$

which is an earth fixed and earth centered coordinate system. Furthermore, the Cartesian body-fixed frame $\underline{\vec{e}}^i$ of vehicle i with its origin positioned at the center of mass (CM), is given by

$$\underline{\vec{e}}^i = [\vec{e}_x^i \quad \vec{e}_y^i]^T. \tag{3.10}$$

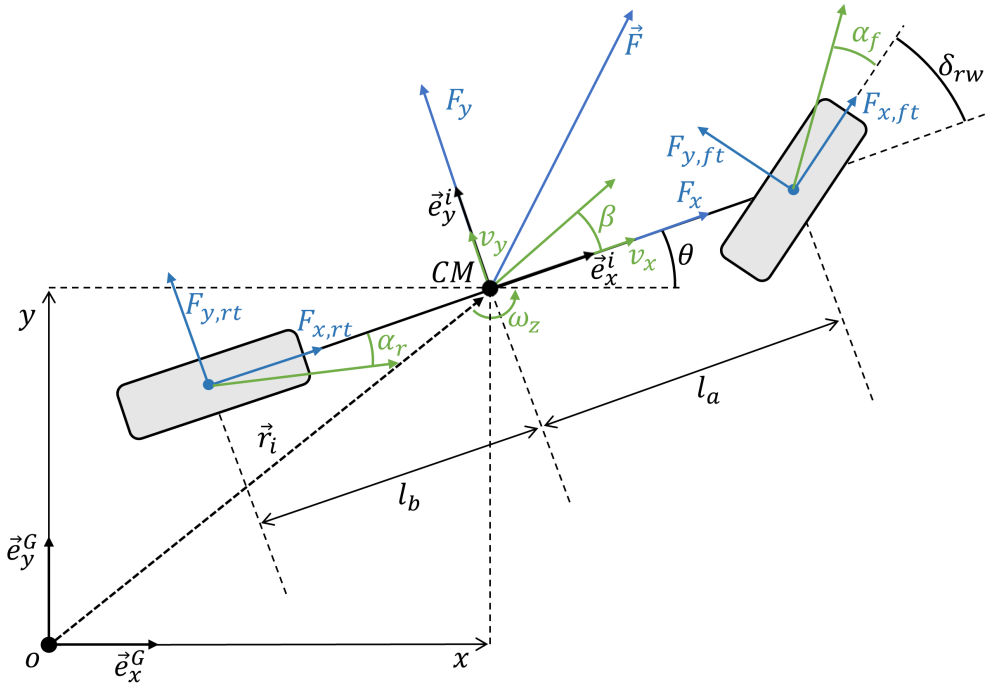

Figure 3.8: The three-degree-of-freedom single-track vehicle model [45].

Since the body-fixed frame rotates with respect to the global frame, the relation between these frames is given by

$$\underline{\vec{e}}^{\,G} = \mathbf{R}(\theta)\,\underline{\vec{e}}^{\,i} = \begin{bmatrix} \cos(\theta) & -\sin(\theta) \\ \sin(\theta) & \cos(\theta) \end{bmatrix} \underline{\vec{e}}^{\,i}, \tag{3.11}$$

where $\mathbf{R}(\theta)$ is the rotation matrix and θ is the heading angle of the vehicle with respect to the $\vec{e}_x^{\,G}$ direction of the global frame [46]. The vector $\vec{r}_i$ represents the position of the center of mass of the vehicle in the global frame and is given by

$$\vec{r}_i = [x \quad y]\underline{\vec{e}}^{\,G}, \tag{3.12}$$

where x is the position in the $\vec{e}_x^{\,G}$ direction and y is the position in the $\vec{e}_y^{\,G}$ direction. By differentiating this position vector, the velocity vector can be determined as follows

$$\dot{\vec{r}}_i = [\dot{x} \quad \dot{y}]\underline{\vec{e}}^{\,G} = [\dot{x} \quad \dot{y}]\mathbf{R}(\theta)\,\underline{\vec{e}}^{\,i} = [v_x \quad v_y]\underline{\vec{e}}^{\,i}. \tag{3.13}$$

Now by differentiating the velocity vector, the acceleration vector can be obtained as follows

$$\ddot{\vec{r}}_i = [\dot{v}_x \quad \dot{v}_y]\underline{\vec{e}}^{\,i} + [v_x \quad v_y]\dot{\underline{\vec{e}}}^{\,i}, \tag{3.14}$$

where $\dot{\underline{\vec{e}}}^{\,i}$ can be determined using (3.11) as follows

$$\dot{\underline{\vec{e}}}^{\,i} = \dot{\mathbf{R}}(\theta)^T\underline{\vec{e}}^{\,G} = \begin{bmatrix} 0 & \omega_z \\ -\omega_z & 0 \end{bmatrix} \underline{\vec{e}}^{\,i}. \tag{3.15}$$

Here, ω_z $(= \dot{\theta})$ is the yaw rate of the vehicle. The acceleration vector can be obtained by implementing (3.15) into (3.14) and is given by

$$\ddot{\vec{r}}_i = [\dot{v}_x \quad \dot{v}_y]\underline{\vec{e}}^{\,i} + [v_x \quad v_y]\begin{bmatrix} 0 & \omega_z \\ -\omega_z & 0 \end{bmatrix} \underline{\vec{e}}^{\,i} = [\dot{v}_x - v_y\omega_z \quad \dot{v}_y + v_x\omega_z]\underline{\vec{e}}^{\,i}. \tag{3.16}$$

As shown in Figure 3.8, the force vector acting on the center of mass of the vehicle is given by

$$\vec{F} = [F_x \quad F_y]\underline{\vec{e}}^i = [F_{x,f} + F_{x,r} + F_{res} \quad F_{y,f} + F_{y,r}]\underline{\vec{e}}^i, \tag{3.17}$$

where $F_{x,f}$ and $F_{y,f}$ are the total forces acting on the front axle, and $F_{x,r}$ and $F_{y,r}$ are the total forces acting on the rear axle. Furthermore, F_{res} is the total longitudinal resistant force acting on the center of mass of the vehicle, which will be derived later in this section. Now, by applying Newton's second law of motion, the equations of motion describing the longitudinal, lateral and yaw motion of the vehicle can be derived, which is done by combining (3.16) with (3.17) for every direction as follows

$$\begin{aligned} \dot{v}_x &= v_y\omega_z + \frac{F_{x,f} + F_{x,r} + F_{res}}{m} \\ \dot{v}_y &= -v_x\omega_z + \frac{F_{y,f} + F_{y,r}}{m} \\ \dot{\omega}_z &= \frac{l_a F_{y,f} - l_b F_{y,r}}{I_{zz}}, \end{aligned} \tag{3.18}$$

where m is the vehicle mass, l_a is the distance between the front axle and the center of mass, l_b is the distance between the rear axle and the center of mass and I_{zz} is the vehicle mass moment of inertia [45]. As the Renault Twizy only steers with the front wheels, the total forces acting on the front and rear axle when assuming a small road wheel angle δ_{rw} can be determined as follows

$$\begin{aligned} F_{x,f} &= F_{x,ft}\cos(\delta_{rw}) - F_{y,ft}\sin(\delta_{rw}) = F_{x,ft} \\ F_{y,f} &= F_{x,ft}\sin(\delta_{rw}) + F_{y,ft}\cos(\delta_{rw}) = F_{y,ft} \\ F_{x,r} &= F_{x,rt} \\ F_{y,r} &= F_{y,rt}, \end{aligned} \tag{3.19}$$

where $F_{x,ft}$ and $F_{y,ft}$ are the tyre forces on the front axle, $F_{x,rt}$ and $F_{y,rt}$ are the tyre forces on the rear axle, and δ_{rw} is the road wheel angle with respect to the $\vec{e}_x^i$ direction of the body-fixed frame. The road wheel angle δ_{rw} can be obtained as follows

$$\delta_{rw} = \frac{\delta_{sw}}{i_{st}}, \tag{3.20}$$

where i_{st} is the steering ratio and δ_{sw} is the steering wheel angle, which is used as an input to the single-track vehicle model. Furthermore, the longitudinal tyre forces $F_{x,ft}$ and $F_{x,rt}$ are also used as inputs to the single-track vehicle model to accelerate and brake the vehicle. The lateral tyre forces $F_{y,ft}$ and $F_{y,rt}$ can be determined by assuming linear cornering characteristics and are given by

$$\begin{aligned} F_{y,ft} &= -C_f\alpha_f \\ F_{y,rt} &= -C_r\alpha_r, \end{aligned} \tag{3.21}$$

where C_f and C_r are the linear cornering stiffnesses of respectively the front and rear axle, and α_f and α_r are the side slip angles of respectively the front and rear tyres [45]. The side slip angles are assumed to be small and can be calculated as follows

$$\begin{aligned} \alpha_f &= -\delta_{rw} + \frac{v_y + l_a\omega_z}{v_x} \\ \alpha_r &= \frac{v_y - l_b\omega_z}{v_x}. \end{aligned} \tag{3.22}$$

3.4.1 Longitudinal vehicle behaviour

The total longitudinal force acting on the center of mass of the vehicle as given in (3.17) consists of the following force contributions

$$F_x = F_{x,f} + F_{x,r} + F_{res}, \tag{3.23}$$

where the total forces acting on the front axle $F_{x,f}$ and rear axle $F_{x,r}$ include the applied forces from the motor and brakes. Furthermore, during driving, a vehicle is subjected to several external resistant forces which influence the acceleration of the vehicle [47]. These forces are included in the total longitudinal resistant force F_{res} acting on the vehicle, which is given by

$$F_{res} = -F_r - F_d - F_v - F_g, \tag{3.24}$$

where F_r represents the rolling resistance force, F_d is the air drag force, F_v is the viscous friction force and F_g is the gravitational force due to road grade influences. The rolling resistance force can be determined by

$$F_r = f_r mg, \tag{3.25}$$

where f_r is the rolling resistance coefficient obtained in previous research by performing a coast down test with the Renault Twizy on a flat road surface [42]. Furthermore, g represents the gravitational acceleration [47]. Next, the air drag force is given by

$$F_d = \frac{1}{2}\rho_{air} C_d A_f (v_x + v_{wind})^2, \tag{3.26}$$

where ρ_{air} is the air density, C_d is the drag coefficient, A_f is the frontal area of the vehicle and v_{wind} is the wind velocity [47]. The wind velocity is assumed to be zero. Furthermore, the viscous friction force can be obtained by

$$F_v = k_{lin} v_x, \tag{3.27}$$

where k_{lin} is the linear viscous friction term, which introduces driveline viscous losses [42]. Finally, the gravitational force due to road grade influences is given by

$$F_g = mg \sin \alpha, \tag{3.28}$$

where α is the road slope angle. It is assumed that the considered vehicles drive on a flat road surface and therefore road grade influences are ignored. The parameters of the Renault Twizy used in the single-track vehicle model are listed in Table 3.4. The same parameters are used to model the vehicle dynamics of the object.

Table 3.4: Parameters single-track vehicle model [40][42][48]

Parameter	Value	Description	Unit
A_f	1.4	Frontal area vehicle	m^2
C_d	0.64	Drag coefficient	-
C_f	38.893	Cornering stiffness front axle	kN/rad
C_r	58.054	Cornering stiffness rear axle	kN/rad
f_r	0.01251	Rolling resistance coefficient	-
g	9.81	Gravitational acceleration	m/s^2
i_{st}	14.02	Steering ratio	-
I_{zz}	350	Vehicle mass moment of inertia	kg m^2
k_{lin}	2.537	Viscous friction	Ns/m
l_a	0.9978	Front axle to the centre of mass	m
l_b	0.6882	Rear axle to the centre of mass	m
m	708	Vehicle mass	kg
ρ_{air}	1.2567	Air density	kg/m^3

3.5 Driving scenarios and simulation parameters

A number of relevant scenarios is chosen to evaluate the performance of the AEB system. For all scenarios, the ground truth trajectories of both the host vehicle and the detected object given in the Cartesian global frame $\underline{\vec{e}}^G$ are shown in Figure 3.9. The first scenario is called a Car-to-Car Rear braking (CCRb) scenario [49]. In this scenario, at first, the host vehicle is following the detected object (target vehicle) and both vehicles are driving straight in the same direction and with a constant velocity. Then, the target vehicle suddenly brakes and a brake intervention by the host vehicle is required to prevent a collision. This scenario is relevant since a large number of road accidents are rear-end collisions and it is desired that the AEB system is able to prevent a collision or at least reduce the severity of the collision for these kind of scenarios.

The second scenario is called a Car-to-Car Rear moving (CCRm) scenario [49]. This scenario is similar to the first scenario, where the host vehicle is following the target vehicle and both vehicles are driving straight in the same direction and with a constant velocity. However, in this scenario the target vehicle does not brake, but keeps driving at a constant velocity lower than the velocity of the host vehicle. As time progresses and the distance between the vehicles becomes smaller, a brake intervention by the host vehicle is required to prevent a collision until the velocity of the host vehicle becomes smaller or equal to the velocity of the target vehicle. This scenario is relevant for the same reason as the first scenario.

The third scenario is called an AEB Vulnerable Road User (VRU) scenario [50]. In this scenario, the host vehicle is driving straight with a constant velocity. Then, suddenly a pedestrian or bicyclist crosses its path from the right side with a constant velocity and a brake intervention by the host vehicle is required to prevent a collision. Situations similar to the one described by this scenario are common in urban areas and it is desired that the AEB system is able to prevent a collision for these kind of scenarios.

Finally, in the fourth scenario, again the host vehicle is following the target vehicle and both vehicles are driving straight in the same direction and with a constant velocity. Then, similar to the first scenario, the target vehicle suddenly brakes. However, before a collision takes place, the host vehicle turns away from the target vehicle. Therefore, in this scenario a brake intervention by the AEB system is not required and considered undesired. This scenario is included since it is a relevant traffic situation and the AEB system is designed to deal with situations in which the host vehicle is cornering.

For every driving scenario, the initial position of the center of mass (CM) of the host vehicle in frame $\underline{\vec{e}}^G$ is set equal to the origin $(x_0^h, y_0^h) = (0, 0)$, the initial heading angle θ_0^h is set equal to 0 rad, and the initial longitudinal velocity of the host vehicle $v_{x,0}^h$ is set equal to 30 km/h (8.33 m/s), which is a common velocity in urban areas. The initial position and velocity of the detected object in frame $\underline{\vec{e}}^G$ are listed in Table 3.5. The simulation duration used throughout this research is 10 s. Since the real-time operating system of the Renault Twizy runs at a base frequency of 100 Hz, the parts of the AEB system that should be implemented on the host vehicle also run at 100 Hz.

Table 3.5: Initial parameters of the detected object in the global frame $\vec{e}^{G}$ for every driving scenario

	1.CCRb	**2.CCRm**	**3.VRU**	**4.Turning**	
Parameter	Value	Value	Value	Value	Description
x_0^t	40	30	60	20	Initial longitudinal position (m)
y_0^t	0	0	-10.5	0	Initial lateral position (m)
θ_0^t	0	0	0.5π	0	Initial heading angle (rad)
$\dot{x}_0^t$	6	4	0	6	Initial longitudinal velocity (m/s)
$\dot{y}_0^t$	0	0	1.5	0	Initial lateral velocity (m/s)

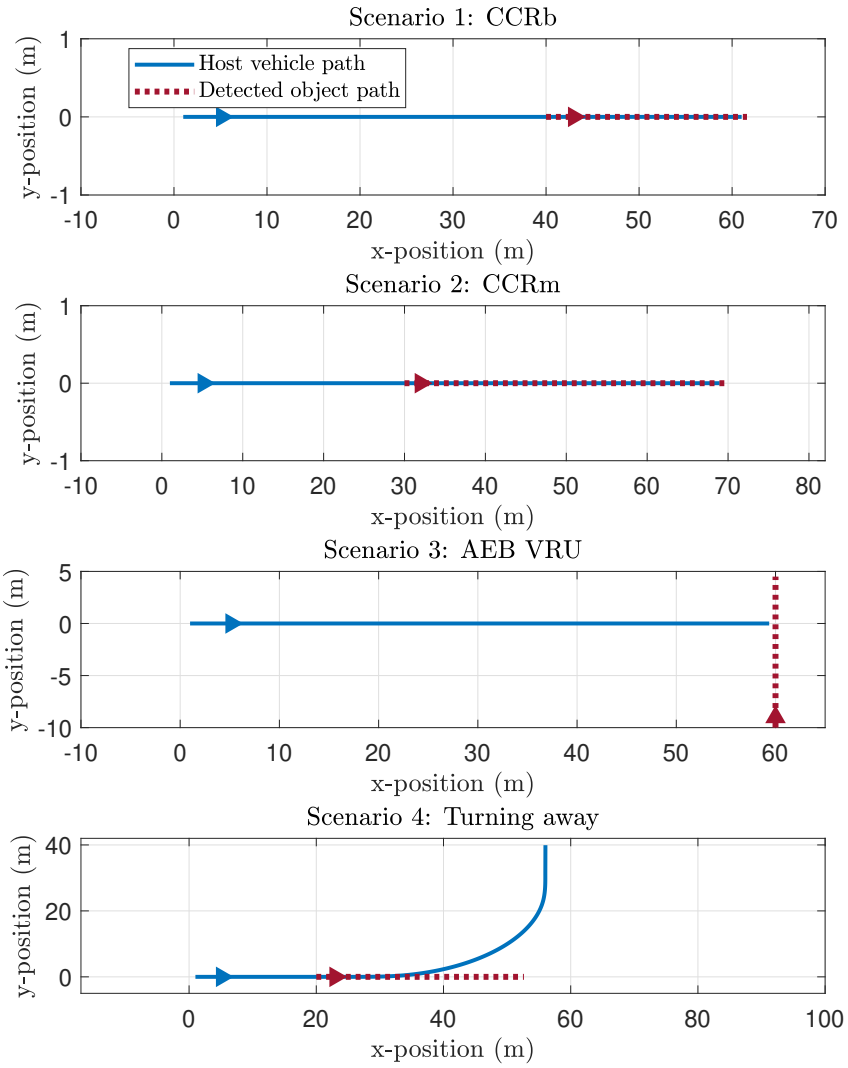

Figure 3.9: The ground truth trajectories of both the host vehicle and the detected object in the global frame $\vec{e}^{G}$ for all driving scenarios.

3.6 Summary

In this chapter, the host vehicle considered in this research has been described together with the sensors equipped on the host vehicle and used by the AEB system, which are the radar sensor, the Inertial Measurement Unit (IMU) and the odometer. These sensors are modelled using realistic operating frequencies and noise levels. In previous research, the conventional brake system of the Renault Twizy has been modified by adding a brake cam actuator to the brake master cylinder. The modified brake system is modelled in the simulation environment, which consists of two main parts, being the brake cam actuator controller followed by the brake cam actuator dynamics. The response delay τ_b of the brake system model is determined as a function of the camshaft angle δ_c. The motion of the host vehicle and the object is modelled using a single-track vehicle model with three degrees of freedom: the longitudinal, lateral and yaw motion.

Different driving scenarios are used to evaluate the performance of the AEB system, which are:

1. Car-to-Car Rear braking (CCRb)
2. Car-to-Car Rear moving (CCRm)
3. AEB VRU
4. Turning away from the target vehicle

All simulation results presented in this research are based on the simulation framework and driving scenarios discussed in this chapter.

Chapter 4

State estimation and path prediction

To determine if a detected object is present in the driving path of the host vehicle and to determine the threat level of the current traffic situation, the absolute motion of the object is required. Typically, not all states of the object can be measured directly by the available sensors on the host vehicle. Therefore, some states need to be estimated from the available sensor measurements, which is also called state estimation or filtering. Sometimes, these sensor measurements are not available at every sample, due to the low sampling rate of the sensor. In this case, a state estimator can be used to estimate the states at the desired sampling rate. Furthermore, measurement noise is often present on the sensor measurements and a state estimator can be used to filter out the noise from these measurements [37]. Finally, another advantage of using a state estimator is the ability to predict the future values of the states [21].

A reliable estimation method is one of the most critical requirements of an AEB system [21]. A state estimator is always based on a model describing the dynamics, which in the case of object tracking applications is a motion model describing how the motion of the object and/or the host vehicle is expected to evolve over time [20]. In general, a motion model is given by

$$\underline{\mathrm{x}}_{k+1} = f_k(\underline{\mathrm{x}}_k, \underline{\mathrm{u}}_k, \underline{\mathrm{w}}_k), \tag{4.1}$$

which is also called the state equation. Here, $\underline{\mathrm{x}}_k$ is the state vector consisting of the states, $\underline{\mathrm{u}}_k$ is the input vector, $\underline{\mathrm{w}}_k$ is the process noise vector and f_k is some vector-valued function [20]. The state equation is given in discrete-time since the sensors work in discrete-time and the host vehicle is operated using a discrete-time platform [38]. From now on, all equations of the state estimator will be expressed in discrete-time as a function of the index number for the current time step k. In addition to a model describing the dynamics, the relation between the sensor measurements and the states are described by a measurement model, which is also called the measurement equation and in general is given by

$$\underline{\mathrm{y}}_k = h_k(\underline{\mathrm{x}}_k, \underline{\mathrm{u}}_k, \underline{\mathrm{v}}_k), \tag{4.2}$$

where $\underline{\mathrm{y}}_k$ is the measurement vector, $\underline{\mathrm{v}}_k$ is the measurement noise vector and h_k is some vector-valued function [20].

A common filter used for state estimation in object tracking applications is the Kalman filter [16]. In general, a Kalman filter has two phases, namely a prediction phase and a measurement update phase as will be explained in Section 4.2 [17]. Since the radar sensor on the host vehicle has a lower sampling rate than the AEB controller, the sensor measurements are not available at every sample. One common approach is to only update the state estimates at the samples where a new measurement is available. At the other samples, only the prediction step of the Kalman filter is

used to estimate the states as will be explained in Section 4.2.3 [38].

In the remainder of this chapter, first the motion model and measurement model are presented after which the state estimator is discussed. Then, the methods used to initialize the state estimator and to select the process noise values are discussed. Thereafter, tuning and the performance of the state estimator are discussed for different driving scenarios. Next, the method used to predict the path of the detected object is discussed and the uncertainty of the predicted path is determined. Finally, the method used to predict the path of the host vehicle is explained and again the uncertainty of the predicted path is determined.

4.1 Motion model and measurement model

A state estimator used for tracking applications is always based on a motion model describing how the motion of the object and/or the host vehicle is expected to evolve over time. Often, these models are represented as a linear state-space model by the following discrete-time state equation

$$\underline{\mathrm{x}}_{k+1} = \mathbf{A}\underline{\mathrm{x}}_k + \mathbf{B}\underline{\mathrm{u}}_k + \mathbf{G}\underline{\mathrm{w}}_k, \tag{4.3}$$

where $\mathbf{A}$ is the system matrix which relates the state vector at the current time step $\underline{\mathrm{x}}_k$ to the state vector at the next time step $\underline{\mathrm{x}}_{k+1}$, $\mathbf{B}$ is the input matrix which relates the input vector $\underline{\mathrm{u}}_k$ to the state vector at the next time step $\underline{\mathrm{x}}_{k+1}$, and $\mathbf{G}$ is the process noise matrix which relates the process noise vector $\underline{\mathrm{w}}_k$ to the state vector at the next time step $\underline{\mathrm{x}}_{k+1}$. Furthermore, the discrete-time measurement equation is given by

$$\underline{\mathrm{y}}_k = \mathbf{C}\underline{\mathrm{x}}_k + \mathbf{D}\underline{\mathrm{u}}_k + \underline{\mathrm{v}}_k, \tag{4.4}$$

where $\mathbf{C}$ is the observation matrix which relates the state vector at the current time step $\underline{\mathrm{x}}_k$ to the measurement vector $\underline{\mathrm{y}}_k$ and $\mathbf{D}$ is the observed input matrix which relates the input vector $\underline{\mathrm{u}}_k$ to the measurement vector $\underline{\mathrm{y}}_k$ [17].

4.1.1 Constant acceleration model

A schematic overview of the host vehicle and the detected object with their states and the available sensor measurements is shown in Figure 4.1, where the object is modelled as a freely moving point mass. The reason for this is that it is not possible to accurately measure or estimate the yaw rate of the object using the available sensors on the host vehicle. All states are given in the current Cartesian body-fixed frame $\underline{\vec{e}}^h_k$, with its origin positioned at the center of mass of the host vehicle. This body-fixed frame is given by

$$\underline{\vec{e}}^h_k = [\vec{e}^h_{x,k} \quad \vec{e}^h_{y,k} \quad \vec{e}^h_{z,k}]^T, \tag{4.5}$$

where the $\vec{e}^h_{x,k}$ direction corresponds with the longitudinal direction of the host vehicle, the $\vec{e}^h_{y,k}$ direction corresponds with the lateral direction of the host vehicle, and $\vec{e}^h_{z,k}$ is pointing upwards. The state vector consisting of the states given in the current body-fixed frame is given by

$$\underline{\mathrm{x}}_k = \begin{bmatrix} d^r_{x,k} & v^t_{x,k} & a^t_{x,k} & d^r_{y,k} & v^t_{y,k} & a^t_{y,k} \end{bmatrix}^T, \tag{4.6}$$

where $d^r_{x,k}$ is the longitudinal relative distance between the object and the radar sensor on the host vehicle, and $v^t_{x,k}$ and $a^t_{x,k}$ are the absolute longitudinal velocity and acceleration of the object (or target vehicle) respectively. Furthermore, $d^r_{y,k}$ is the lateral relative distance, and $v^t_{y,k}$ and $a^t_{y,k}$ are the absolute lateral velocity and acceleration of the object respectively. At every sample, the longitudinal velocity $v^h_{x,k}$ and the longitudinal acceleration $a^h_{x,k}$ of the host vehicle are assumed to

be known from the IMU and the odometer on the host vehicle. These are included in the input vector, which is given by

$$\underline{u}_k = \begin{bmatrix} v^h_{x,k} & a^h_{x,k} \end{bmatrix}^T. \tag{4.7}$$

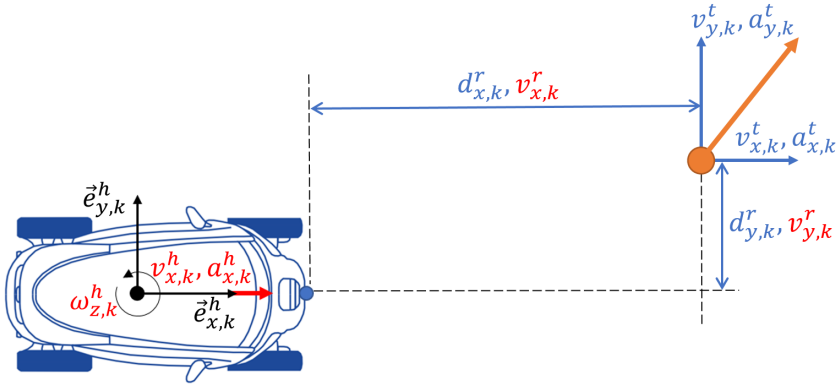

Figure 4.1: Schematic overview of the host vehicle and the detected object with their states (blue) and the available sensor measurements (red).

Since both the host vehicle and the object are likely to accelerate and brake in the driving scenarios described in Section 3.5, it is decided to use a constant acceleration model instead of a constant velocity model to improve the accuracy of the estimations. Furthermore, the constant acceleration model is a simple linear kinematic motion model which does not require the yaw rate of the object and enables the use of a Kalman filter as a state estimator. Normally, the constant acceleration model is a relative model. However, in this research, the constant acceleration model is slightly modified by using the absolute velocity and acceleration of the object. The estimated absolute motion of the object is required to predict its path and to determine if the object is relevant for the AEB system, which will be discussed in Section 4.4.

When using the constant acceleration model it is assumed that the object has uncorrelated motions in both the longitudinal and the lateral direction of the current body-fixed frame. Furthermore, it is assumed that the host vehicle has no side slip, and therefore the lateral velocity of the host vehicle is assumed to be zero. Finally, the longitudinal acceleration of the host vehicle and the longitudinal and lateral acceleration of the object are assumed to be constant over the sample time T_s and the jerk is assumed to be a white noise process [20]. The resulting process noise vector is given by

$$\underline{w}_k = \begin{bmatrix} w^h_{j_x,k} & w^t_{j_x,k} & w^h_{j_y,k} & w^t_{j_y,k} \end{bmatrix}^T, \tag{4.8}$$

where $w^h_{j_x,k}$ and $w^t_{j_x,k}$ are zero-mean Gaussian white noise on the longitudinal jerk of the host vehicle and the object respectively. Furthermore, $w^h_{j_y,k}$ and $w^t_{j_y,k}$ are zero-mean Gaussian white noise on the lateral jerk of the host vehicle and the object respectively.

Given the assumptions described above, the discrete-time state equation as described by (4.3) for

the constant acceleration model is given by

$$\begin{bmatrix} d^r_{x,k+1} \\ v^t_{x,k+1} \\ a^t_{x,k+1} \\ d^r_{y,k+1} \\ v^t_{y,k+1} \\ a^t_{y,k+1} \end{bmatrix} = \begin{bmatrix} 1 & T_s & \frac{T_s^2}{2} & 0 & 0 & 0 \\ 0 & 1 & T_s & 0 & 0 & 0 \\ 0 & 0 & 1 & 0 & 0 & 0 \\ 0 & 0 & 0 & 1 & T_s & \frac{T_s^2}{2} \\ 0 & 0 & 0 & 0 & 1 & T_s \\ 0 & 0 & 0 & 0 & 0 & 1 \end{bmatrix} \begin{bmatrix} d^r_{x,k} \\ v^t_{x,k} \\ a^t_{x,k} \\ d^r_{y,k} \\ v^t_{y,k} \\ a^t_{y,k} \end{bmatrix} + \begin{bmatrix} -T_s & -\frac{T_s^2}{2} \\ 0 & 0 \\ 0 & 0 \\ 0 & 0 \\ 0 & 0 \\ 0 & 0 \end{bmatrix} \begin{bmatrix} v^h_{x,k} \\ a^h_{x,k} \end{bmatrix} + \begin{bmatrix} -\frac{T_s^3}{6} & \frac{T_s^3}{6} & 0 & 0 \\ 0 & \frac{T_s^2}{2} & 0 & 0 \\ 0 & T_s & 0 & 0 \\ 0 & 0 & -\frac{T_s^3}{6} & \frac{T_s^3}{6} \\ 0 & 0 & 0 & \frac{T_s^2}{2} \\ 0 & 0 & 0 & T_s \end{bmatrix} \begin{bmatrix} w^h_{j_x,k} \\ w^t_{j_x,k} \\ w^h_{j_y,k} \\ w^t_{j_y,k} \end{bmatrix}. \tag{4.9}$$

4.1.2 Measurement model

The measurement model of a state estimator describes how the sensor measurements given by the measurement vector $\underline{\mathrm{y}}_k$ are related to the states given by the state vector $\underline{\mathrm{x}}_k$. The measurement model can be described by a discrete-time measurement equation as given in (4.4). The front facing radar sensor on the Renault Twizy is able to measure both the longitudinal relative distance $d^r_{x,k}$ and velocity $v^r_{x,k}$, as well as the lateral relative distance $d^r_{y,k}$ and velocity $v^r_{y,k}$, which results in the following measurement vector

$$\underline{\mathrm{y}}_k = \begin{bmatrix} d^r_{x,k} & v^r_{x,k} & d^r_{y,k} & v^r_{y,k} \end{bmatrix}^T. \tag{4.10}$$

The corresponding measurement noise vector is given by

$$\underline{\mathrm{v}}_k = \begin{bmatrix} \mathrm{v}_{d^r_{x,k}} & \mathrm{v}_{v^r_{x,k}} & \mathrm{v}_{d^r_{y,k}} & \mathrm{v}_{v^r_{y,k}} \end{bmatrix}^T. \tag{4.11}$$

When comparing the measurement vector $\underline{\mathrm{y}}_k$ with the state vector $\underline{\mathrm{x}}_k$ given in (4.6), it can be concluded that both vectors include the longitudinal and lateral relative distances $d^r_{x,k}$ and $d^r_{y,k}$. However, the longitudinal and lateral relative velocities $v^r_{x,k}$ and $v^r_{y,k}$ are only included in the measurement vector $\underline{\mathrm{y}}_k$ and not in the state vector $\underline{\mathrm{x}}_k$. Instead, the velocity components of the state vector $\underline{\mathrm{x}}_k$ are the absolute velocities of the object $v^t_{x,k}$ and $v^t_{y,k}$.

In Figure 4.2 a measurement overview is given, where the object is assumed to be stationary and the host vehicle is driving with a longitudinal velocity v^h_x and yaw rate ω^h_z. Although the object is stationary, the radar sensor measures a velocity component $v^\perp$ on the object perpendicular to the vector $\vec{r}_{T/R}$, which is due to the turning behaviour of the host vehicle. To determine the relation between the measured relative velocities and the estimated absolute velocities of the object, first expressions for the longitudinal velocity $v^\perp_x$ and the lateral velocity $v^\perp_y$ need to be found, which can be done by considering the host vehicle and the object as one rigid body. In this case, $v^\perp_x$ and $v^\perp_y$ are components of the time-derivative of the body-fixed vector $\vec{r}_{T/R}$, denoted by $\dot{\vec{r}}_{T/R}$.

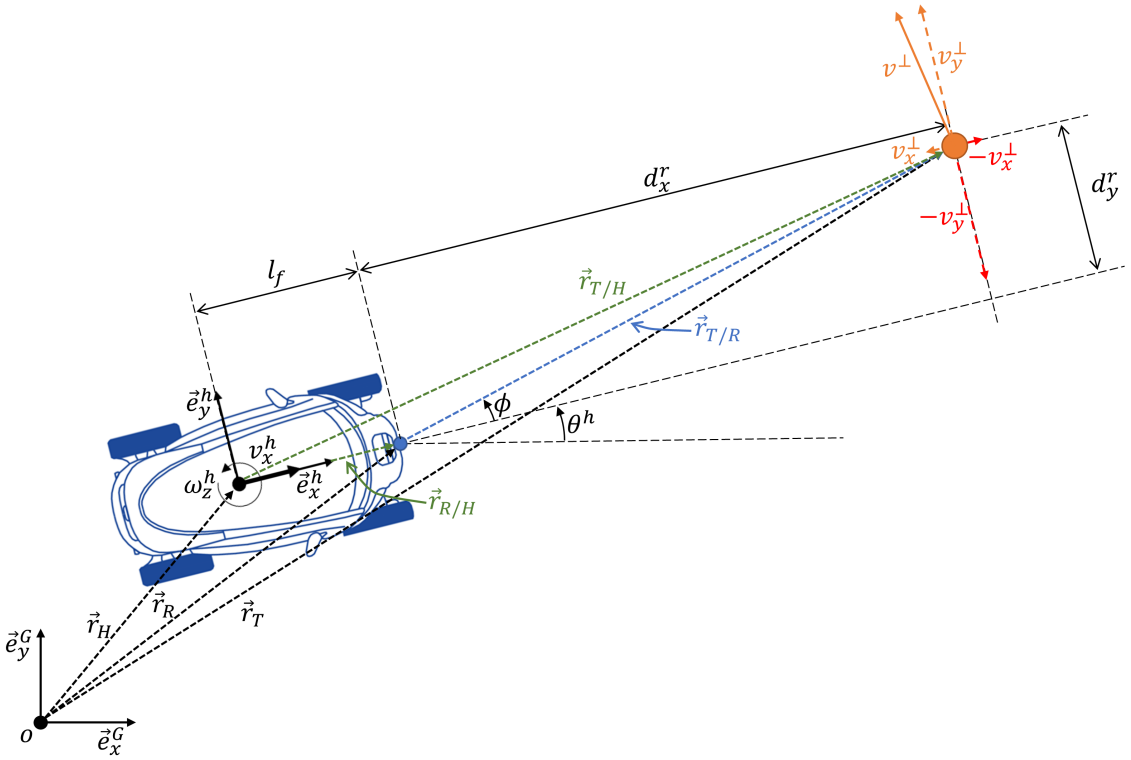

Figure 4.2: Measurement overview of the radar sensor.

Before determining $\dot{\vec{r}}_{T/R}$, first the different frames and vectors as shown in Figure 4.2 will be discussed. The vectors $\vec{r}_H$, $\vec{r}_R$ and $\vec{r}_T$ represent the positions of the host vehicle, radar sensor and object respectively in the Cartesian global frame $\underline{\vec{e}}^G$, which is given by

$$\underline{\vec{e}}^G = [\vec{e}_x^G \quad \vec{e}_y^G \quad \vec{e}_z^G]^T, \tag{4.12}$$

where the $\vec{e}_x^G$ and $\vec{e}_y^G$ directions correspond with the east and north direction of an earth fixed and earth centered coordinate system, and the $\vec{e}_z^G$ direction is pointing upwards. As mentioned earlier, frame $\underline{\vec{e}}^h$ is a Cartesian body-fixed frame with its origin positioned at the center of mass of the host vehicle. The relation between both frames is given by

$$\underline{\vec{e}}^G = \mathbf{R}(\theta^h)\,\underline{\vec{e}}^h = \begin{bmatrix} \cos(\theta^h) & -\sin(\theta^h) & 0 \\ \sin(\theta^h) & \cos(\theta^h) & 0 \\ 0 & 0 & 1 \end{bmatrix} \underline{\vec{e}}^h, \tag{4.13}$$

where $\mathbf{R}(\theta^h)$ is the rotation matrix and θ^h is the heading angle of the host vehicle with respect to the $\vec{e}_x^G$ direction of the global frame [46]. Next, the vector $\vec{r}_{R/H}$ represents the position of the radar sensor in the body-fixed frame and is given by

$$\vec{r}_{R/H} = [l_f \quad 0 \quad 0]\underline{\vec{e}}^h, \tag{4.14}$$

where l_f is the longitudinal distance between the center of mass of the host vehicle and the front facing radar sensor. Furthermore, the vector $\vec{r}_{T/R}$ represents the position of the object in the body-fixed frame as measured by the radar sensor and is given by

$$\vec{r}_{T/R} = [d_x^r \quad d_y^r \quad 0]\underline{\vec{e}}^h, \tag{4.15}$$

and finally the vector $\vec{r}_{T/H}$ represents the position of the object in the body-fixed frame and is given by

$$\vec{r}_{T/H} = \vec{r}_{R/H} + \vec{r}_{T/R} = [d_x^r + l_f \quad d_y^r \quad 0]\underline{\vec{e}}^h. \tag{4.16}$$

Expressions for $v_x^\perp$ and $v_y^\perp$ in the body-fixed frame can now be found by determining the time-derivative of vector $\vec{r}_{T/R}$, which is given by

$$\dot{\vec{r}}_{T/R} = \dot{\vec{r}}_T - \dot{\vec{r}}_R = [v_x^\perp \quad v_y^\perp \quad 0]\underline{\vec{e}}^h. \tag{4.17}$$

where $\dot{\vec{r}}_T$ and $\dot{\vec{r}}_R$ are the time-derivatives of respectively the vectors $\vec{r}_T$ and $\vec{r}_R$. Here, the time-derivative of vector $\vec{r}_R$ can be found as follows

$$\begin{aligned}
\dot{\vec{r}}_R &= \dot{\vec{r}}_H + \dot{\vec{r}}_{R/H} = \dot{\vec{r}}_H + \vec{\omega} \times \vec{r}_{R/H} \\
&= [v_x^h \quad 0 \quad 0]\mathbf{R}(\theta^h)^T \underline{\vec{e}}^G + \left([0 \quad 0 \quad \omega_z^h]\underline{\vec{e}}^G\right) \times \left([l_f \quad 0 \quad 0]\mathbf{R}(\theta^h)^T \underline{\vec{e}}^G\right) \\
&= [v_x^h \cos(\theta^h) \quad v_x^h \sin(\theta^h) \quad 0]\underline{\vec{e}}^G + [0 \quad 0 \quad \omega_z^h]\left(\underline{\vec{e}}^G \times \underline{\vec{e}}^{G^T}\right)\mathbf{R}(\theta^h)[l_f \quad 0 \quad 0]^T \\
&= v_x^h \cos(\theta^h)\vec{e}_x^G + v_x^h \sin(\theta^h)\vec{e}_y^G + [\omega_z^h \vec{e}_y^G \quad -\omega_z^h \vec{e}_x^G \quad 0]\mathbf{R}(\theta^h)[l_f \quad 0 \quad 0]^T \\
&= v_x^h C(\theta^h)\vec{e}_x^G + v_x^h S(\theta^h)\vec{e}_y^G + ... \\
&...[(\omega_z^h C(\theta^h)\vec{e}_y^G - \omega_z^h S(\theta^h)\vec{e}_x^G) \quad (-\omega_z^h S(\theta^h)\vec{e}_y^G - \omega_z^h C(\theta^h)\vec{e}_x^G) \quad 0][l_f \quad 0 \quad 0]^T \\
&= \left(v_x^h C(\theta^h) - \omega_z^h l_f S(\theta^h)\right)\vec{e}_x^G + \left(v_x^h S(\theta^h) + \omega_z^h l_f C(\theta^h)\right)\vec{e}_y^G,
\end{aligned} \tag{4.18}$$

where $C(\theta^h)$ denotes $\cos(\theta^h)$ and $S(\theta^h)$ denotes $\sin(\theta^h)$ [46]. Furthermore, as given in [46], the following relation is used

$$\underline{\vec{e}}^G \times \underline{\vec{e}}^{G^T} = \begin{bmatrix} \overrightarrow{0} & \vec{e}_z^G & -\vec{e}_y^G \\ -\vec{e}_z^G & \overrightarrow{0} & \vec{e}_x^G \\ \vec{e}_y^G & -\vec{e}_x^G & \overrightarrow{0} \end{bmatrix}. \tag{4.19}$$

Similarly, the time-derivative of vector $\vec{r}_T$ is given by

$$\begin{aligned}
\dot{\vec{r}}_T &= \dot{\vec{r}}_H + \dot{\vec{r}}_{T/H} = \dot{\vec{r}}_H + \vec{\omega} \times \vec{r}_{T/H} \\
&= \left(v_x^h C(\theta^h) - \omega_z^h (d_x^r + l_f) S(\theta^h) - \omega_z^h d_y^r C(\theta^h)\right)\vec{e}_x^G + ... \\
&... \left(v_x^h S(\theta^h) + \omega_z^h (d_x^r + l_f) C(\theta^h) - \omega_z^h d_y^r S(\theta^h)\right)\vec{e}_y^G.
\end{aligned} \tag{4.20}$$

Finally, using (4.18) and (4.20), the time-derivative of vector $\vec{r}_{T/R}$ can be determined as follows

$$\begin{aligned}
\dot{\vec{r}}_{T/R} &= \dot{\vec{r}}_T - \dot{\vec{r}}_R \\
&= \left(-\omega_z^h d_x^r S(\theta^h) - \omega_z^h d_y^r C(\theta^h)\right)\vec{e}_x^G + \left(\omega_z^h d_x^r C(\theta^h) - \omega_z^h d_y^r S(\theta^h)\right)\vec{e}_y^G \\
&= [(-\omega_z^h d_x^r S(\theta^h) - \omega_z^h d_y^r C(\theta^h)) \quad (\omega_z^h d_x^r C(\theta^h) - \omega_z^h d_y^r S(\theta^h)) \quad 0]\mathbf{R}(\theta^h)\,\underline{\vec{e}}^h \\
&= [-\omega_z^h d_y^r (C^2(\theta^h) + S^2(\theta^h)) \quad \omega_z^h d_x^r (C^2(\theta^h) + S^2(\theta^h)) \quad 0]\underline{\vec{e}}^h \\
&= [-\omega_z^h d_y^r \quad \omega_z^h d_x^r \quad 0]\underline{\vec{e}}^h,
\end{aligned} \tag{4.21}$$

which results in the following expressions for $v_x^\perp$ and $v_y^\perp$

$$\begin{aligned}
v_x^\perp &= -\omega_z^h d_y^r \\
v_y^\perp &= \omega_z^h d_x^r.
\end{aligned} \tag{4.22}$$

Using these expressions, the relations between the measured relative velocity and the absolute velocity of the object in both directions are given by

$$\begin{aligned}
v_x^r &= v_x^t - v_x^h - v_x^\perp = v_x^t - v_x^h + \omega_z^h d_y^r \\
v_y^r &= v_y^t - v_y^\perp = v_y^t - \omega_z^h d_x^r.
\end{aligned} \tag{4.23}$$

Here, it is assumed again that the host vehicle has no lateral velocity component. Using the relations given in (4.23), the discrete-time measurement equation as described by (4.4) is given by

$$\begin{bmatrix} d_{x,k}^r \\ v_{x,k}^r \\ d_{y,k}^r \\ v_{y,k}^r \end{bmatrix} = \begin{bmatrix} 1 & 0 & 0 & 0 & 0 & 0 \\ 0 & 1 & 0 & \omega_{z,k}^h & 0 & 0 \\ 0 & 0 & 0 & 1 & 0 & 0 \\ -\omega_{z,k}^h & 0 & 0 & 0 & 1 & 0 \end{bmatrix} \begin{bmatrix} d_{x,k}^r \\ v_{x,k}^t \\ a_{x,k}^t \\ d_{y,k}^r \\ v_{y,k}^t \\ a_{y,k}^t \end{bmatrix} + \begin{bmatrix} 0 & 0 \\ -1 & 0 \\ 0 & 0 \\ 0 & 0 \end{bmatrix} \begin{bmatrix} v_{x,k}^h \\ a_{x,k}^h \end{bmatrix} + ... \\ ... \begin{bmatrix} \mathrm{v}_{d_{x,k}^r} \\ \mathrm{v}_{v_{x,k}^r} \\ \mathrm{v}_{d_{y,k}^r} \\ \mathrm{v}_{v_{y,k}^r} \end{bmatrix}, \tag{4.24}$$

where the yaw rate of the host vehicle $\omega_{z,k}^h$ is included in the observation matrix $\mathbf{C}_k$, which makes the discrete-time measurement equation given above nonlinear and time-variant. However, the yaw rate $\omega_{z,k}^h$ is assumed to be slowly varying and therefore the nonlinearity is ignored, which is a valid assumption for the driving scenarios described in Section 3.5. At every sample, the yaw rate of the host vehicle $\omega_{z,k}^h$ is assumed to be known from the IMU.

4.2 State estimator

To estimate the states described by $\underline{\mathrm{x}}_k$, a discrete-time Kalman filter is used. In this section, the Kalman filter and its general equations will be discussed. Thereafter, an additional correction step on the estimated states will be introduced, which is required to correct the states for the rotation of the host vehicle. Then, the method used to deal with the low sampling rate of the radar sensor will be explained. Finally, the methods used to initialize the state estimator and to select the process noise values are discussed.

4.2.1 Kalman filter equations

Given a model of the system is known, a Kalman filter can be used to estimate the states described by $\underline{\mathrm{x}}_k$ using the available noisy measurements $\underline{\mathrm{y}}_k$ together with the knowledge of the system dynamics, when assuming that both the process noise and measurement noise are zero-mean, white and uncorrelated noise processes with covariance matrices $\mathbf{Q}_k$ and $\mathbf{R}_k$ respectively [17]. Depending on the available measurements, different state estimates of the state vector $\underline{\mathrm{x}}_k$ can be made. If at time k all measurements up to and including time $k-1$ are available, then a so-called a-priori state estimate can be formed, which is indicated by $\underline{\hat{\mathrm{x}}}_{k|k-1}$. Here, the first index, in this case k, indicates the time of the state estimate and the second index indicates whether the state estimate is a-priori or a-posteriori. So, $\underline{\hat{\mathrm{x}}}_{k|k-1}$ is an estimate of $\underline{\mathrm{x}}_k$ before the measurement at time k has been processed. Determining the a-priori state estimate $\underline{\hat{\mathrm{x}}}_{k|k-1}$ and the a-priori state estimation covariance $\mathbf{P}_{k|k-1}$ corresponds with the first phase of the discrete-time Kalman filter, which is called the prediction phase [17]. When the measurement at time k becomes available, a so-called a-posteriori state estimate can be formed, which is indicated by $\underline{\hat{\mathrm{x}}}_{k|k}$. So, $\underline{\hat{\mathrm{x}}}_{k|k}$ is an estimate of $\underline{\mathrm{x}}_k$ after the measurement at time k is being processed. Determining the a-posteriori state estimate $\underline{\hat{\mathrm{x}}}_{k|k}$ and the a-posteriori state estimation covariance $\mathbf{P}_{k|k}$ corresponds with the second phase of the discrete-time Kalman filter, which is called the measurement update phase [17]. Figure 4.3 gives a schematic overview of the two phases of a discrete-time Kalman filter.

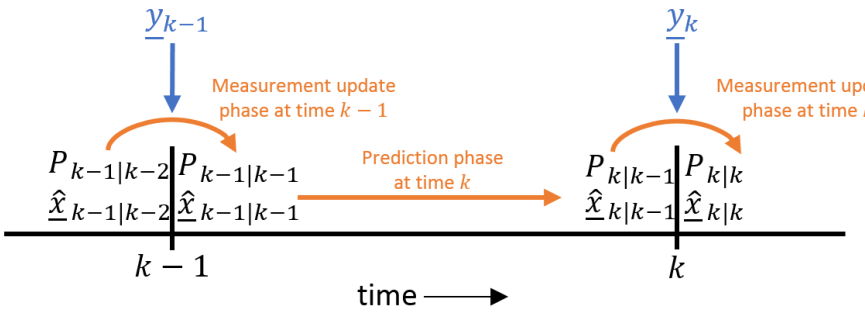

Figure 4.3: A schematic overview of the two phases of a discrete-time Kalman filter together with the a-posteriori and the a-priori state estimates and the corresponding state estimation covariances [17].

In the first phase of the discrete-time Kalman filter, which is the prediction phase, the a-priori state estimate is determined as follows

$$\hat{\underline{x}}_{k|k-1} = \mathbf{A}\hat{\underline{x}}_{k-1|k-1} + \mathbf{B}\underline{u}_k, \tag{4.25}$$

where $\hat{\underline{x}}_{k-1|k-1}$ is the a-posteriori state estimate of the previous time step [17]. Then, the predicted a-priori state estimation covariance can be determined as follows

$$\mathbf{P}_{k|k-1} = \mathbf{A}\mathbf{P}_{k-1|k-1}\mathbf{A}^T + \mathbf{Q}_k, \tag{4.26}$$

where $\mathbf{P}_{k-1|k-1}$ is the a-posteriori state estimation covariance of the previous time step. The second phase of the discrete-time Kalman filter is the measurement update phase, which is only executed if a new measurement is available as will be explained in Section 4.2.3. In the measurement update phase, first the predicted innovation is determined, which is the error made in estimating the output $\underline{y}_k$ and is given by

$$\tilde{\underline{y}}_k = \underline{y}_k - \hat{\underline{y}}_k = \underline{y}_k - \mathbf{C}_k\hat{\underline{x}}_{k|k-1} - \mathbf{D}\underline{u}_k. \tag{4.27}$$

Furthermore, the innovation covariance matrix is given by

$$\mathbf{S}_k = \mathbf{C}_k\mathbf{P}_{k|k-1}\mathbf{C}_k^T + \mathbf{R}_k. \tag{4.28}$$

Using the innovation covariance matrix, the Kalman gain can be determined as follows

$$\mathbf{K}_k = \mathbf{P}_{k|k-1}\mathbf{C}_k^T\mathbf{S}_k^{-1}. \tag{4.29}$$

Finally, the updated a-posteriori state estimate is given by

$$\hat{\underline{x}}_{k|k} = \hat{\underline{x}}_{k|k-1} + \mathbf{K}_k\tilde{\underline{y}}_k = \hat{\underline{x}}_{k|k-1} + \mathbf{K}_k\left(\underline{y}_k - \hat{\underline{y}}_k\right), \tag{4.30}$$

and the updated a-posteriori state estimation covariance is given by

$$\mathbf{P}_{k|k} = (\mathbf{I} - \mathbf{K}_k\mathbf{C}_k)\mathbf{P}_{k|k-1}. \tag{4.31}$$

Since the time-varying observation matrix $\mathbf{C}_k$ is included in the equations of the measurement update phase, this could result in instability if the yaw rate of the host vehicle $\omega_{z,k}^h$ becomes too large. However, for the driving scenarios discussed in Section 3.5, the yaw rate remains relatively small and is slowly varying. Therefore, this possible instability will not be discussed further.

The process noise covariance matrix is given by

$$\mathbf{Q}_k = \mathbf{G}\mathbf{q}_k\mathbf{G}^T, \tag{4.32}$$

where $\mathbf{q}_k$ is determined using the expected value operator similar to the measurement noise covariance matrix, which can both be determined as follows

$$\begin{aligned}\mathbf{q}_k &= E\left\{\underline{\mathrm{w}}_n \underline{\mathrm{w}}_m^T\right\} = \begin{bmatrix} \sigma^2_{w^h_{j_x}} & 0 & 0 & 0 \\ 0 & \sigma^2_{w^t_{j_x}} & 0 & 0 \\ 0 & 0 & \sigma^2_{w^h_{j_y}} & 0 \\ 0 & 0 & 0 & \sigma^2_{w^t_{j_y}} \end{bmatrix} \delta_{nm} = \mathbf{q} \\ \mathbf{R}_k &= E\left\{\underline{\mathrm{v}}_n \underline{\mathrm{v}}_m^T\right\} = \begin{bmatrix} \sigma^2_{d^r_x} & 0 & 0 & 0 \\ 0 & \sigma^2_{v^r_x} & 0 & 0 \\ 0 & 0 & \sigma^2_{d^r_y} & 0 \\ 0 & 0 & 0 & \sigma^2_{v^r_y} \end{bmatrix} \delta_{nm} = \mathbf{R}.\end{aligned} \tag{4.33}$$

Here, σ^2 is the variance of the signals present in respectively the process noise vector $\underline{\mathrm{w}}$ and the measurement noise vector $\underline{\mathrm{v}}$. Both the process noise and the measurement noise are assumed to be zero-mean Gaussian white noise processes and due to the Kroneckerdelta function δ_{nm} both covariance matrices do not depend on time, resulting in $\mathbf{Q}_k = \mathbf{Q}$ and $\mathbf{R}_k = \mathbf{R}$ [17]. Furthermore, both $\mathbf{q}$ and $\mathbf{R}$ are square, positive definite and also diagonal, since the motions of the object in the longitudinal and lateral direction of the current body-fixed frame are assumed to be uncorrelated. The noise levels of the measurement signals included in $\mathbf{R}$ are listed in Table 3.2.

4.2.2 Additional correction step Kalman filter

In this research, the constant acceleration model is slightly adapted by using the absolute motion of the object instead of the relative motion. To reduce the state estimation errors when the host vehicle is cornering ($\omega_z^h \neq 0$), the a-posteriori state estimate of the previous time step $\underline{\hat{\mathrm{x}}}_{k-1|k-1}$ is corrected for the rotation of the host vehicle before the prediction phase of the Kalman filter is executed.

If the host vehicle is cornering, the current body-fixed frame $\vec{\underline{e}}_k^h$ will rotate with respect to the previous body-fixed frame $\vec{\underline{e}}_{k-1}^h$. Figure 4.4 shows the estimated relative distances of the previous time step before correction in frame $\vec{\underline{e}}_{k-1}^h$ together with the measured relative distances in frame $\vec{\underline{e}}_k^h$, where the rotation between both frames is clearly visible. Without correcting $\underline{\hat{\mathrm{x}}}_{k-1|k-1}$ for the rotation of the host vehicle, the a-priori state estimate $\underline{\hat{\mathrm{x}}}_{k|k-1}$ as calculated by (4.25) will still be given in the previous body-fixed frame $\vec{\underline{e}}_{k-1}^h$, whereas the measurement vector $\underline{\mathrm{y}}_k$ is given in the current body-fixed frame $\vec{\underline{e}}_k^h$. By correcting $\underline{\hat{\mathrm{x}}}_{k-1|k-1}$ before the prediction phase, both the a-priori state estimate $\underline{\hat{\mathrm{x}}}_{k|k-1}$ and the measurement vector $\underline{\mathrm{y}}_k$ are given in the current body-fixed frame $\vec{\underline{e}}_k^h$ when performing the measurement update phase of the Kalman filter as given in (4.30). In this way the state estimation errors can be reduced.

The relation between the previous body-fixed frame $\vec{\underline{e}}_{k-1}^h$ and the current body-fixed frame $\vec{\underline{e}}_k^h$ is given by

$$\vec{\underline{e}}_{k-1}^h = \mathbf{R}(\Delta\theta^h)\, \vec{\underline{e}}_k^h = \begin{bmatrix} \cos(\Delta\theta^h) & -\sin(\Delta\theta^h) & 0 \\ \sin(\Delta\theta^h) & \cos(\Delta\theta^h) & 0 \\ 0 & 0 & 1 \end{bmatrix} \vec{\underline{e}}_k^h, \tag{4.34}$$

where $\mathbf{R}(\Delta\theta^h)$ is the rotation matrix and $\Delta\theta^h$ is the difference in heading angle between two samples, which can be obtained as follows

$$\Delta\theta^h = \omega^h_{z,k-1} T_s. \tag{4.35}$$

Here, at every sample, the yaw rate of the previous time step $\omega^h_{z,k-1}$ is assumed to be known from the IMU. Furthermore, the yaw rate of the host vehicle is assumed to be constant again over the

sample time T_s. The corrected a-posteriori state estimate of the previous time step is given by

$$\underline{\hat{x}}^*_{k-1|k-1} = \begin{bmatrix} \hat{d}r^*_{x,k-1|k-1} & \hat{v}^{t^*}_{x,k-1|k-1} & \hat{a}^{t^*}_{x,k-1|k-1} & \hat{d}r^*_{y,k-1|k-1} & \hat{v}^{t^*}_{y,k-1|k-1} & \hat{a}^{t^*}_{y,k-1|k-1} \end{bmatrix}^T. \tag{4.36}$$

Using (4.34), the a-posteriori estimate of the longitudinal relative distance can be corrected as follows

$$\hat{d}r^*_{x,k-1|k-1} = \hat{d}r_{x,k-1|k-1}\cos(\Delta\theta^h) + \hat{d}r_{y,k-1|k-1}\sin(\Delta\theta^h), \tag{4.37}$$

In a similar way the a-posteriori estimates of the absolute longitudinal velocity and acceleration of the object can be corrected.

The a-posteriori estimate of the lateral relative distance can be corrected using (4.34) as follows

$$\hat{d}r^*_{y,k-1|k-1} = -\hat{d}r_{x,k-1|k-1}\sin(\Delta\theta^h) + \hat{d}r_{y,k-1|k-1}\cos(\Delta\theta^h). \tag{4.38}$$

Again, the a-posteriori estimates of the absolute lateral velocity and acceleration of the object can be corrected in a similar way. The correction step can be implemented in the Kalman filter by replacing the a-posteriori state estimate $\underline{\hat{x}}_{k-1|k-1}$ in (4.25) by the corrected a-posteriori state estimate $\underline{\hat{x}}^*_{k-1|k-1}$.

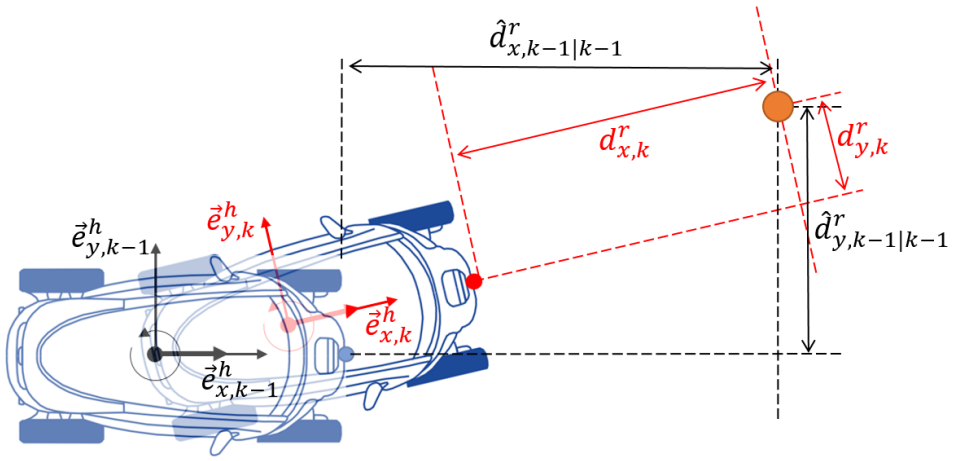

Figure 4.4: The estimated relative distances of the previous time step before correction in frame $\underline{\vec{e}}^h_{k-1}$ together with the measured relative distances in frame $\underline{\vec{e}}^h_k$.

4.2.3 Low sampling rate of the radar sensor

When using the Kalman filter as discussed so far, the measurements are assumed to be available at every sample. However, in reality this is not the case since the sample rate of the radar sensor differs from the operating frequency of the AEB controller (including the Kalman filter). The sample rate of the radar sensor is 16.7 Hz, whereas the operating frequency of the AEB controller is 100 Hz. This means that at approximately every sixth sample new measurements from the radar sensor are available, and in between these measurements the Kalman filter should estimate the states without a measurement update. Here, it is assumed that there are no inter-sample measurements and the sample rate of the radar sensor is a multitude of the operating frequency of the Kalman filter. In the literature, a common approach to the problem described above is to only perform the measurement update phase in case new measurements are available [51] [52]. In [51], this approach results in a size-varying measurement vector $\underline{y}_k$, observation matrix $\mathbf{C}_k$, observed input matrix $\mathbf{D}$, and measurement noise vector $\underline{v}_k$. However, this method ensures that the state estimates are only updated when new measurements are available, which is achieved by removing the elements of $\underline{y}_k$, $\mathbf{C}_k$, $\mathbf{D}$, and $\underline{v}_k$ that do not belong to new measurements. If at time k the only components available of the measurement vector $\underline{y}_k$ are $i_1, ..., i_{m_k}$ (with $1 \leq i_1 \leq ... \leq i_{m_k} \leq m$), then the corrected measurement vector is given by

$$\underline{y}_k^* = \mathbf{L}_k \underline{y}_k, \tag{4.39}$$

where $\mathbf{L}_k$ is a $m_k \times m$ matrix with m_k being the number of new measurements at time k and with m being the number of rows of the observation matrix $\mathbf{C}_k$. The matrix $\mathbf{L}_k$ has ones at the positions $((1, i_1), ..., (m_k, i_{m_k}))$ and zeros elsewhere. Furthermore, the corrected observation matrix, observed input matrix and measurement noise vector are given by

$$\mathbf{C}_k^* = \mathbf{L}_k \mathbf{C}_k \quad \mathbf{D}_k^* = \mathbf{L}_k \mathbf{D} \quad \underline{v}_k^* = \mathbf{L}_k \underline{v}_k. \tag{4.40}$$

This method can be implemented by replacing $\underline{y}_k$, $\mathbf{C}_k$, $\mathbf{D}$ and $\underline{v}_k$ in (4.25) to (4.31) with the corrected $\underline{y}_k^*$, $\mathbf{C}_k^*$, $\mathbf{D}_k^*$ and $\underline{v}_k^*$. Furthermore, this method can be used for setups with multiple sensors with different sample rates. In [53], another method is proposed where the unavailable measurements are considered to be exactly equal to the predicted measurements. Therefore, similar to the method discussed before, the state estimates are not corrected with the measurements and the a-posteriori state estimate $\underline{\hat{x}}_{k|k}$ is equal to the a-priori state estimate $\underline{\hat{x}}_{k|k-1}$. However, the method proposed in [53] results in a modified a-posteriori state estimation covariance $\mathbf{P}_{k|k}$. In [54], the Kalman gain $\mathbf{K}_k$ is set to zero in case a measurement is missing, which similar to the method presented in [51] results in an a-posteriori state estimate $\underline{\hat{x}}_{k|k}$ equal to the a-priori state estimate $\underline{\hat{x}}_{k|k-1}$ and an a-posteriori state estimation covariance $\mathbf{P}_{k|k}$ equal to the a-priori state estimation covariance $\mathbf{P}_{k|k-1}$. It should be noted that these methods are not necessarily mathematically proven, but implementing them can improve the performance of the Kalman filter.

The method used to deal with the low sampling rate of the radar sensor is similar to the methods presented in [51] and [54]. However, in the setup considered in this research only the radar sensor provides the measurements included in the measurement vector $\underline{y}_k$. Therefore, in contrast to the method presented in [51], there is no need to correct $\underline{y}_k$, $\mathbf{C}_k$, $\mathbf{D}$ and $\underline{v}_k$ in case no new measurements are available. If the radar sensor does not provide a new measurement, the state estimates are only based on the prediction step of the Kalman filter and the a-posteriori state estimate $\underline{\hat{x}}_{k|k}$ is set equal to the predicted a-priori state estimate $\underline{\hat{x}}_{k|k-1}$, and the a-posteriori state estimation covariance $\mathbf{P}_{k|k}$ is set equal to the predicted a-priori state estimation covariance $\mathbf{P}_{k|k-1}$.

4.2.4 Initialization of the state estimator

When the object enters the field of view of the radar sensor, the Kalman filter should be initialized first. This involves making an initial estimate of the states included in the state vector $\underline{\mathrm{x}}_k$ as given in (4.6). The initial estimate of these states is given by

$$\hat{\underline{\mathrm{x}}}_0 = \begin{bmatrix} \hat{d}^r_{x,0} & \hat{v}^t_{x,0} & \hat{a}^t_{x,0} & \hat{d}^r_{y,0} & \hat{v}^t_{y,0} & \hat{a}^t_{y,0} \end{bmatrix}^T. \tag{4.41}$$

Here, the initial estimates of the longitudinal and lateral relative distances are set equal to the initial measured longitudinal and lateral relative distances obtained by the radar sensor as follows

$$\begin{aligned} \hat{d}^r_{x,0} &= d^r_{x,0} \\ \hat{d}^r_{y,0} &= d^r_{y,0}. \end{aligned} \tag{4.42}$$

Furthermore, the initial estimates of the absolute longitudinal and lateral velocity of the object are obtained from the initial measurements of the radar sensor, the IMU and the odometer using the relations given in (4.23) as follows

$$\begin{aligned} \hat{v}^t_{x,0} &= v^r_{x,0} + v^h_{x,0} - \omega^h_{z,0} d^r_{y,0} \\ \hat{v}^t_{y,0} &= v^r_{y,0} + \omega^h_{z,0} d^r_{x,0}. \end{aligned} \tag{4.43}$$

Finally, the initial estimates of the absolute longitudinal and lateral acceleration of the object are set to zero, since they are unknown. By initializing the Kalman filter with the initial estimates as described above, the initialization errors are reduced and the state estimates will converge sooner towards their actual values.

In addition to the states, also the state estimation covariance needs to be initialized. Since the initial state estimates are obtained directly from the initial radar measurements, the measurement noise levels of the radar measurements as given in Table 3.2 are used to determine the initial state estimation covariance as follows

$$\mathbf{P}_0 = \mathbf{A} \begin{bmatrix} \sigma^2_{d^r_x} & 0 & 0 & 0 & 0 & 0 \\ 0 & \sigma^2_{v^r_x} & 0 & 0 & 0 & 0 \\ 0 & 0 & 0 & 0 & 0 & 0 \\ 0 & 0 & 0 & \sigma^2_{d^r_y} & 0 & 0 \\ 0 & 0 & 0 & 0 & \sigma^2_{v^r_y} & 0 \\ 0 & 0 & 0 & 0 & 0 & 0 \end{bmatrix} \mathbf{A}^T + \mathbf{Q}. \tag{4.44}$$

4.2.5 Selecting the process noise values

In general, the performance of the Kalman filter largely depends on the ratio between the covariance matrices $\mathbf{Q}$ and $\mathbf{R}$. As discussed earlier, the noise levels of the measurement signals included in the measurement noise covariance matrix $\mathbf{R}$ are known from the product data sheet of the radar sensor and are listed in Table 3.2. Therefore, the performance of the Kalman filter is optimized by solely tuning the process noise values of the process noise covariance matrix $\mathbf{Q}$. This is done by minimizing a cost function for different process noise values. As shown in (4.33), the process noise covariance matrix $\mathbf{Q}$ of the constant acceleration model consists of four noise terms on the longitudinal and lateral jerk for both the host vehicle and the object (or target). The process noise matrix $\mathbf{G}$ relates these noise terms to all states. Here, the process noise values of the host vehicle and the object are assumed to be equal, which results in a two-parameter optimization problem. The resulting process noise covariance matrix including the process noise values to be

tuned is given by

$$\begin{aligned}\mathbf{Q} = \mathbf{GqG}^T &= \mathbf{G}\begin{bmatrix} \sigma^2_{w^h_{j_x}} & 0 & 0 & 0 \\ 0 & \sigma^2_{w^t_{j_x}} & 0 & 0 \\ 0 & 0 & \sigma^2_{w^h_{j_y}} & 0 \\ 0 & 0 & 0 & \sigma^2_{w^t_{j_y}} \end{bmatrix}\mathbf{G}^T \\ &= \mathbf{G}\begin{bmatrix} 10^{P_x} & 0 & 0 & 0 \\ 0 & 10^{P_x} & 0 & 0 \\ 0 & 0 & 10^{P_y} & 0 \\ 0 & 0 & 0 & 10^{P_y} \end{bmatrix}\mathbf{G}^T,\end{aligned} \tag{4.45}$$

where P_x and P_y are the parameters used to vary the process noise values. By varying P_x and P_y, the performance of the Kalman filter can be compared for different process noise values, and by minimizing a cost function the process noise values resulting in the lowest cost C can be found. The cost function C used to find these process noise values is given by

$$C = \sum_{n=1}^{N} \frac{\text{RMS}\left(x^{gt}_{k,n} - \hat{x}_{k,n}\right)}{\max\left(\left|x^{gt}_{k,n} - \hat{x}_{k,n}\right|\right)} = \sum_{n=1}^{N} \frac{\sqrt{\frac{1}{K}\sum_{k=1}^{K}\left(x^{gt}_{k,n} - \hat{x}_{k,n}\right)^2}}{\max\left(\left|x^{gt}_{k,n} - \hat{x}_{k,n}\right|\right)}, \tag{4.46}$$

where N is the total number of states in the state vector $\underline{\mathrm{x}}_k$ as given in (4.6), K is the total number of samples used to calculate C and superscript gt is used to indicate the ground truth signal. The cost function is the summation of the root-mean-square (RMS) error divided by the maximum estimation error for every single state of all simulations. In this way, the RMS error is normalised with the maximum error, resulting in a cost between 0 and 1 and thus allowing the summation of the costs for different states since they all contribute equally to the cost function.

4.3 Tuning and performance of the state estimator

To evaluate the performance of the Kalman filter, simulations are performed for the driving scenarios described in Chapter 3. The outputs of the vehicle models are used as the ground truth signals in the simulation results presented in this section. Furthermore, in this section, it is assumed that there is no measurement noise present on the longitudinal velocity $v^h_{x,k}$ and the longitudinal acceleration $a^h_{x,k}$ of the host vehicle measured by the odometer and IMU. The reason for this assumption is that these signals are included in the input vector given in (4.7), meaning the measurement noise on these signals is not taken into account by the Kalman filter. For the same reason it is assumed that there is no measurement noise present on the yaw rate of the host vehicle ω^h_z obtained by the IMU, and used in the measurement equation given in (4.24) and in the additional correction step of the Kalman filter. Finally, the field of view of the radar sensor as given in Figure 3.3 is not considered in this section and it is assumed that the radar sensor is able to "see" the object at any time.

In this section, first the process noise values are selected using the method discussed in the previous section. Thereafter, the performance of the Kalman filter is analyzed for different driving scenarios.

4.3.1 Selection of the process noise values

To find the process noise values resulting in the lowest cost C, the method described in Section 4.2.5 is used. Here, the cost function given in (4.46) is minimized for different process noise values. Due to the assumption that the process noise values of the host vehicle and the object are equal, the process noise values are varied using only two parameters, being P_x and P_y. The process noise values are tuned for one driving scenario, such that the remaining scenarios give a more objective

indication of the performance of the Kalman filter. The scenario used to tune the process noise values is the fourth scenario, which is the most complex scenario of the proposed scenarios, where the host vehicle turns away from a braking target vehicle with a varying yaw rate. Therefore, both the constant acceleration assumption and the constant yaw rate assumption do not hold for this scenario, which makes this scenario closest to reality. To compare the values of the cost function C for different combinations of P_x and P_y, the same noise seeds are used for the measurement noise added to the radar measurements for every combination of P_x and P_y. Using different noise seeds resulted in the same process noise values resulting in the lowest cost C as presented in this section. Furthermore, to ensure that the cost function C is not affected by any initialization errors, the estimation errors used to calculate the cost function C are first included after 1 second of simulation time.

Figure 4.5 shows the cost function C for different combinations of the parameters P_x and P_y. These results are obtained by varying P_x and P_y in steps of 0.5 from -4 to 4. Here, the red dot indicates the minimal value of C, which is obtained when both P_x and P_y are set to 1. This means that for the fourth driving scenario, the lowest cost C is reached if the process noise values are set relatively high compared to the measurement noise values. Therefore, in this setting, the Kalman filter mostly relies on the measurements to estimate the states. Furthermore, Figure 4.5 shows the performance of the Kalman filter gets worse for lower values of P_x.

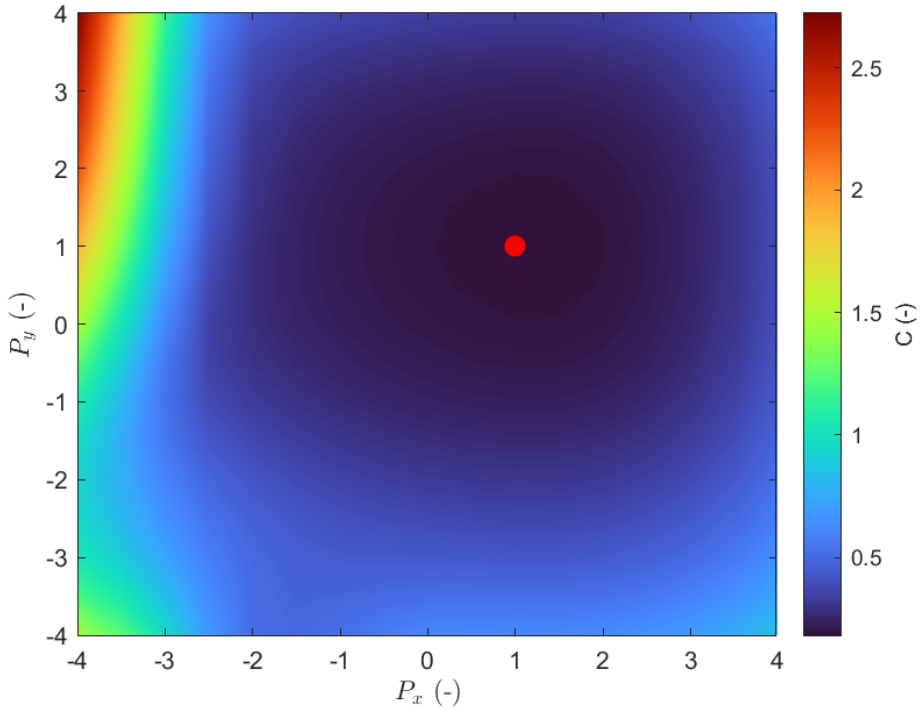

Figure 4.5: The cost function C for different combinations of the parameters P_x and P_y, where the red dot indicates the combination resulting in the minimal value of C.

4.3.2 Performance of the state estimator

In this section the performance of the Kalman filter with the process noise values found in the previous section is evaluated for the driving scenarios described in Chapter 3. The performance of the Kalman filter is evaluated by determining the errors between the estimated states and the corresponding ground truth signals and comparing them for different driving scenarios. More specifically, the RMS values and the absolute maximum values of these state estimation errors are compared, which are listed in the top part of Table 4.1. Furthermore, the RMS values and the absolute maximum values of the errors between the direct state measurements and the corresponding ground truth signals are listed in the bottom part of Table 4.1. The only direct state measurements available are the longitudinal relative distance d_x^r and the lateral relative distance d_y^r. As an example, the RMS value and the absolute maximum value of the state estimation error of a certain state x are given by

$$\begin{aligned} \text{RMS}(x^{gt} - \hat{x}) &= \sqrt{\frac{1}{K}\sum_{k=1}^{K}\left(x_k^{gt} - \hat{x}_k\right)^2} \\ \max(x^{gt} - \hat{x}) &= \max\left(\left|x_k^{gt} - \hat{x}_k\right|\right) \end{aligned} \tag{4.47}$$

where x_k^{gt} is the ground truth value and $\hat{x}_k$ is the state estimate of state x at time k. Again, to ensure that the RMS values and the absolute maximum values of the state estimation errors are not affected by any initialization errors, the state estimation errors are first included after 1 second of simulation time.

Table 4.1: The RMS errors and the absolute maximum errors of all state estimates (top part) and of the direct state measurements (bottom part) for all driving scenarios.

	1.CCRb		**2.CCRm**		**3.VRU**		**4.Turning**	
Error	RMS	max	RMS	max	RMS	max	RMS	max
$d_x^{r,gt} - \hat{d}_x^r\,(m)$	0.058	0.083	0.058	0.088	0.060	0.084	0.048	0.101
$v_x^{t,gt} - \hat{v}_x^t\,(m/s)$	0.070	0.141	0.058	0.141	0.059	0.141	0.084	0.258
$a_x^{t,gt} - \hat{a}_x^t\,(m/s^2)$	0.293	1.047	0.102	0.230	0.103	0.230	0.247	0.497
$d_y^{r,gt} - \hat{d}_y^r\,(m)$	0.018	0.022	0.018	0.022	0.019	0.020	0.257	0.021
$v_y^{t,gt} - \hat{v}_y^t\,(m/s)$	0.050	0.128	0.050	0.128	0.050	0.128	0.062	0.128
$a_y^{t,gt} - \hat{a}_y^t\,(m/s^2)$	0.103	0.225	0.103	0.225	0.103	0.225	0.294	0.226
$d_x^{r,gt} - d_x^r\,(m)$	0.124	0.371	0.124	0.371	0.124	0.371	0.124	0.371
$d_y^{r,gt} - d_y^r\,(m)$	0.120	0.414	0.120	0.414	0.120	0.414	0.120	0.414

When comparing the state estimation errors giving in the top part of Table 4.1 for the different driving scenarios, it can be concluded that the errors are similar in magnitude for all scenarios. However, scenario 2 and 3 result in smaller or similar errors compared to scenarios 1 and 4. This could be explained by the fact that scenarios 2 and 3 are the simplest scenarios, since both the constant acceleration assumption and the constant yaw rate assumption hold for these scenarios. Furthermore, as expected, it can be seen that most errors increase when a cornering maneuver is included, which is the case in scenario 4. This scenario is used to select the process noise values. Compared to the other scenarios, most RMS values and absolute maximum values of the state estimation errors are larger for scenario 4. Therefore, it can be concluded that the selected process noise values in the previous section can be used for different driving scenarios.

The bottom part of Table 4.1 includes the RMS values and the absolute maximum values of the errors between the direct state measurements and the corresponding ground truth signals. Comparing these errors with the state estimation errors in the top part of Table 4.1 also gives useful insights in the performance of the Kalman filter. Since the measurement noise added to the radar

sensor measurements (as given in Table 3.2) is equal for every scenario, also the RMS values and the absolute maximum values of the direct state measurement errors are equal for all scenarios. When comparing the state estimation errors of the longitudinal and lateral relative distances with the direct state measurement errors, it can be concluded that by using the Kalman filter, the measurement noise can be reduced significantly. Compared to the direct state measurement errors, the state estimation errors are two to six times smaller. The only exception here is the state estimation error of the lateral relative distance for scenario 4, which is about twice as large as the corresponding direct state measurement error. This can be explained by the assumption made in the motion model of the Kalman filter, where the lateral velocity of the host vehicle is assumed to be zero. However, for the cornering maneuver included in scenario 4 this assumption is not valid, which causes the larger state estimation error of the lateral relative distance for this scenario.

The ground truth signals and the estimation of all states for all driving scenarios together with the measured longitudinal and lateral relative distance are shown in Figure B.1 in Appendix B.1. Here, the Kalman filter is initialized using the method discussed in Section 4.2.4. The effects of the initialization method on the performance of the Kalman filter will not be discussed. Figure B.1 shows that for all driving scenarios the estimations of all states correspond well with the ground truth signals and the estimation errors are limited considering the quality of the available measurements. Therefore, for the simulated driving scenarios, the Kalman filter is able to estimate the states accurately with an acceptable error. Furthermore, by using the Kalman filter, the state estimates are available at every sample and the measurement noise levels on the longitudinal and lateral relative distance are significantly reduced.

4.4 Path prediction of the detected object

To determine if a detected object is relevant for the AEB system, the paths of both the host vehicle and the detected object are predicted first. Once the predicted paths are known, a possible collision between the host vehicle and the object can be found and a brake intervention by the AEB system can be initiated if necessary. At every time step k, the paths of both the host vehicle and the detected object are predicted in the current body-fixed frame $\vec{e}^{\,h}_k$. Figure 4.6 shows the current and predicted states describing the position and motion of the object in the current body-fixed frame.

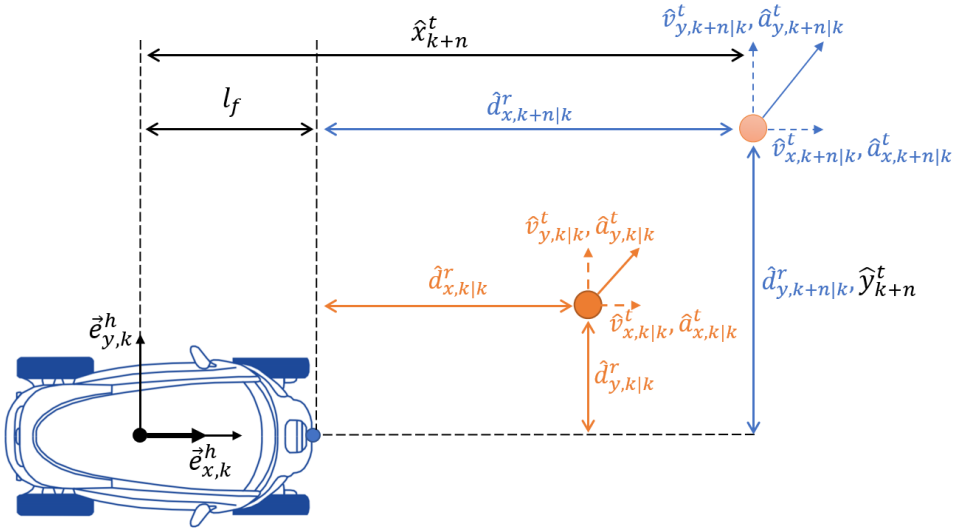

Figure 4.6: The current and the predicted position and motion of the detected object in the current body-fixed frame.

The states describing the position and motion of the object are included in the state vector $\underline{\mathrm{x}}_k$ given in (4.6). The position of the object is predicted over the time horizon $[k, k+n]$, where n is the prediction horizon in samples. This can be done by using the last available a-posteriori state estimate $\underline{\hat{\mathrm{x}}}_{k|k}$ to determine the predicted state estimate $\underline{\hat{\mathrm{x}}}_{k+n|k}$, which is also called a n-step a-priori prediction [17][22]. Since the prediction horizon n is fixed, this type of prediction is also called a fixed-lead prediction [16]. As will be discussed in the next section, the larger the prediction horizon n, the larger the uncertainty of the predicted position will be. The predicted state estimate $\underline{\hat{\mathrm{x}}}_{k+n|k}$ can be obtained by iterating the prediction phase of the Kalman filter n times. This means the constant acceleration model is used again to predict the position and motion of the object, where it is assumed that the object has uncorrelated motions in both the longitudinal and the lateral direction of the current body-fixed frame. Furthermore, the longitudinal and lateral acceleration of the object are assumed to be constant during the time horizon $[k, k+n]$, which introduces some model uncertainty since the acceleration of the object could change during this time horizon. Using the a-posteriori state estimate $\underline{\hat{\mathrm{x}}}_{k|k}$, the predicted state estimate for one time step ahead of the current time step k can be determined in a similar way as the a-priori state estimate given in (4.25) and is given by

$$\underline{\hat{\mathrm{x}}}_{k+1|k} = \mathbf{A}\underline{\hat{\mathrm{x}}}_{k|k} + \mathbf{B}\underline{\mathrm{u}}_k. \tag{4.48}$$

Now, by using (4.48), the predicted state estimate for two time steps ahead of the current time step k can be determined as follows

$$\begin{aligned} \underline{\hat{\mathrm{x}}}_{k+2|k} &= \mathbf{A}\underline{\hat{\mathrm{x}}}_{k+1|k} + \mathbf{B}\underline{\mathrm{u}}_k \\ &= \mathbf{A}\left(\mathbf{A}\underline{\hat{\mathrm{x}}}_{k|k} + \mathbf{B}\underline{\mathrm{u}}_k\right) + \mathbf{B}\underline{\mathrm{u}}_k \\ &= \mathbf{A}^2\underline{\hat{\mathrm{x}}}_{k|k} + \mathbf{A}\mathbf{B}\underline{\mathrm{u}}_k + \mathbf{B}\underline{\mathrm{u}}_k. \end{aligned} \tag{4.49}$$

From (4.48) and (4.49), the general equation of the predicted state estimate $\underline{\hat{\mathrm{x}}}_{k+n|k}$ can be derived, which is given by [55]

$$\underline{\hat{\mathrm{x}}}_{k+n|k} = \mathbf{A}^n\underline{\hat{\mathrm{x}}}_{k|k} + \sum_{m=1}^{n}\mathbf{A}^{m-1}\mathbf{B}\underline{\mathrm{u}}_k. \tag{4.50}$$

Here, as given in (4.7), the input vector $\underline{\mathrm{u}}_k$ consists of the longitudinal velocity $v^h_{x,k}$ and the longitudinal acceleration $a^h_{x,k}$ of the host vehicle. Since the motion of the host vehicle does not influence the predicted position of the object in the current body-fixed frame, (4.50) can be simplified as follows

$$\begin{aligned} \underline{\hat{\mathrm{x}}}_{k+n|k} &= \mathbf{A}^n\underline{\hat{\mathrm{x}}}_{k|k} \\ \begin{bmatrix} \hat{d}^r_{x,k+n|k} \\ \hat{v}^t_{x,k+n|k} \\ \hat{a}^t_{x,k+n|k} \\ \hat{d}^r_{y,k+n|k} \\ \hat{v}^t_{y,k+n|k} \\ \hat{a}^t_{y,k+n|k} \end{bmatrix} &= \begin{bmatrix} 1 & T_s & \frac{T_s^2}{2} & 0 & 0 & 0 \\ 0 & 1 & T_s & 0 & 0 & 0 \\ 0 & 0 & 1 & 0 & 0 & 0 \\ 0 & 0 & 0 & 1 & T_s & \frac{T_s^2}{2} \\ 0 & 0 & 0 & 0 & 1 & T_s \\ 0 & 0 & 0 & 0 & 0 & 1 \end{bmatrix}^n \begin{bmatrix} \hat{d}^r_{x,k|k} \\ \hat{v}^t_{x,k|k} \\ \hat{a}^t_{x,k|k} \\ \hat{d}^r_{y,k|k} \\ \hat{v}^t_{y,k|k} \\ \hat{a}^t_{y,k|k} \end{bmatrix}, \end{aligned} \tag{4.51}$$

where $\hat{d}^r_{x,k+n|k}$ and $\hat{d}^r_{y,k+n|k}$ now indicate the predicted longitudinal and lateral distance between the object and the position of the radar sensor at time k in the current body-fixed frame. Here, it should be noted that $\hat{d}^r_{x,k+n|k}$ and $\hat{d}^r_{y,k+n|k}$ do not indicate the predicted relative distance between the object and the host vehicle, since the motion of the host vehicle is not included in (4.51).

As is shown in Figure 4.6, the predicted absolute longitudinal and lateral position of the object (or target vehicle) in the current body-fixed frame can be determined in a similar way as the vector $\vec{r}_{T/H}$ given by (4.16) as follows

$$\begin{aligned} \hat{x}^t_{k+n} &= \hat{d}^r_{x,k+n|k} + l_f \\ \hat{y}^t_{k+n} &= \hat{d}^r_{y,k+n|k}, \end{aligned} \tag{4.52}$$

where $\hat{x}^t_{k+n}$ indicates the predicted absolute longitudinal position of the object in the $\vec{e}^h_{x,k}$ direction and $\hat{y}^h_{k+n}$ indicates the predicted absolute lateral position of the object in the $\vec{e}^h_{y,k}$ direction. Furthermore, l_f is the distance between the center of mass of the host vehicle and the radar sensor, which is set equal to the known distance a between the center of mass and the front axle of the host vehicle distance as given in Table 3.4.

At every time step k, the absolute longitudinal and lateral position of the object is predicted for multiple prediction times t_{pre}, which together form the predicted path of the object at sample k. The prediction horizon in samples n can be determined from the prediction time as follows

$$n = \frac{t_{pre}}{T_s}, \tag{4.53}$$

where T_s is the sample time of the AEB system being equal to 0.01 s and the prediction horizon in samples n is rounded to the nearest integer. In Figure 4.7 the actual path of the object is shown together with its predicted path in the current body-fixed frame. Here, the prediction time t_{pre} is changed from one to three seconds in steps of a half-second. For the driving scenarios discussed in Section 3.5, where the host vehicle drives with a velocity of 30 km/h, a prediction horizon of three seconds is assumed to be sufficient to prevent a collision. In Figure 4.7a, the predicted path for the CCRb driving scenario is shown, where the predicted positions start to deviate from the ground truth positions once the object starts to brake. Furthermore, in Figure 4.7b, the predicted path for the AEB VRU scenario is shown, where a small deviation is noticeable between the predicted positions and the ground truth positions. This deviation is caused by the uncertainty of the predicted positions as will be discussed in the next section. In the end, it can be concluded that the error between the actual path and the predicted path is acceptable, and therefore the method proposed in this section to predict the path of the detected object will be used in the remainder of this research.

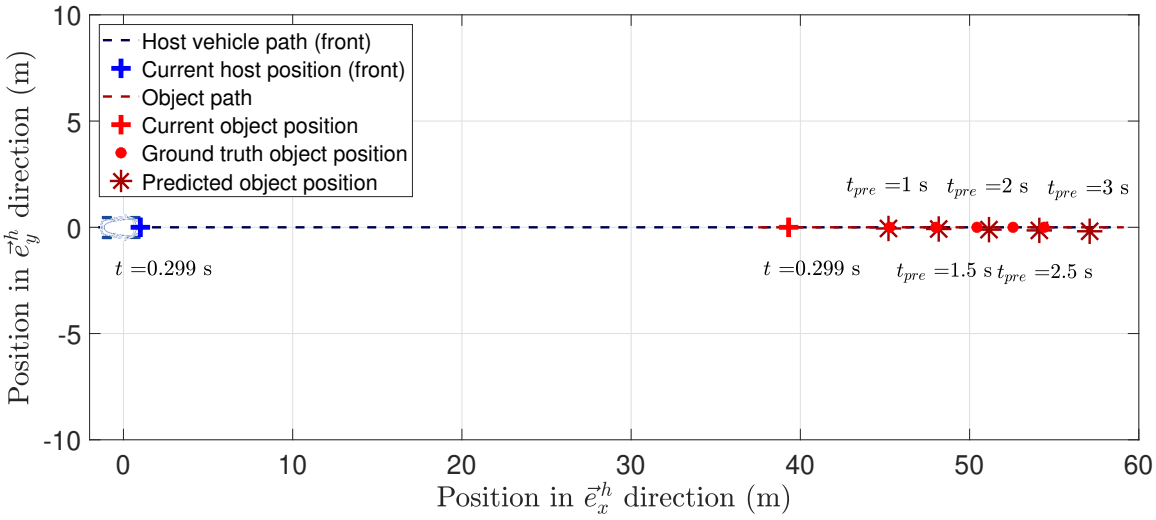

(a) Scenario 1: CCRb.

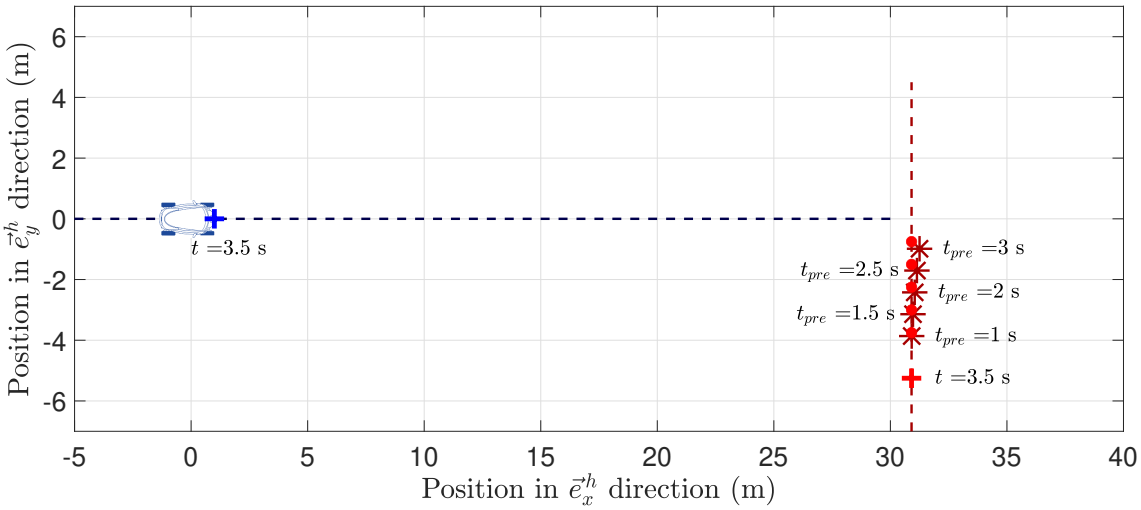

(b) Scenario 3: AEB VRU.

Figure 4.7: The actual path and the predicted path of the detected object in the current body-fixed frame.

4.4.1 Uncertainty of the predicted path

As discussed in the previous section, the predicted positions of the detected object are uncertain due to the model uncertainty of the constant acceleration model and the presence of measurement noise on the sensor measurements. To determine the level of uncertainty on the predicted positions of the object, the state estimation covariance needs to be predicted over the time horizon $[k, k+n]$. This can be done by using the last available a-posteriori state estimation covariance $\mathbf{P}_{k|k}$ to determine the predicted state estimation covariance $\mathbf{P}_{k+n|k}$. Again, the predicted state estimation covariance $\mathbf{P}_{k+n|k}$ can be obtained by iterating the prediction phase of the Kalman filter n times. Using the a-posteriori state estimation covariance $\mathbf{P}_{k|k}$, the predicted state estimation covariance for one time step ahead of the current time step k can be determined in a similar way as the

a-priori state estimation covariance in (4.26) and is given by

$$\mathbf{P}_{k+1|k} = \mathbf{A}\mathbf{P}_{k|k}\mathbf{A}^T + \mathbf{G}\mathbf{Q}\mathbf{G}^T. \tag{4.54}$$

By using (4.54), the predicted state estimation covariance for two time steps ahead of the current time step k can be determined as follows

$$\begin{aligned}\mathbf{P}_{k+2|k} &= \mathbf{A}\mathbf{P}_{k+1|k}\mathbf{A}^T + \mathbf{G}\mathbf{Q}\mathbf{G}^T \\ &= \mathbf{A}\left(\mathbf{A}\mathbf{P}_{k|k}\mathbf{A}^T + \mathbf{G}\mathbf{Q}\mathbf{G}^T\right)\mathbf{A}^T + \mathbf{G}\mathbf{Q}\mathbf{G}^T \\ &= \mathbf{A}^2\mathbf{P}_{k|k}{\mathbf{A}^T}^2 + \mathbf{A}\mathbf{G}\mathbf{Q}\mathbf{G}^T\mathbf{A}^T + \mathbf{G}\mathbf{Q}\mathbf{G}^T.\end{aligned} \tag{4.55}$$

Now, from (4.54) and (4.55), the general equation of the predicted state estimation covariance $\mathbf{P}_{k+n|k}$ can be derived, which is given by

$$\mathbf{P}_{k+n|k} = \mathbf{A}^n\mathbf{P}_{k|k}{\mathbf{A}^T}^n + \sum_{m=1}^{n}\mathbf{A}^{m-1}\mathbf{G}\mathbf{Q}\mathbf{G}^T{\mathbf{A}^T}^{m-1}. \tag{4.56}$$

where the system matrix $\mathbf{A}$ to the power of the prediction horizon n shows that the state estimation errors grow exponentially when the prediction horizon n becomes larger [55]. The resulting predicted state estimation covariance $\mathbf{P}_{k+n|k}$ has the following form

$$\mathbf{P}_{k+n|k} = \begin{bmatrix} \sigma(\hat{d}_x^r,\hat{d}_x^r) & \sigma(\hat{d}_x^r,\hat{v}_x^t) & \sigma(\hat{d}_x^r,\hat{a}_x^t) & 0 & 0 & 0 \\ \sigma(\hat{v}_x^t,\hat{d}_x^r) & \sigma(\hat{v}_x^t,\hat{v}_x^t) & \sigma(\hat{v}_x^t,\hat{a}_x^t) & 0 & 0 & 0 \\ \sigma(\hat{a}_x^t,\hat{d}_x^r) & \sigma(\hat{a}_x^t,\hat{v}_x^t) & \sigma(\hat{a}_x^t,\hat{a}_x^t) & 0 & 0 & 0 \\ 0 & 0 & 0 & \sigma(\hat{d}_y^r,\hat{d}_y^r) & \sigma(\hat{d}_y^r,\hat{v}_y^t) & \sigma(\hat{d}_y^r,\hat{a}_y^t) \\ 0 & 0 & 0 & \sigma(\hat{v}_y^t,\hat{d}_y^r) & \sigma(\hat{v}_y^t,\hat{v}_y^t) & \sigma(\hat{v}_y^t,\hat{a}_y^t) \\ 0 & 0 & 0 & \sigma(\hat{a}_y^t,\hat{d}_y^r) & \sigma(\hat{a}_y^t,\hat{v}_y^t) & \sigma(\hat{a}_y^t,\hat{a}_y^t) \end{bmatrix}, \tag{4.57}$$

where the variances are located on the diagonal of the covariance matrix and the covariances are located on the off-diagonal. As shown in (4.57), there is a correlation between the position, velocity and acceleration in both the longitudinal and the lateral direction, which is expected since the constant acceleration model is used, where it is assumed that the object has uncorrelated motions in both the longitudinal and the lateral direction of the current body-fixed frame. The goal is to determine the level of uncertainty on the predicted positions of the object, which can be indicated by the variances $\sigma^2_{\hat{d}_x^r}$ and $\sigma^2_{\hat{d}_y^r}$. These variances are not exactly equal to $\sigma(\hat{d}_x^r,\hat{d}_x^r)$ and $\sigma(\hat{d}_y^r,\hat{d}_y^r)$ as given in (4.57), since this would imply that there is no correlation between the position, velocity and acceleration. When taking into account these correlations and the corresponding units of the covariances, the variances $\sigma^2_{\hat{d}_x^r}$ and $\sigma^2_{\hat{d}_y^r}$ given in m^2 can be obtained. These variances are determined as follows

$$\begin{aligned}\sigma^2_{\hat{d}_x^r} &= \sigma(\hat{d}_x^r,\hat{d}_x^r) + T_s\sigma(\hat{d}_x^r,\hat{v}_x^t) + \frac{T_s^2\sigma(\hat{d}_x^r,\hat{a}_x^t)}{2} \\ \sigma^2_{\hat{d}_y^r} &= \sigma(\hat{d}_y^r,\hat{d}_y^r) + T_s\sigma(\hat{d}_y^r,\hat{v}_y^t) + \frac{T_s^2\sigma(\hat{d}_y^r,\hat{a}_y^t)}{2}.\end{aligned} \tag{4.58}$$

4.5 Path prediction of the host vehicle

Similar to the path prediction of the detected object, the path of the host vehicle is also predicted in the current body-fixed frame $\vec{e}_k^h$. However, in contrast to the path prediction of the object, which uses the state estimates obtained by the Kalman filter, the path of the host vehicle is predicted directly from the sensor measurements of the longitudinal velocity $v_{x,k}^h$, the longitudinal acceleration $a_{x,k}^h$ and the yaw rate of the host vehicle $\omega_{z,k}^h$. Figure 4.8 shows the current states and the predicted position and heading angle of the host vehicle in the current body-fixed frame. Here, $\hat{x}_{k+n}^h$ represents the predicted longitudinal position of the center of mass of the host vehicle in the $\vec{e}_{x,k}^h$ direction, $\hat{y}_{k+n}^h$ represents the predicted lateral position of the center of mass of the host vehicle in the $\vec{e}_{y,k}^h$ direction, and $\hat{\theta}_{k+n}^h$ represents the predicted heading angle of the host vehicle with respect to the $\vec{e}_{x,k}^h$ direction of the current body-fixed frame.

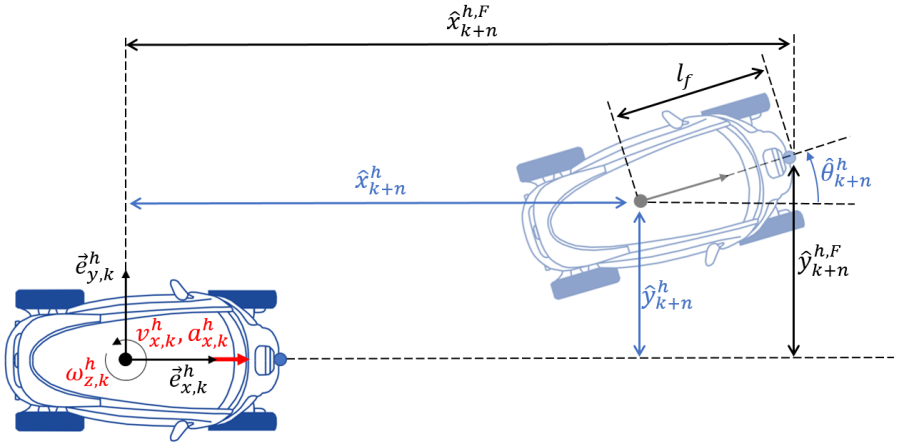

Figure 4.8: The current states and the predicted position and heading angle of the host vehicle in the current body-fixed frame.

To predict the path of the host vehicle, the constant yaw rate and acceleration model is used [23]. The same prediction time t_{pre} is used for the path prediction of both the host vehicle and the object. The predicted position and heading angle of the host vehicle are given by

$$
\begin{aligned}
\hat{x}_{k+n}^h &= x_k^h + \frac{a_{x,k}^h \left(\cos(\hat{\theta}_{k+n}^h) - \cos(\theta_k^h)\right)}{(\omega_{z,k}^h)^2} + \frac{\left(v_{x,k}^h + a_{x,k}^h t_{pre}\right)\sin(\hat{\theta}_{k+n}^h) - v_{x,k}^h \sin(\theta_k^h)}{\omega_{z,k}^h} \\
&= \frac{a_{x,k}^h \left(\cos(\hat{\theta}_{k+n}^h) - 1\right)}{(\omega_{z,k}^h)^2} + \frac{\left(v_{x,k}^h + a_{x,k}^h t_{pre}\right)\sin(\hat{\theta}_{k+n}^h)}{\omega_{z,k}^h} \\
\hat{y}_{k+n}^h &= y_k^h + \frac{a_{x,k}^h \left(\sin(\hat{\theta}_{k+n}^h) - \sin(\theta_k^h)\right)}{(\omega_{z,k}^h)^2} - \frac{\left(v_{x,k}^h + a_{x,k}^h t_{pre}\right)\cos(\hat{\theta}_{k+n}^h) - v_{x,k}^h \cos(\theta_k^h)}{\omega_{z,k}^h} \\
&= \frac{a_{x,k}^h \sin(\hat{\theta}_{k+n}^h)}{(\omega_{z,k}^h)^2} - \frac{\left(v_{x,k}^h + a_{x,k}^h t_{pre}\right)\cos(\hat{\theta}_{k+n}^h) - v_{x,k}^h}{\omega_{z,k}^h} \\
\hat{\theta}_{k+n}^h &= \theta_k^h + \omega_{z,k}^h t_{pre} = \omega_{z,k}^h t_{pre}.
\end{aligned}
\tag{4.59}
$$

Since the position and heading angle of the host vehicle are predicted in the current body-fixed frame, the initial longitudinal position x_k^h, the initial lateral position y_k^h and the initial heading angle θ_k^h of the host vehicle are all equal to zero. At every time step, the yaw rate $\omega_{z,k}^h$ and the longitudinal acceleration $a_{x,k}^h$ of the host vehicle are assumed to be known from the IMU and the

longitudinal velocity $v^h_{x,k}$ of the host vehicle is assumed to be known from the odometer. Furthermore, both the yaw rate $\omega^h_{z,k}$ and the longitudinal acceleration $a^h_{x,k}$ are assumed to be constant over the prediction time t_{pre}, which introduces some model uncertainty since they could change during this period.

Instead of predicting the position of the center of mass of the host vehicle, the predicted position of the front of the host vehicle needs to be known to detect a possible collision between the host vehicle and the object. In Figure 4.8, the predicted longitudinal position of the front of the host vehicle in the $\vec{e}^h_{x,k}$ direction is indicated by $\hat{x}^{h,F}_{k+n}$ and the predicted lateral position of the front of the host vehicle in the $\vec{e}^h_{y,k}$ direction is indicated by $\hat{y}^{h,F}_{k+n}$, which can be obtained as follows

$$\begin{aligned} \hat{x}^{h,F}_{k+n} &= \hat{x}^h_{k+n} + l_f \cos(\hat{\theta}^h_{k+n}) \\ \hat{y}^{h,F}_{k+n} &= \hat{y}^h_{k+n} + l_f \sin(\hat{\theta}^h_{k+n}). \end{aligned} \tag{4.60}$$

Figure 4.9 shows the actual path of the host vehicle together with the predicted path in the current body-fixed frame for the 'turning away' driving scenario. This driving scenario clearly shows the benefit of using the constant yaw rate and acceleration model to predict the path of the host vehicle. Here, in Figure 4.9a, the host vehicle is still driving straight, which means the current yaw rate of the host vehicle is zero ($\omega^h_{z,k} = 0$). The predicted positions start to deviate from the ground truth positions once the host vehicle starts to turn and the actual yaw rate of the host vehicle becomes nonzero. Then, in Figure 4.9b, the host vehicle is turning away, which means the current yaw rate of the host vehicle is nonzero ($\omega^h_{z,k} \neq 0$). Here, a small deviation is noticeable between the predicted positions and the ground truth positions. Again, this deviation is caused by the uncertainty of the predicted positions as will be discussed in the next section. However, it can be concluded that the error between the actual path and the predicted path is acceptable, and therefore the method proposed in this section to predict the path of the host vehicle will be used in the remainder of this research.

4.5.1 Uncertainty of the predicted path

The predicted positions of the host vehicle are uncertain due to the model uncertainty of the constant yaw rate and acceleration model, but also due to the measurement noise present on the sensor measurements. It is assumed that the uncertainty of the predicted path is only influenced by the measurement noise. The goal is to determine the level of uncertainty on the predicted positions of the host vehicle, which can be expressed in standard deviations by $\sigma_{\hat{x}^h}$ and $\sigma_{\hat{y}^h}$ indicating the level of uncertainty on the predicted longitudinal and lateral position respectively. To determine $\sigma_{\hat{x}^h}$ and $\sigma_{\hat{y}^h}$, the noise levels of the measured longitudinal velocity $\sigma_{v^h_x}$, the measured longitudinal acceleration $\sigma_{a^h_x}$ and the measured yaw rate $\sigma_{\omega^h_z}$ as given in Table 3.2 and expressed in standard deviations are used.

The level of uncertainty on the predicted positions of the host vehicle can be obtained by implementing the measurement noise levels of the longitudinal velocity and acceleration, and the yaw rate into the constant yaw rate and acceleration model given in (4.59) as follows

$$\begin{aligned} \sigma_{\hat{x}^h} &= \frac{\sigma_{a^h_x}\left(\cos(\sigma_{\omega^h_z} t_{pre}) - 1\right)}{(\sigma_{\omega^h_z})^2} + \frac{\left(\sigma_{v^h_x} + \sigma_{a^h_x} t_{pre}\right)\sin(\sigma_{\omega^h_z} t_{pre})}{\sigma_{\omega^h_z}} \\ \sigma_{\hat{y}^h} &= \frac{\sigma_{a^h_x}\sin(\sigma_{\omega^h_z} t_{pre})}{(\sigma_{\omega^h_z})^2} - \frac{\left(\sigma_{v^h_x} + \sigma_{a^h_x} t_{pre}\right)\cos(\sigma_{\omega^h_z} t_{pre}) - \sigma_{v^h_x}}{\sigma_{\omega^h_z}}. \end{aligned} \tag{4.61}$$

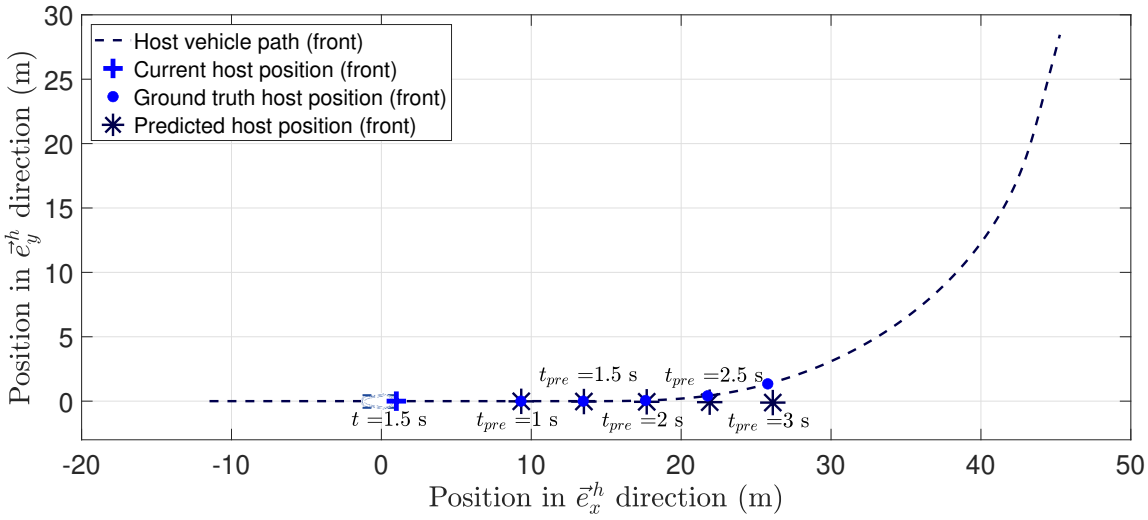

(a) Current yaw rate is zero ($\omega_{z,k}^h = 0$).

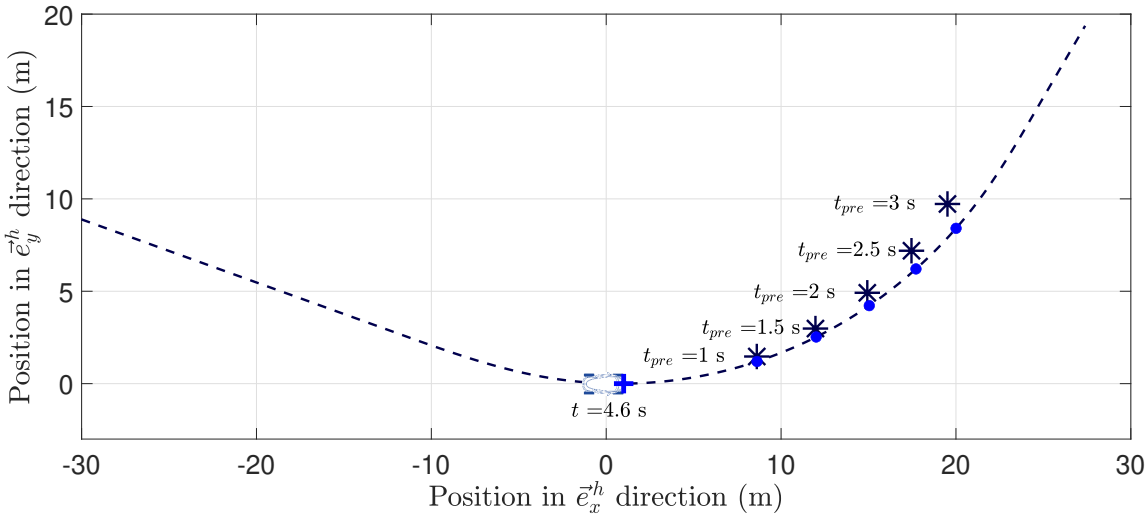

(b) Current yaw rate is nonzero ($\omega_{z,k}^h \neq 0$).

Figure 4.9: The actual path and the predicted path of the host vehicle in the current body-fixed frame for the 'turning away' scenario.

4.6 Summary

In this chapter, the absolute motion of the detected object is estimated from the available sensor measurements using a linear discrete-time Kalman filter. The motion model used in the Kalman filter is the constant acceleration model, which normally describes the relative motion between the host vehicle and the object. However, in this research, the motion model is slightly adapted, since the absolute motion of the object is required. Furthermore, an additional correction step is proposed for the Kalman filter to reduce the state estimation errors when the host vehicle is cornering. Since the radar sensor on the host vehicle has a lower sampling rate than the AEB controller (including the Kalman filter), the state estimates are only updated in case a new measurement becomes available. In between measurements, only the prediction step of the Kalman filter is used to estimate the states. By performing simulations for the most complex driving scenario, the process noise values of the process noise covariance matrix $\mathbf{Q}$ resulting in the lowest cost C are found. For all simulated driving scenarios, the Kalman filter performs well and is able to estimate the states accurately with an acceptable error.

To determine if a detected object is relevant for the AEB system, the paths of both the host vehicle and the object are predicted. The position of the object is predicted by making a n-step a-priori prediction using the last available state estimates from the Kalman filter. The level of uncertainty on the predicted positions of the object is determined from the predicted state estimation covariance. Furthermore, the position of the host vehicle is predicted directly from the available sensor measurements and the level of uncertainty on the predicted positions is determined from the corresponding sensor measurement noise levels.

Chapter 5

AEB controller

Once the predicted paths of the host vehicle and the detected object are known, a possible collision between the host vehicle and the object can be found. After determining if a detected object is relevant and present in the driving path of the host vehicle, the AEB controller uses a risk metric called the Brake-Threat-Number (BTN) to determine if a brake intervention is required, which is a measure of the threat level and indicates the effort that is required to avoid a collision with the object. The BTN is defined as the required acceleration of the host vehicle a^h_{req} needed to avoid a collision divided by the minimal achievable host vehicle acceleration a^h_{min} [33] and is given by

$$\text{BTN} = \frac{a^h_{req}}{a^h_{min}}, \tag{5.1}$$

where a^h_{min} is chosen to be -7 m/s^2 as explained in Section 3.3.3. In practice, the BTN ranges from 0 to 1, since a BTN larger than 1 indicates a collision with the object cannot be avoided by braking the vehicle due to the physical limitations of the brake system.

In this chapter, first a new method is proposed to determine if a detected object is relevant for the AEB system. Thereafter, the method used to determine the required acceleration of the host vehicle will be given. Then, the method used to compensate for the response delay of the brake system will be discussed. Finally, the AEB controller in the form of a state machine will be discussed together with all its states and conditions, and the AEB controller will be tuned to optimize its performance.

5.1 Object relevance

Compared to the existing methods proposed in Section 2.2 used to determine if an object is relevant, in this section a new method is proposed, which uses the predicted positions and the corresponding levels of uncertainty of the host vehicle and the object as determined in the previous chapter. At every time step k, the positions of the host vehicle and the object are predicted for multiple prediction times t_{pre}, which is changed from one to three seconds in steps of a half-second. For every prediction time t_{pre}, uncertainty ellipses are drawn around the corresponding predicted positions of the host vehicle and the object. An elliptic shape is chosen due to the probabilistic uncertainty model. These ellipses indicate where the host vehicle or the object has a large probability to be at time t_{pre} [24]. A possible collision between the host vehicle and the object is found if for a certain prediction time t_{pre} the corresponding uncertainty ellipses intersect.

5.1.1 Uncertainty ellipse detected object

Figure 5.1 shows the uncertainty ellipse around the predicted position of the detected object $(\hat{x}^t_{k+n}, \hat{y}^t_{k+n})$ in the current body-fixed frame. Here, the radius of the major axis is indicated by a^t and the radius of the minor axis is indicated by b^t. Given the levels of uncertainty on the predicted position of the object in standard deviations, the general equation of a standard axis-aligned ellipse centered at the predicted position of the object becomes [56]

$$\left(\frac{x - \hat{x}^t_{k+n}}{\sigma_{\hat{d}^r_x}}\right)^2 + \left(\frac{y - \hat{y}^t_{k+n}}{\sigma_{\hat{d}^r_y}}\right)^2 = s, \tag{5.2}$$

where s indicates the scale of the ellipse. The scale s depends on the desired confidence level and can be obtained using the so called Chi-Square distribution [57], which will not be discussed further. The scale s is set to 9.210, which corresponds with a confidence interval of 99%. This means that the actual position of the object at time t_{pre} lies within the corresponding uncertainty ellipse with 99% certainty. The radii of the uncertainty ellipse can be determined from (5.2) as follows

$$\begin{aligned} a^t &= \sigma_{\hat{d}^r_x}\sqrt{s} \\ b^t &= \sigma_{\hat{d}^r_y}\sqrt{s}. \end{aligned} \tag{5.3}$$

Finally, using the determined radii, the parametric representation of the uncertainty ellipse for the object becomes

$$\begin{aligned} x^t_{ell}(\kappa) &= a^t \cos(\kappa) + \hat{x}^t_{k+n} \\ y^t_{ell}(\kappa) &= b^t \sin(\kappa) + \hat{y}^t_{k+n}, \end{aligned} \tag{5.4}$$

where κ is a linearly spaced vector with points between 0 and 2π.

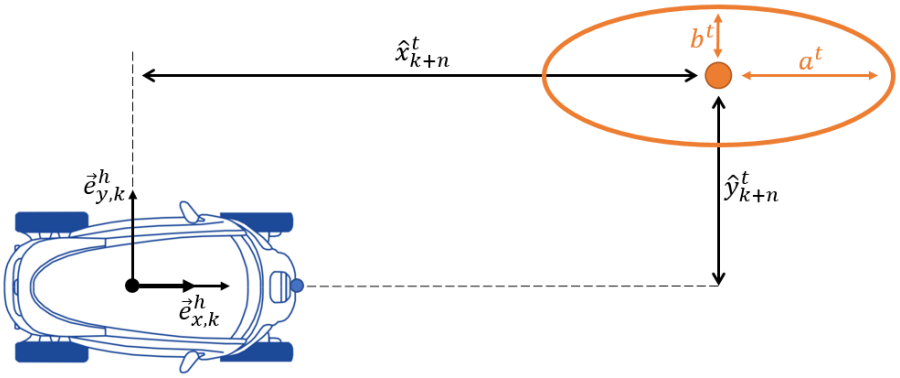

Figure 5.1: Uncertainty ellipse around the predicted position of the detected object in the current body-fixed frame.

5.1.2 Uncertainty ellipse host vehicle

Figure 5.2 shows the uncertainty ellipse around the predicted position of the host vehicle $(\hat{x}^{h,F}_{k+n}, \hat{y}^{h,F}_{k+n})$ in the current body-fixed frame. Here, the radius of the major axis is indicated by a^h and the radius of the minor axis is indicated by b^h. Furthermore, it can be seen that the uncertainty ellipse is rotated over the predicted heading angle $\hat{\theta}^h_{k+n}$. Given the levels of uncertainty on the predicted position of the host vehicle in standard deviations, the equation of a rotated ellipse centered at the predicted position of the host vehicle and rotated over an angle $\hat{\theta}^h_{k+n}$ can be derived from (5.2) and is given by

$$\begin{aligned}&\left(\frac{(x-\hat{x}^{h,F}_{k+n})\cos(\hat{\theta}^h_{k+n})+(y-\hat{y}^{h,F}_{k+n})\sin(\hat{\theta}^h_{k+n})}{\sigma_{\hat{x}^h}}\right)^2+\dots\\ \dots&\left(\frac{(x-\hat{x}^{h,F}_{k+n})\sin(\hat{\theta}^h_{k+n})-(y-\hat{y}^{h,F}_{k+n})\cos(\hat{\theta}^h_{k+n})}{\sigma_{\hat{y}^h}}\right)^2=s.\end{aligned} \tag{5.5}$$

Similar as for the uncertainty ellipse of the object, the scale s for the uncertainty ellipse of the host vehicle is chosen such that the actual position of the host vehicle at time t_{pre} lies within the corresponding uncertainty ellipse with 99% certainty. Furthermore, the width w of the host vehicle is included in the radius of the minor axis b^h such that the uncertainty ellipse of the host vehicle is drawn around the front edges of the host vehicle. The resulting radii of the uncertainty ellipse are given by

$$\begin{aligned}a^h&=\sigma_{\hat{x}^h}\sqrt{s}\\ b^h&=\sigma_{\hat{y}^h}\sqrt{s}+\frac{1}{2}w.\end{aligned} \tag{5.6}$$

Finally, using the determined radii, the parametric representation of the rotated uncertainty ellipse for the host vehicle becomes

$$\begin{aligned}x^h_{ell}(\kappa)&=a^h\cos(\hat{\theta}^h_{k+n})\cos(\kappa)-b^h\sin(\hat{\theta}^h_{k+n})\sin(\kappa)+\hat{x}^{h,F}_{k+n}\\ y^h_{ell}(\kappa)&=a^h\sin(\hat{\theta}^h_{k+n})\cos(\kappa)+b^h\cos(\hat{\theta}^h_{k+n})\sin(\kappa)+\hat{y}^{h,F}_{k+n}.\end{aligned} \tag{5.7}$$

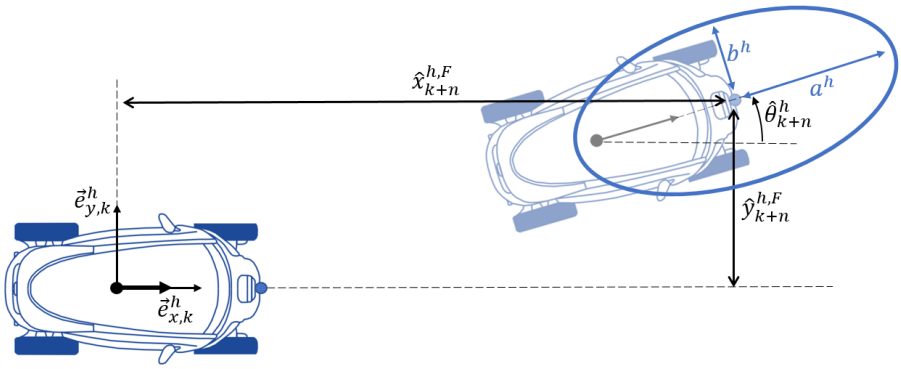

Figure 5.2: Uncertainty ellipse around the predicted position of the host vehicle in the current body-fixed frame.

5.1.3 Collision detection

A possible collision is found if for a certain prediction time t_{pre} the corresponding uncertainty ellipses of the host vehicle and the object intersect. To determine if the uncertainty ellipses intersect, the points representing the rotated uncertainty ellipse of the host vehicle (x^h_{ell}, y^h_{ell}) are inserted in the equation of the uncertainty ellipse of the object. The uncertainty ellipses intersect if for a certain point (x^h_{ell}, y^h_{ell}) the following condition holds

$$\left(\frac{x^h_{ell} - \hat{x}^t_{k+n}}{a^t}\right)^2 + \left(\frac{y^h_{ell} - \hat{y}^t_{k+n}}{b^t}\right)^2 \leq 1. \tag{5.8}$$

Figure 5.3 shows an example of a relevant object, where the uncertainty ellipses of the host vehicle and the object intersect for a certain prediction time t_{pre}. In reality, a collision between the host vehicle and the object will only occur if at time t_{pre} the actual position of the object overlaps with the actual position of the front of the host vehicle. Therefore, to determine the probability of a collision, the probability of both the host vehicle and the object being present within the overlapping area needs to be determined. However, determining this probability is considered to be future work and will not be discussed further. An object is considered to be relevant for the AEB system if the uncertainty ellipses intersect for a certain prediction time t_{pre}. Using this method will increase the number of false positives of the AEB system, since there is a large probability that the actual position of either the host vehicle or the object lies outside the overlapping area as is shown in Figure 5.3, meaning a brake intervention by the AEB system is unnecessary. An object is also considered to be relevant if it is expected to be present right in front of the host vehicle, which is the case if the absolute estimated lateral relative distance is smaller or equal to half of the vehicle width w, described by the following condition

$$|\hat{d}^r_{y,k|k}| \leq \frac{1}{2}w. \tag{5.9}$$

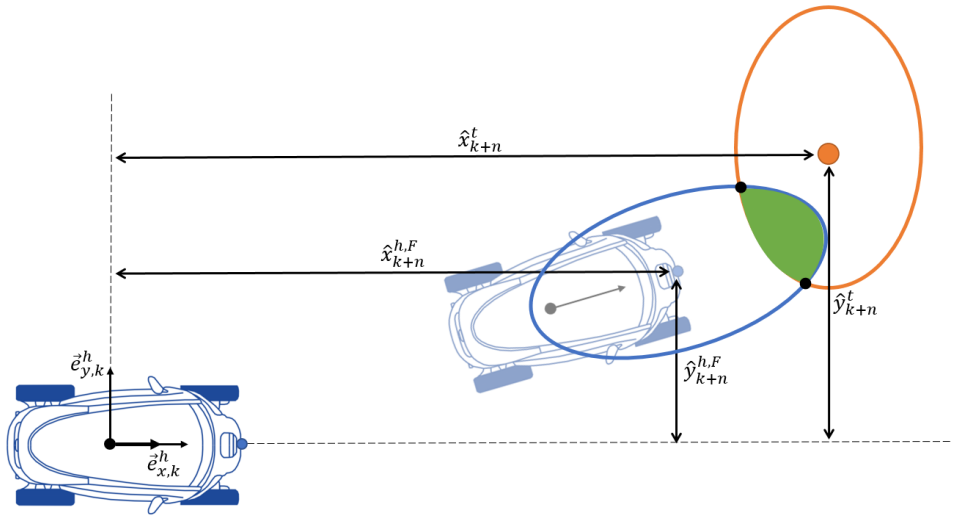

Figure 5.3: Example of a relevant object, where the uncertainty ellipses of the host vehicle and the object intersect.

5.2 Calculation of the required host acceleration

To determine the required acceleration of the host vehicle, two cases are considered in which the detected object is either stationary or moving in the longitudinal direction of the current body-fixed frame $\vec{e}^h_k$. For these cases, the calculation methods of the required host acceleration a^h_{req} are

slightly different [33], which will both be discussed in the remainder of this section. Note that the object is not moving in the longitudinal direction of the current body-fixed frame in every driving scenario. For example in the 'turning away' scenario, the object will also move in the lateral direction of the current body-fixed frame once the host vehicle is turning away from the object. However, this issue is solved when using the method proposed in the previous section to determine if the object is relevant. If the host vehicle turns away from the object, a brake intervention will not be initiated by the AEB system, since the object is not considered to be relevant anymore.

5.2.1 Required host acceleration with a stationary detected object

In the first case, the detected object is either standing still or moving initially and coming to a standstill before the host vehicle comes to a standstill. To derive the required host acceleration, it is assumed that the longitudinal acceleration of both the host vehicle a_x^h and the object a_x^t are constant. Given the current longitudinal position, velocity and acceleration of both the host vehicle and the object as shown in Figure 5.4, the longitudinal position of the host vehicle and the object along their path at time t is given by

$$\begin{aligned} d_x^h(t) &= d_x^h(0) + v_x^h(0)t + \frac{1}{2}a_x^h(0)t^2 \\ d_x^t(t) &= d_x^t(0) + v_x^t(0)t + \frac{1}{2}a_x^t(0)t^2, \end{aligned} \tag{5.10}$$

and the longitudinal velocity of the host vehicle and the object at time t is given by

$$\begin{aligned} v_x^h(t) &= v_x^h(0) + a_x^h(0)t \\ v_x^t(t) &= v_x^t(0) + a_x^t(0)t, \end{aligned} \tag{5.11}$$

where the current states of the host vehicle and the object are taken at $t = 0$.

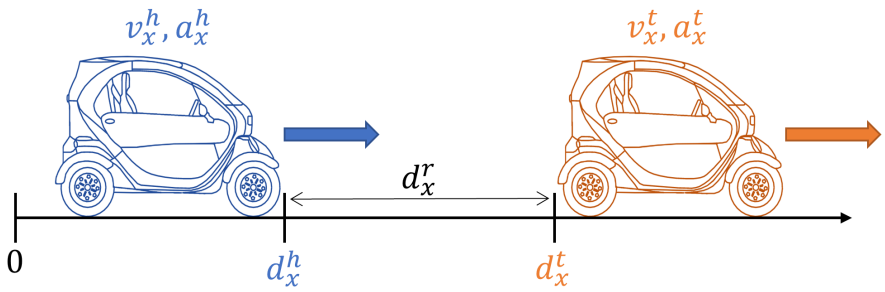

Figure 5.4: Longitudinal motion of the host vehicle and the detected object.

From (5.10) and (5.11), the required acceleration of the host vehicle a_{req}^h can be determined as follows [33]

$$a_{req}^h = -\frac{1}{2}\frac{{v_x^h}^2(0)}{d_x^r(0) + d_{stop}^t}, \tag{5.12}$$

where d_{stop}^t is the stopping distance of the object, which is given by

$$d_{stop}^t = -\frac{1}{2}\frac{{v_x^t}^2(0)}{a_x^t(0)}. \tag{5.13}$$

The full derivations of the required host acceleration a_{req}^h for the first case and the stopping distance d_{stop}^t are given in Appendix C.1.

5.2.2 Required host acceleration with a moving detected object

In the second case, the detected object is moving and the host vehicle needs to brake until its velocity is equal to the velocity of the object. The relative longitudinal distance between the host vehicle and the object at time t can be derived from (5.10) as follows

$$\begin{aligned} d_x^r(t) &= \left(d_x^t(0) - d_x^h(0)\right) + \left(v_x^t(0) - v_x^h(0)\right) t + \frac{1}{2}\left(a_x^t(0) - a_x^h(0)\right) t^2 \\ &= d_x^r(0) + v_x^r(0)t + \frac{1}{2} a_x^r(0) t^2. \end{aligned} \tag{5.14}$$

Furthermore, the relative longitudinal velocity between the host vehicle and the object at time t can be derived from (5.11) as follows

$$\begin{aligned} v_x^r(t) &= \left(v_x^t(0) - v_x^h(0)\right) + \left(a_x^t(0) - a_x^h(0)\right) t \\ &= v_x^r(0) + a_x^r(0) t. \end{aligned} \tag{5.15}$$

In this second case, a collision between the host vehicle and the object is avoided when their velocities are equal at a time instant called Time-to-Touch (t_{TTT}) [33]. Solving (5.14) for the Time-to-Touch gives the required acceleration of the host vehicle a_{req}^h

$$a_{req}^h = a_x^t(0) - \frac{\left(v_x^t(0) - v_x^h(0)\right)^2}{2 d_x^r(0)}. \tag{5.16}$$

The full derivations of the required host acceleration a_{req}^h for the second case and the Time-to-Touch t_{TTT} are given in Appendix C.2. The second case holds if the velocity of the object at the Time-to-Touch is positive ($v_x^t(t_{TTT}) > 0$). Otherwise, the first case holds and the required acceleration of the host vehicle a_{req}^h is calculated using (5.12).

5.3 Compensation for the brake response delay

Instead of using the current motions of the host vehicle and the detected object to determine the required host acceleration a_{req}^h and the BTN, the motions are predicted into the future over the brake response delay τ_b. When using these predicted motions, a brake intervention by the AEB system can be initiated earlier to compensate for the response delay of the brake system. The method used to determine the brake response delay τ_b of the modelled brake system is discussed in Section 3.3.3, where Figure 3.7 shows the response delay of the brake system τ_b as a function of the camshaft angle δ_c of the brake cam actuator. In this figure it can be seen that the response delay decreases non-linearly for an increasing camshaft angle.

As discussed in the previous chapter, the states describing the motion of the host vehicle and the detected object are uncertain. When predicting these states into the future over the time spanned by the brake response delay τ_b the uncertainty of the predicted states will grow. Therefore, using the predicted states to calculate the required host acceleration and the BTN will also affect their uncertainty.

In the remainder of this section the methods used to predict the motions of the detected object and the host vehicle will be discussed. Furthermore, the method used to determine required host acceleration and the BTN from the predicted motions will be discussed.

5.3.1 Predicted motion of the detected object

To determine the required host acceleration a_{req}^h using (5.12) or (5.16), several states describing the longitudinal motion of the detected object need to be predicted, which are the longitudinal relative distance d_x^r, the longitudinal velocity v_x^t and the longitudinal acceleration a_x^t. The method

used to predict the motion of the detected object over the time spanned by the brake response delay is almost similar to the method used to predict the path of the object as discussed in Section 4.4. However, in contrast to the method used to predict the path of the object, now the longitudinal relative distance d_x^r instead of the longitudinal position of the detected object should be predicted in the current body-fixed frame $\vec{e}_k^h$, which means also the motion of the host vehicle should be taken into account.

At every current time step k, the motion of the object is predicted in the current body-fixed frame as is shown in Figure 4.6. The states describing the motion of the object are included in the state vector $\underline{\mathrm{x}}_k$ given in (4.6). The motion of the object is predicted over the time horizon $[k, k+n_b]$, where n_b is the prediction horizon in samples. The prediction horizon n_b can be obtained from the brake response delay τ_b as follows

$$n_b = \frac{\tau_b}{T_s}, \tag{5.17}$$

which is rounded to the nearest integer. Again, the motion of the object is predicted by making a n-step a-priori prediction, resulting in the predicted state estimate $\underline{\hat{\mathrm{x}}}_{k+n_b|k}$ [17][22]. The constant acceleration model is used to predict the motion of the object, where it is assumed that the object has uncorrelated motions in both the longitudinal and the lateral direction of the current body-fixed frame. Besides, the longitudinal and lateral acceleration of the object as well as the longitudinal acceleration of the host vehicle are assumed to be constant during the time horizon $[k, k+n_b]$, which introduces some model uncertainty since the acceleration of the object or the host vehicle could change during this time horizon. Using (4.50), the predicted state estimate can be obtained as follows

$$\begin{aligned}
\underline{\hat{\mathrm{x}}}_{k+n_b|k} &= \mathbf{A}^{n_b}\underline{\hat{\mathrm{x}}}_{k|k} + \sum_{m=1}^{n_b}\mathbf{A}^{m-1}\mathbf{B}\underline{\mathrm{u}}_k \\
\begin{bmatrix} \hat{d}^r_{x,k+n_b|k} \\ \hat{v}^t_{x,k+n_b|k} \\ \hat{a}^t_{x,k+n_b|k} \\ \hat{d}^r_{y,k+n_b|k} \\ \hat{v}^t_{y,k+n_b|k} \\ \hat{a}^t_{y,k+n_b|k} \end{bmatrix} &= \begin{bmatrix} 1 & T_s & \frac{T_s^2}{2} & 0 & 0 & 0 \\ 0 & 1 & T_s & 0 & 0 & 0 \\ 0 & 0 & 1 & 0 & 0 & 0 \\ 0 & 0 & 0 & 1 & T_s & \frac{T_s^2}{2} \\ 0 & 0 & 0 & 0 & 1 & T_s \\ 0 & 0 & 0 & 0 & 0 & 1 \end{bmatrix}^{n_b} \begin{bmatrix} \hat{d}^r_{x,k|k} \\ \hat{v}^t_{x,k|k} \\ \hat{a}^t_{x,k|k} \\ \hat{d}^r_{y,k|k} \\ \hat{v}^t_{y,k|k} \\ \hat{a}^t_{y,k|k} \end{bmatrix} \\
&\quad + \sum_{m=1}^{n_b} \begin{bmatrix} 1 & T_s & \frac{T_s^2}{2} & 0 & 0 & 0 \\ 0 & 1 & T_s & 0 & 0 & 0 \\ 0 & 0 & 1 & 0 & 0 & 0 \\ 0 & 0 & 0 & 1 & T_s & \frac{T_s^2}{2} \\ 0 & 0 & 0 & 0 & 1 & T_s \\ 0 & 0 & 0 & 0 & 0 & 1 \end{bmatrix}^{m-1} \begin{bmatrix} -T_s & -\frac{T_s^2}{2} \\ 0 & 0 \\ 0 & 0 \\ 0 & 0 \\ 0 & 0 \\ 0 & 0 \end{bmatrix} \begin{bmatrix} v^h_{x,k} \\ a^h_{x,k} \end{bmatrix}.
\end{aligned} \tag{5.18}$$

Note that in contrast to the predicted state estimate used for the path prediction given in (4.51), now also the longitudinal motion of the host vehicle included in the input vector u_k is predicted in (5.18). Therefore, in contrast to the predicted state estimate given in (4.51), $\hat{d}^r_{x,k+n_b|k}$ now indicates the predicted longitudinal relative distance between the host vehicle and the object.

5.3.2 Predicted motion of the host vehicle

In addition to the states describing the motion of the detected object, also the longitudinal velocity of the host vehicle v_x^h needs to be predicted to determine the required host acceleration a^h_{req} using (5.12) or (5.16). In contrast to the predicted motion of the object, which is obtained by making a n-step a-priori prediction using the state estimates from the Kalman filter, the

longitudinal velocity of the host vehicle is predicted directly from the (virtual) sensor measurements of the longitudinal velocity $v^h_{x,k}$ and the longitudinal acceleration $a^h_{x,k}$. When assuming that the longitudinal acceleration of the host vehicle remains constant over the time spanned by the brake response delay τ_b, the predicted longitudinal velocity of the host vehicle can be obtained from the sensor measurements as follows

$$\hat{v}^h_{x,k+n_b} = v^h_{x,k} + \tau_b a^h_{x,k}, \tag{5.19}$$

which introduces some model uncertainty since the longitudinal acceleration of the host vehicle could change during this time period.

5.3.3 Required host acceleration using the predicted motions

For a stationary object, the required acceleration of the host vehicle in discrete-time can be determined by substituting the predicted states of the object and the host vehicle into (5.12) as follows

$$a^h_{req,k} = -\frac{1}{2}\frac{\hat{v}^{h^2}_{x,k+n_b}}{\hat{d}^r_{x,k+n_b|k} + d^t_{stop,k}}, \tag{5.20}$$

where the stopping distance of the object $d^t_{stop,k}$ can be obtained as follows

$$d^t_{stop,k} = -\frac{1}{2}\frac{\hat{v}^{t^2}_{x,k+n_b|k}}{\hat{a}^t_{x,k+n_b|k}}. \tag{5.21}$$

For a moving object, the required acceleration of the host vehicle in discrete-time can be determined by substituting the predicted states of the object and the host vehicle into (5.16) as follows

$$a^h_{req,k} = \hat{a}^t_{x,k+n_b|k} - \frac{\left(\hat{v}^t_{x,k+n_b|k} - \hat{v}^h_{x,k+n_b}\right)^2}{2\hat{d}^r_{x,k+n_b|k}}. \tag{5.22}$$

For both cases, an arbitrary number functioning as a constant safety margin is subtracted from the predicted relative distance $\hat{d}^r_{x,k+n_b|k}$ before determining the required host acceleration. This is done to ensure that the host vehicle comes to a standstill at a fixed distance from the object.

The Brake-Threat-Number (BTN) can now be obtained by substituting the required host acceleration $a^h_{req,k}$ into (5.1). Since the predicted states are uncertain, using them to calculate the required host acceleration $a^h_{req,k}$ and consecutively the BTN will also affect their uncertainty. By using the levels of uncertainty on the predicted states, a certain range in which the actual BTN lies can be determined. However, the BTN used by the AEB controller is obtained directly from the predicted states. Therefore, determining the range in which the actual BTN lies is considered as future work.

5.4 AEB controller design

Depending on the threat level of the current traffic situation, indicated by the BTN, the AEB controller determines if a brake intervention is required. The value of the BTN determines if the AEB system should be activated or deactivated and in which operating mode the AEB system should operate. The AEB system can operate in four different operating modes, as is shown in Figure 5.5. For each operating mode the required brake acceleration $a_{b,req}$ differs, which is the output of the AEB controller and is used by the brake cam actuator controller, as explained in Section 3.3.2. Next, the operating modes of the AEB system will be discussed together with the conditions that must hold to activate or deactivate the AEB system.

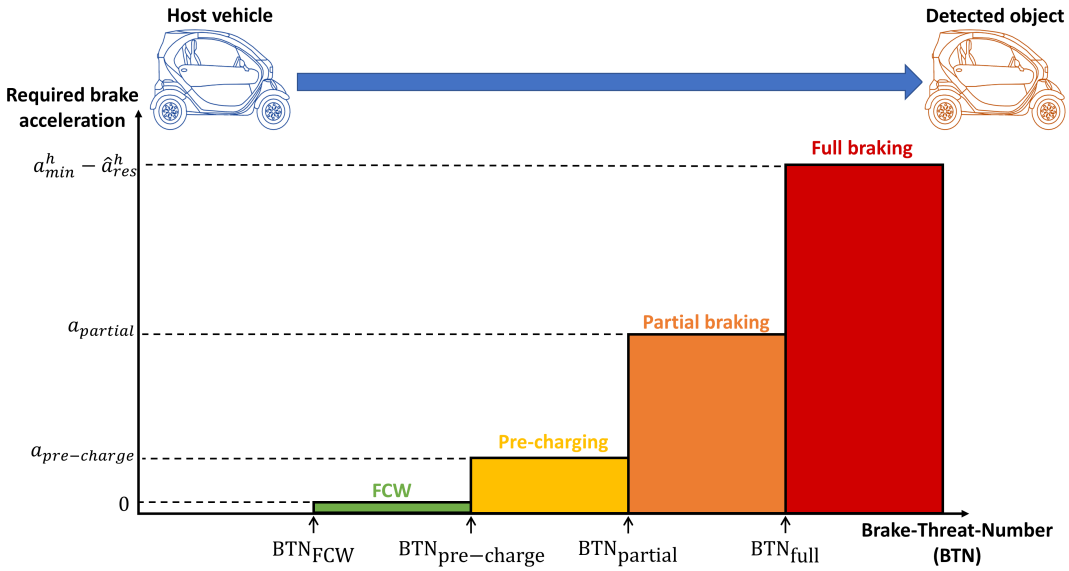

Figure 5.5: Operating modes of the AEB system.

5.4.1 Operating modes

In the first operating mode, a Forward Collision Warning (FCW) is given, which is an audio-visual warning to alert the driver for a likely collision [49]. If the FCW is given soon enough, the driver can possibly avoid the collision by himself. However, the warning should not be given too early in order to avoid the system from issuing a warning in non-critical situations, which could lower the credibility of the AEB system [6]. To activate the AEB system and in this way the first operating mode, the following conditions must hold:

- The current BTN value is larger than the value of the BTN threshold parameter BTN_{FCW}.
- The object is considered to be relevant using the method discussed in the previous chapter.
- The current longitudinal velocity of the host vehicle $v^h_{x,k}$ is larger than a predefined minimal required velocity v^h_{xmin} to prevent the AEB system from being activated when for example parking the vehicle.

The values of the parameters used by the AEB controller and described in this section are chosen by performing simulations and will therefore not be discussed further in this research. The chosen values of these parameters will be given in the following section.

Next, in the second operating mode, the vehicle brakes are being pre-charged to decrease the response delay of the brake system, as given in Figure 3.7. In this way, a subsequent brake intervention by the AEB system or driver can be carried out more quickly [6]. This operating mode is activated once the current BTN value exceeds the value of the BTN threshold parameter $\text{BTN}_{\text{pre-charge}}$. In this operating mode, the required brake acceleration $a_{b,req}$ is set equal to a small predefined acceleration $a_{pre-charge}$ and a signal is sent to the cruise controller of the host vehicle to stop accelerating the vehicle. For example, a small acceleration of 0.5 m/s^2 already increases the camshaft angle significantly to a value of 1.75 rad. Now, when looking at Figure 3.7, the response delay of the brake system τ_b is given as a function of the camshaft angle δ_c. Here, it can be seen that a camshaft angle of 1.75 rad makes the response delay of the brake system decrease by approximately 0.2 s and therefore a subsequent brake intervention can be carried out quicker.

Then, if the driver does not notice the FCW, and the BTN value increases further, the third operating mode of the AEB system is initiated in which the vehicle is partially braked. In this way a haptic warning is given to the driver and the velocity of the host vehicle reduces slightly [6]. This operating mode is activated once the current BTN value exceeds the value of the BTN threshold parameter $\text{BTN}_{\text{partial}}$. Furthermore, in this operating mode the required brake acceleration $a_{b,req}$ is set equal to the predefined acceleration $a_{partial}$.

Finally, in case the driver still shows no (sufficient) response to avoid a collision with the detected object, the last operating mode is activated in which a full brake intervention is initiated. This operating mode is activated once the current BTN value exceeds the value of the BTN threshold parameter BTN_{full}. In this operating mode, the required brake acceleration $a_{b,req}$ can be determined using the minimal achievable acceleration of the host vehicle a^h_{min} as follows

$$a_{b,req} = a^h_{min} - \hat{a}^h_{res}, \tag{5.23}$$

where $\hat{a}^h_{res}$ is the estimated acceleration from resistant forces, which can be obtained as follows

$$\hat{a}^h_{res} = \frac{\hat{F}^h_{res}}{m_{eff}} \tag{5.24}$$

where $\hat{F}^h_{res}$ is the estimated longitudinal resistant force acting on the host vehicle, which can be obtained by using the predicted longitudinal velocity of the host vehicle $\hat{v}^h_{x,k+n_b}$ and substituting it into (3.24).

To deactivate the AEB system, one of the following conditions must be satisfied:

- The current BTN value is smaller than the value of the BTN threshold parameter $\text{BTN}_{\text{deactivate}}$.
- The object is not considered to be relevant anymore and a full brake intervention has not been initiated yet.
- The host vehicle comes to a standstill.
- The longitudinal velocity of the detected object is larger than the longitudinal velocity of the host vehicle.

The conditions mentioned above to activate or deactivate the AEB system should hold for a specified number of consecutive samples to prevent undesired activations or deactivations.

5.4.2 Tuning of the AEB controller

The performance of the AEB system is influenced by the parameters used by the AEB controller as defined in the previous section. The chosen values of these parameters are summarised in Table 5.1. Here, it can be seen that the BTN threshold parameter BTN_{FCW}, which determines the BTN value at which the AEB system is activated, is set to 0.5. In previous research, a traffic situation is considered critical when the BTN is larger than or equal to 0.5, which indicates a medium to high threat [33]. The BTN threshold parameters $\text{BTN}_{\text{pre-charge}}$ and $\text{BTN}_{\text{partial}}$ should lie somewhere between 0.5 and 1, since a BTN larger than 1 means a collision with the object cannot be avoided. The values of these parameters are chosen by performing simulations, where $\text{BTN}_{\text{pre-charge}}$ is set to 0.65 and $\text{BTN}_{\text{partial}}$ is set to 0.8. Finally, the value of the acceleration in partial braking mode $a_{partial}$ is set to -3 m/s^2, which gives other road users the possibility to react in time and allows the use of the regenerative braking system of the Renault Twizy.

The value of the BTN threshold parameter BTN_{full} is tuned to optimize the performance of the AEB system. The driving scenario used to tune this parameter is the AEB Vulnerable Road User (VRU) scenario, since in this scenario the detected object does not move in the longitudinal direction of the current body-fixed frame $\vec{e}^h_k$. Two criteria will be considered in order to tune the parameter BTN_{full}, being

1. The distance between the host vehicle and the detected object should be at least 0.5 m.
2. A full brake intervention by the AEB system should be initiated as late as possible.

Here, the safety distance d_{safe} is used as a measure of the first criterion, which is defined as the ground truth relative distance $d_x^{r,gt}$ at the moment the host vehicle comes to a standstill. Setting the BTN threshold parameter BTN_{full} to a value around 1 should in theory result in a safety distance d_{safe} around 0.5 m, since a constant safety margin of 0.5 m is subtracted from the predicted relative distance before the required host acceleration and the BTN are determined. However, due to the various uncertainties and assumptions introduced throughout this research, this is not exactly the case and the parameter BTN_{full} needs to be tuned to ensure a safety distance d_{safe} of at least 0.5 m. Determining the effects of all uncertainties on d_{safe} is considered as future work.

The distance d_{full} is used as a measure of the second criterion, which is defined as the ground truth relative distance $d_x^{r,gt}$ at the moment a full brake intervention is initiated. Intuitively, a larger value of the parameter BTN_{full} will result in a later initiation of a full brake intervention of the AEB system and thus resulting in a smaller distance d_{full}. Therefore, the optimal value of the parameter BTN_{full} is the largest possible value which still results in a safety distance d_{safe} of at least 0.5 m.

Table 5.1: AEB controller parameters

Parameter	Value	Description	Unit
$a_{partial}$	-3	Acceleration for partial braking	m/s^2
$a_{pre-charge}$	-0.5	Acceleration for pre-charging	m/s^2
$\text{BTN}_{\text{deactivate}}$	0.2	BTN threshold for deactivation	-
BTN_{FCW}	0.5	BTN threshold for FCW activation	-
$\text{BTN}_{\text{partial}}$	0.8	BTN threshold for partial braking activation	-
$\text{BTN}_{\text{pre-charge}}$	0.65	BTN threshold for pre-charging activation	-

Since the value of the parameter BTN_{full} should lie somewhere around 1, the parameter is changed from 0.95 to 1 in steps of 0.01. For every value of BTN_{full}, 100 simulations are performed with different and incoherent noise seeds for the used virtual sensor measurements. The same noise seeds are used for the simulations of every value of BTN_{full}. The optimal value of the parameter BTN_{full} is the largest possible value resulting in a worst-case safety distance $WC_{d_{safe}}$ of at least 0.5 m. The worst-case safety distance is given by

$$WC_{d_{safe}} = \mu_{d_{safe}} - 3\sigma_{d_{safe}}, \tag{5.25}$$

where $\mu_{d_{safe}}$ is the mean of the safety distance and $\sigma_{d_{safe}}$ is the standard deviation of the safety distance, which is multiplied by 3 to ensure that the actual safety distance is larger or equal to the worst-case safety distance $WC_{d_{safe}}$ with 99.7% certainty. Given a set of simulation results for a certain value of BTN_{full}, the mean of the safety distance is given by

$$\mu_{d_{safe}} = \frac{\sum_{i=1}^{N} d_{safe}(i)}{N}, \tag{5.26}$$

where N is the total number of simulations, being equal to 100. Furthermore, the standard deviation of the safety distance is given by

$$\sigma_{d_{safe}} = \sqrt{\frac{1}{N}\sum_{i=1}^{N}\left(d_{safe}(i) - \mu_{d_{safe}}\right)^2}. \tag{5.27}$$

Figure 5.6 shows the simulation results of the criteria used to tune the AEB controller. Here, Figure 5.6a shows the distance d_{safe} as a function of the BTN threshold parameter BTN_{full},

where it can be seen that 0.99 is the largest possible value of BTN_{full} resulting in a worst-case safety distance $WC_{d_{safe}}$ of at least 0.5 m. Furthermore, Figure 5.6b shows the distance d_{full} as a function of BTN_{full}, which as expected shows a larger value of BTN_{full} results in a smaller distance d_{full} and thus a later initiation of a full brake intervention by the AEB system. Therefore, the optimal value of the parameter BTN_{full} used in the remainder of this research is 0.99.

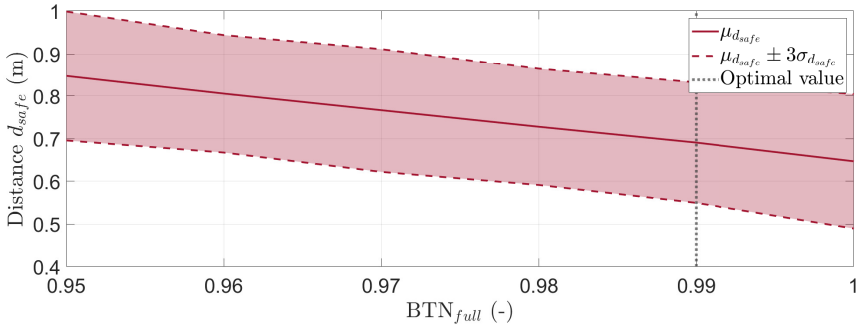

(a) The distance d_{safe} as a function of the BTN threshold parameter BTN_{full}.

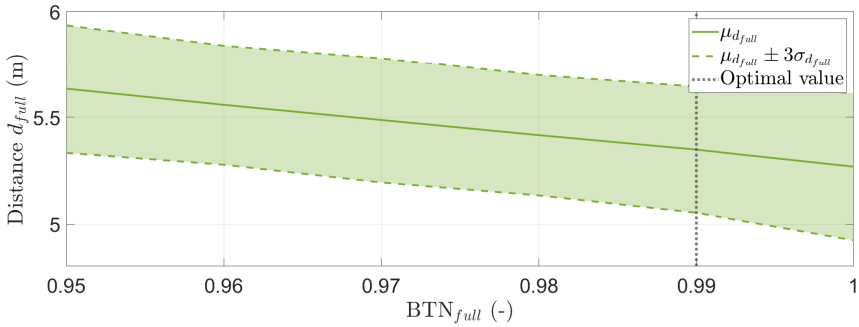

(b) The distance d_{full} as a function of the BTN threshold parameter BTN_{full}.

Figure 5.6: Simulation results of the criteria used to tune the AEB controller.

5.5 Summary

A new method is proposed to determine if an object is relevant, which uses the predicted positions and the corresponding levels of uncertainty to draw uncertainty ellipses around the predicted positions of the host vehicle and the object. A possible collision between the host vehicle and the object is found if for a certain prediction time t_{pre} the corresponding uncertainty ellipses intersect.

To determine if a brake intervention is needed to avoid a collision with a detected object, the AEB controller uses a parameter called the Brake-Threat-Number (BTN), which is a measure of the threat level and indicates the effort that is required to avoid a collision with the object. The BTN is defined as the required host acceleration to avoid a collision divided by the minimal achievable host acceleration. Two cases are considered to determine the required host acceleration, in which the detected object is either stationary or moving in the longitudinal direction of the current body-fixed frame. To compensate for the response delay of the brake system, the threat level is determined using the predicted future motions of the host vehicle and the object, which are predicted over the time spanned by the brake response delay τ_b. When activated, the AEB system can operate in four different operating modes, being Forward Collision Warning (FCW), pre-charging of the brakes, partial braking and full braking.

Chapter 6

Simulation of the AEB system

In this chapter the performance of the AEB system will be evaluated via simulations for different driving scenarios. The simulation results presented in this chapter are based on the vehicles, simulation framework and driving scenarios discussed in Chapter 3. The noise levels of the virtual sensor measurements are set equal to the noise levels given in Table 3.2. Here, to reduce the noise level of the measured longitudinal velocity v_x^h and acceleration a_x^h, they are first filtered using a first-order low-pass filter with a time constant of 0.1 s before being used by the various components of the AEB system. By using this low-pass filter, the noise levels on the longitudinal velocity v_x^h and acceleration a_x^h are reduced significantly with a relatively small phase lag (time delay). Therefore, the effect of the low-pass filter on the state estimates of the Kalman filter is small and will be ignored. The parameters of the AEB controller used to obtain the simulation results presented in this chapter are given in Table 5.1 and the BTN threshold parameter BTN_{full} is set equal to the tuned value found in Section 5.4.2. In the remainder of this chapter first the simulation results of the closed-loop tests performed for different driving scenarios will be discussed together with the performance of the AEB system for these scenarios. Thereafter, the results of the open-loop tests performed with the Renault Twizy using real sensor measurements will be discussed.

6.1 Closed-loop testing using simulations

In this section the simulation results of the closed-loop tests performed for three different driving scenarios will be discussed together with the performance of the AEB system for these scenarios. The tested driving scenarios are the AEB Vulnerable Road User (VRU) scenario, the Car-to-Car Rear moving (CCRm) scenario and the Turning away scenario, which are all discussed in Section 3.5. The tests are called closed-loop since the required brake acceleration $a_{b,req}$ as determined by the AEB controller is fed back to the modelled brake system of the host vehicle.

6.1.1 AEB Vulnerable Road User (VRU) scenario

In the AEB VRU scenario, the host vehicle is driving straight with a constant velocity and a pedestrian or bicyclist crosses its path from the right side with a constant velocity. Since the detected object is not present right in front of the host vehicle, determining if the object is relevant is of great importance for this scenario. A brake intervention should only be initiated if the object is considered to be relevant for the AEB system, meaning a possible collision between the host vehicle and the object is found.

Figure 6.1 shows the predicted paths of the object at different times, where Figure 6.1a shows the predicted paths of the object together with the corresponding ground truth positions of the host vehicle. In general, the longitudinal error between the predicted paths and the actual object path

is small compared to the longitudinal relative distance between the host vehicle and the object. In Figure 6.1b a close up of the predicted paths is given, where it can be seen that for most of the predicted paths the maximal absolute longitudinal error between the predicted path and the actual object path is smaller than 1 m.

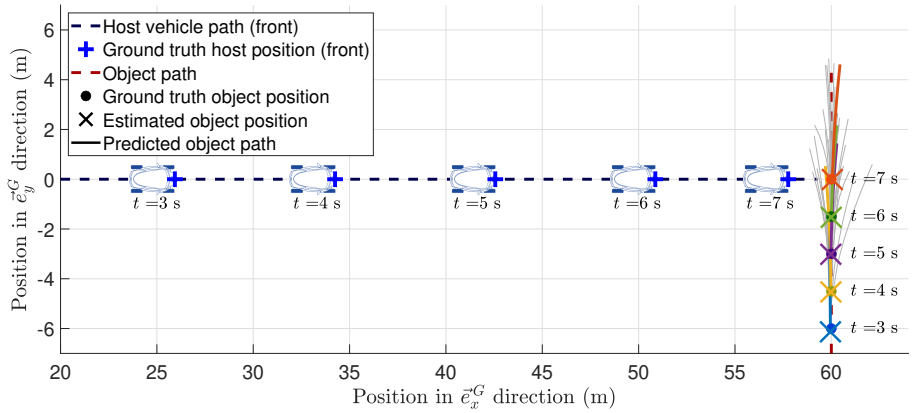

(a) Predicted paths together with the ground truth positions of the host vehicle.

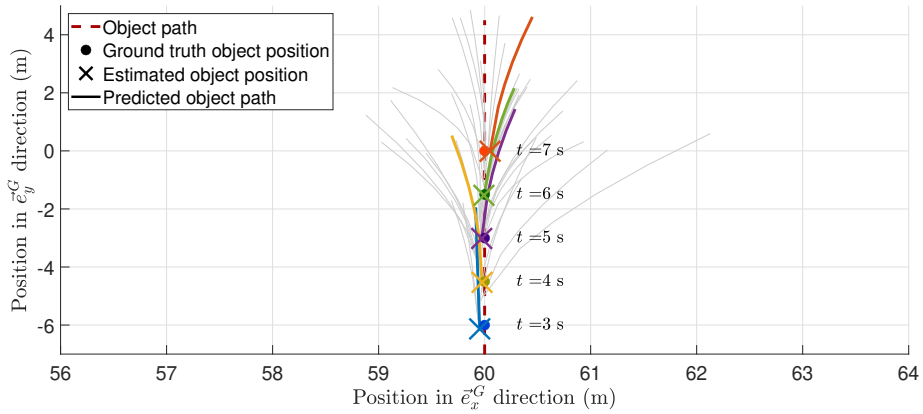

(b) Close up of the predicted paths.

Figure 6.1: Predicted paths of the detected object at different times for the third driving scenario AEB VRU.

Figure 6.2 shows the predicted positions of the host vehicle and the object together with the corresponding uncertainty ellipses at different times. Here, Figure 6.2a shows the object is not considered to be relevant for the AEB system at $t = 3$ s, since none of the uncertainty ellipses of the host vehicle and the object intersect at a certain prediction time t_{pre}. However, as shown in Figure 6.2b, the object is considered to be relevant at $t = 4$ s, since the uncertainty ellipses intersect at a prediction time t_{pre} of 3 s. Here, it can be seen clearly that the error between the predicted object position and the ground truth object position grows as the prediction time t_{pre} becomes larger, which makes sense since the level of uncertainty on the predicted position also grows as t_{pre} becomes larger. At $t = 5.5$ s, the object is still considered to be relevant as is shown in Figure 6.2c, since the uncertainty ellipses intersect at a prediction time t_{pre} of 1.5 s. At this moment the AEB system is activated and a brake intervention by the AEB system is required to prevent a collision, which will be discussed next.

The simulation results of the AEB VRU scenario are shown in Figure 6.3, where the four operating modes of the AEB system are indicated by the coloured areas. The simulation results include the predicted and ground truth longitudinal relative distance in Figure 6.3a. Furthermore, the predicted and ground truth longitudinal host velocity and the predicted and ground truth absolute longitudinal velocity of the object are shown in Figure 6.3b. Then, Figure 6.3c shows the ground truth longitudinal host acceleration and the predicted and ground truth absolute longitudinal acceleration of the object. Besides, the required brake acceleration $a_{b,req}$ is also shown in Figure 6.3c. All predicted and ground truth signals are given in the current body-fixed frame $\vec{e}_k^{\,h}$. Finally, the Brake-Threat-Number (BTN) together with the brake response delay τ_b are shown in Figure 6.3d. Furthermore, Figure 6.3d also shows if the object is present in the field of view of the radar sensor and if the object is considered to be relevant for the AEB system.

Figure 6.3 shows the BTN rises from zero once the object enters the field of view of the radar sensor. The BTN rises as the longitudinal relative distance decreases and the host vehicle approaches the detected object. Once the BTN exceeds the value of the BTN threshold parameter $\mathrm{BTN}_{\mathrm{FCW}}$, the Forward Collision Warning (FCW) is initiated. Thereafter, once the BTN exceeds the value of the BTN threshold parameter $\mathrm{BTN}_{\text{pre-charge}}$, the brakes are being pre-charged, resulting in a small acceleration of the host vehicle as is shown in Figure 6.3c and a reduction of the brake response delay τ_b as is desired, which is shown in Figure 6.3d. Then, once the BTN exceeds the value of the BTN threshold parameter $\mathrm{BTN}_{\mathrm{partial}}$, the host vehicle is being partially braked, resulting in an acceleration of approximately -3 $\mathrm{m/s^2}$. Finally, once the BTN exceeds the value of the BTN threshold parameter $\mathrm{BTN}_{\mathrm{full}}$, full braking is initiated. The sudden drop of the BTN at the start of this operating mode is caused by the large reduction of the brake response delay τ_b once a full brake intervention is initiated. Since the value of the brake response delay determines the time horizon over which the motions of the host vehicle and the detected object used to calculate the BTN are predicted, the reduction of the brake response delay causes a sudden rise in the predicted motions as is shown in Figures 6.3a and 6.3b, and consecutively a sudden drop of the BTN. As the host vehicle is being fully braked and its velocity decreases to zero, the BTN also decreases and drops to zero once the object leaves the field of view of the radar sensor. Finally, the AEB system is deactivated once the host vehicle comes to a standstill, which it does at a desired distance of at least 0.5 m from the object.

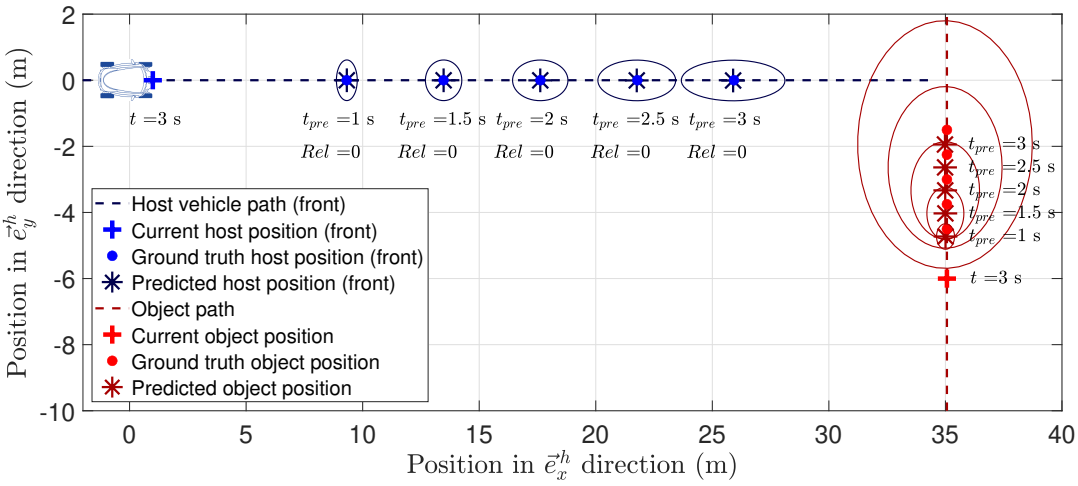

(a) At t = 3 s, the object is not considered to be relevant.

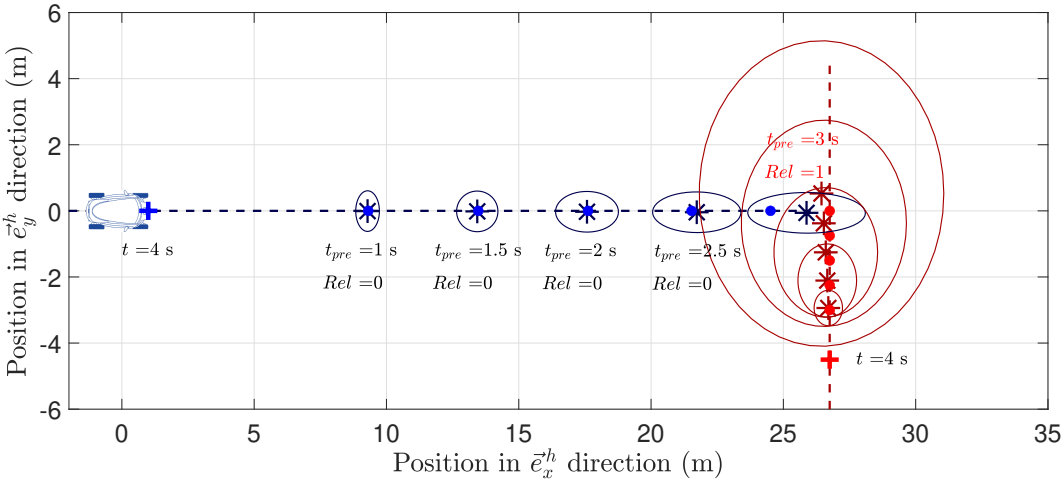

(b) At t = 4 s, the object is considered to be relevant.

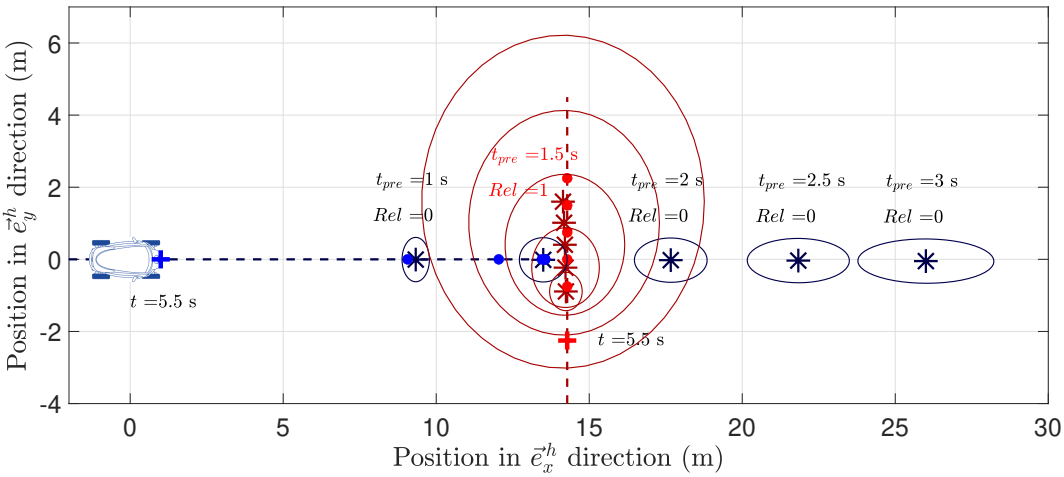

(c) At t = 5.5 s, the object is considered to be relevant and the AEB system is activated.

Figure 6.2: Predicted positions of the host vehicle and the detected object together with the corresponding uncertainty ellipses at different times for the third driving scenario AEB VRU.

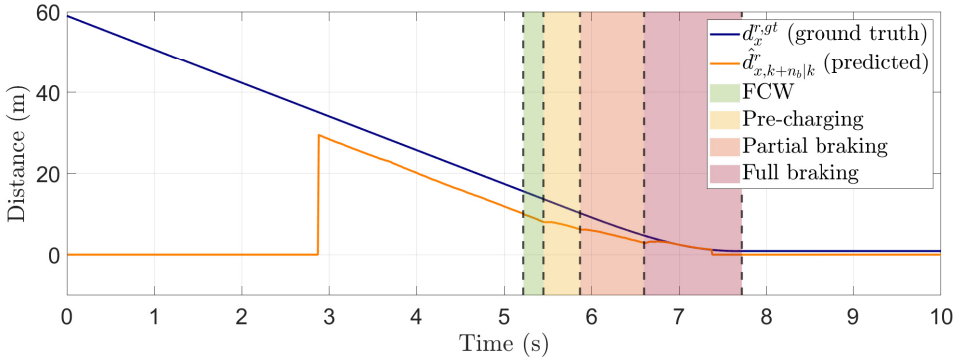

(a) Longitudinal relative distance.

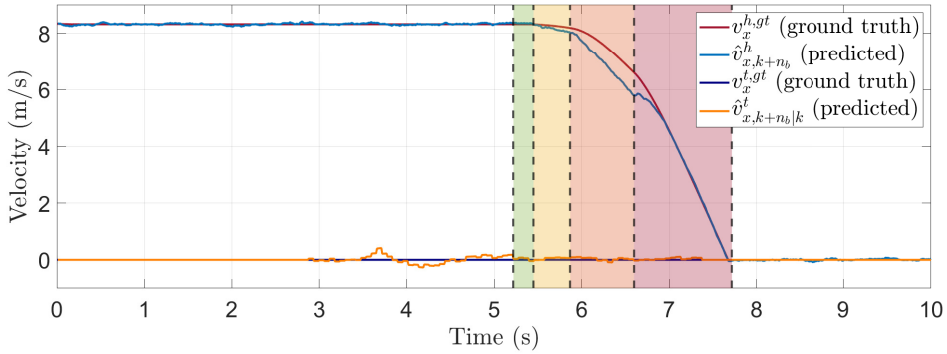

(b) Longitudinal host velocity and longitudinal object velocity.

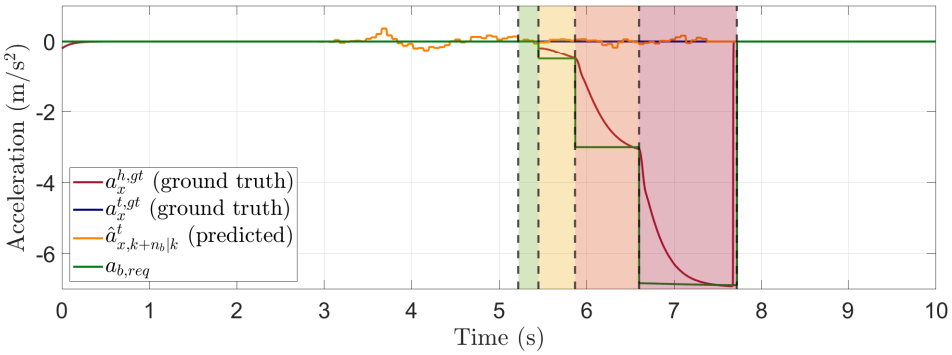

(c) Longitudinal host acceleration, longitudinal object acceleration and the required brake acceleration.

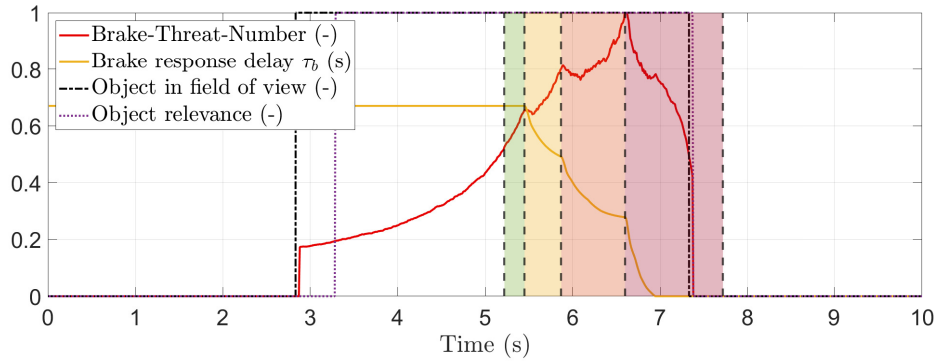

(d) Brake-Threat-Number (BTN) together with the brake response delay of the modelled brake system.

Figure 6.3: Simulation results of the third driving scenario AEB VRU.

6.1.2 Car-to-Car Rear moving (CCRm) scenario

In the CCRm scenario, the host vehicle is following the target vehicle and both vehicles are driving straight in the same direction and with a constant velocity. Since the detected object is present in front of the host vehicle, the object is considered to be relevant for the AEB system over the entire simulation time. As the velocity of the object is lower than the velocity of the host vehicle, a brake intervention by the AEB system is required to prevent a collision until the velocity of the host vehicle matches the velocity of the object.

The simulation results of the CCRm scenario are shown in Figure 6.4, where all predicted and ground truth signals are given in the current body-fixed frame. Here, it can be seen that the BTN rises as the longitudinal relative distance decreases and the host vehicle approaches the object. Again, the operating modes FCW, pre-charging, partial braking and full braking are initiated consecutively once the BTN exceeds the value of the corresponding BTN threshold parameter as given in Table 5.1. As explained in the previous section, the sudden drop of the BTN at the start of the partial braking and full braking operating modes is caused by the large reduction of the brake response delay τ_b once a brake intervention is initiated. Once the host vehicle is being fully braked and the velocity of the host vehicle approaches the velocity of the object, meaning the relative velocity approaches zero, the BTN drops to zero accordingly, which can be explained by looking at (5.16) used to calculate the required acceleration of the host vehicle with a moving object. After the velocity of the host vehicle becomes smaller than the velocity of the object, the BTN rises again. The AEB system is deactivated once the velocity of the host vehicle is smaller or equal to the velocity of the object for a certain number of consecutive samples as is shown in Figure 6.4b. As desired, the minimal relative distance between the host vehicle and the object is at least 0.5 m. After deactivation of the AEB system, the velocity of the host vehicle still decreases slightly, which is caused by the resistant forces acting on the host vehicle and because the throttle of the host vehicle is set to zero by the AEB controller. Furthermore, due to the dynamics of the modelled brake system, it takes some time for the acceleration of the host vehicle to approach 0 m/s^2 after deactivation of the AEB system.

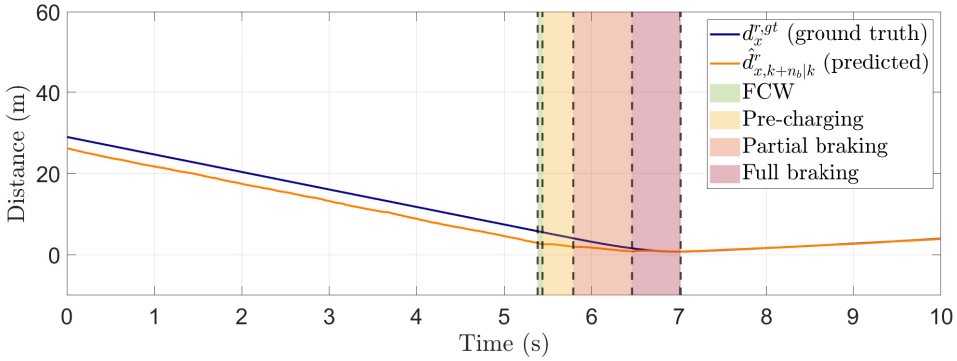

(a) Longitudinal relative distance.

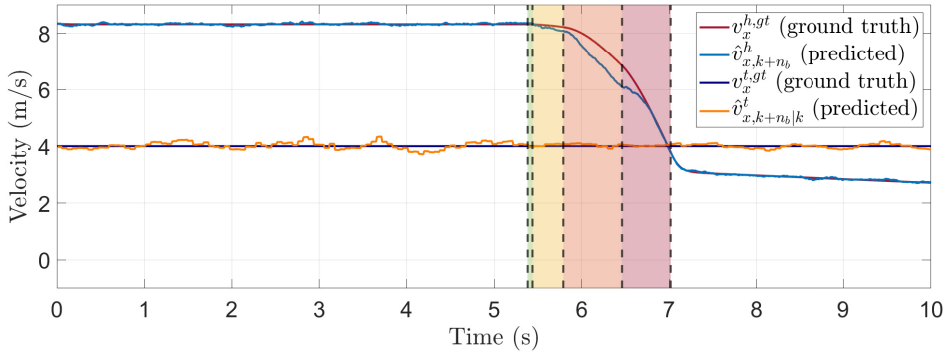

(b) Longitudinal host velocity and longitudinal object velocity.

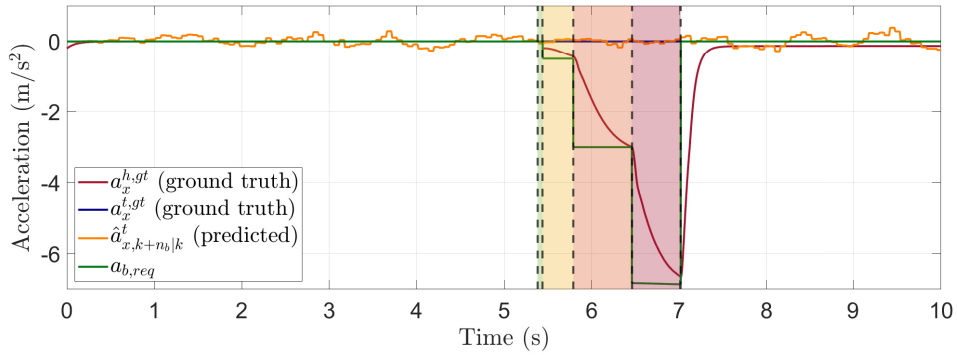

(c) Longitudinal host acceleration, longitudinal object acceleration and the required brake acceleration.

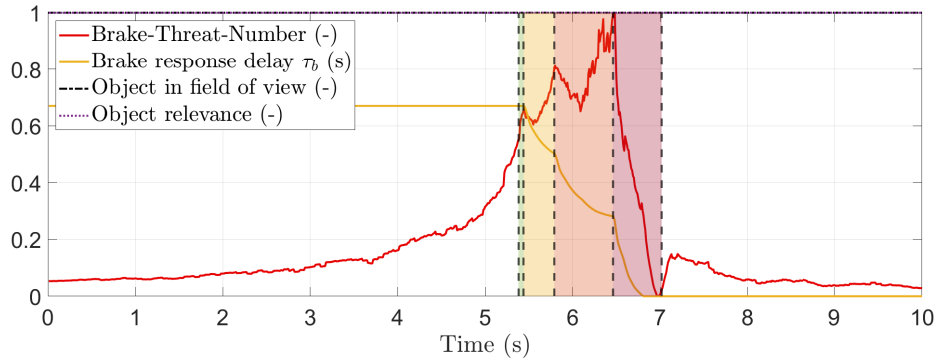

(d) Brake-Threat-Number (BTN) together with the brake response delay of the modelled brake system.

Figure 6.4: Simulation results of the second driving scenario CCRm.

6.1.3 Turning away scenario

In the turning away scenario, at first the host vehicle is following the target vehicle and both vehicles are driving straight in the same direction and with a constant velocity. Then, the target vehicle brakes and before a collision takes place the host vehicle turns away from the target vehicle. Therefore, for this scenario, a brake intervention by the AEB system is not required to prevent a collision and is undesired. Since the host vehicle turns away from the object, determining if the object is relevant is of great importance for this scenario and a brake intervention should only be initiated if the object is considered to be relevant for the AEB system.

Figure 6.5 shows the predicted positions of the host vehicle and the object together with the corresponding uncertainty ellipses at different times. Here, Figure 6.5a shows the object is considered to be relevant for the AEB system at $t = 1$ s, since the object is present right in front of the host vehicle. In this driving scenario, the host vehicle starts to turn away from the object at $t = 3$ s. Figure 6.5b shows the object is still considered to be relevant at $t = 3.3$ s, since the uncertainty ellipses intersect at a prediction time t_{pre} of 2 s. As shown in Figure 6.5b, the ground truth positions of the host vehicle do not lie within the corresponding ellipses of uncertainty. The reason for this is that the yaw rate of the host vehicle is still changing at $t = 3.3$ s, whereas the positions of the host vehicle are predicted by making a constant yaw rate assumption. Only the measurement uncertainty of the available sensor measurements is taken into account here and the model uncertainty is neglected, which explains why the ground truth positions lie outside the corresponding ellipses of uncertainty. Finally, at $t = 3.95$ s, the object is not considered to be relevant as is shown in Figure 6.5c, since none of the uncertainty ellipses intersect, which means the object is not present in the path of the host vehicle anymore.

The simulation results of the fourth driving scenario turning away are shown in Figure 6.6, where all predicted and ground truth signals are given in the current body-fixed frame. For this scenario, the ground truth yaw rate of the host vehicle is also included in Figure 6.6d. Figure 6.6 shows the BTN rises as the host vehicle approaches the object and the longitudinal relative distance decreases. At $t = 3$ s, the host vehicle starts to turn away from the object as can be seen by looking at the yaw rate of the host vehicle in Figure 6.6d. Around $t = 3.6$ s, the object is not considered to be relevant for the AEB system anymore. Therefore, the first operating mode of the AEB system is not activated once the BTN exceeds the value of the BTN threshold parameter $\mathrm{BTN_{FCW}}$ as given in Table 5.1. Once the object remains outside the field of view of the radar sensor for a certain number of consecutive samples, the BTN drops to zero. As desired, no brake intervention is initiated by the AEB system for this driving scenario.

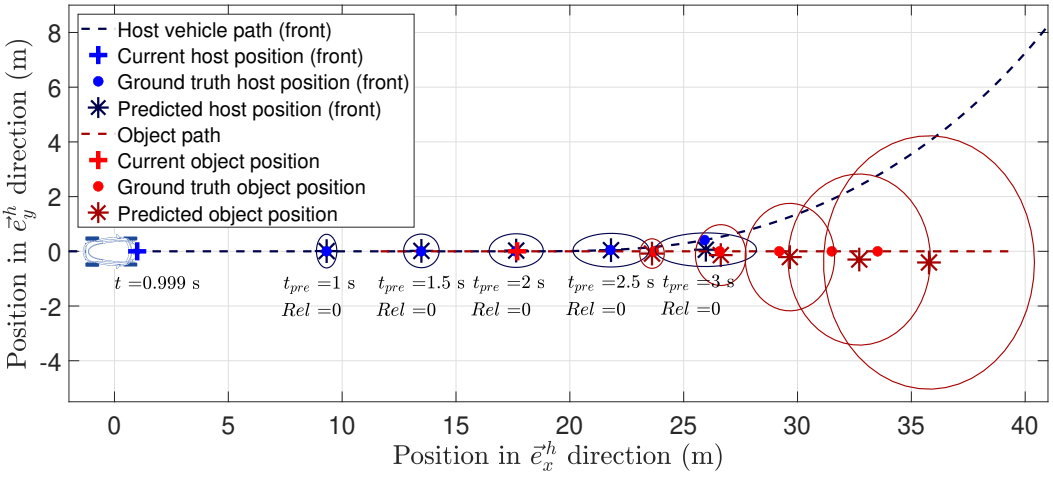

(a) At $t = 1$ s, the object is present right in front of the host vehicle and is therefore considered relevant.

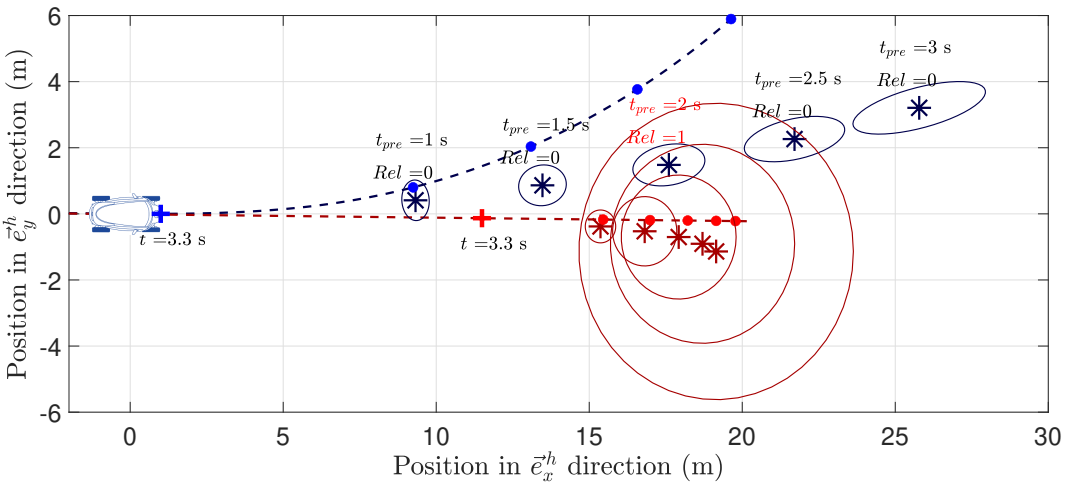

(b) At $t = 3.3$ s, the object is still considered to be relevant.

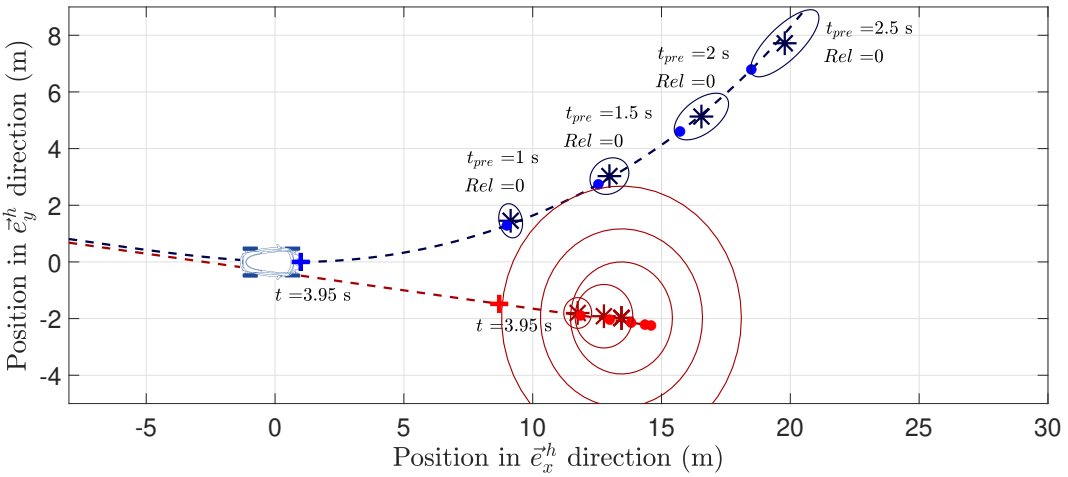

(c) At $t = 3.95$ s, the object is not considered to be relevant anymore.

Figure 6.5: Predicted positions of the host vehicle and the detected object together with the corresponding uncertainty ellipses at different times for the fourth driving scenario turning away.

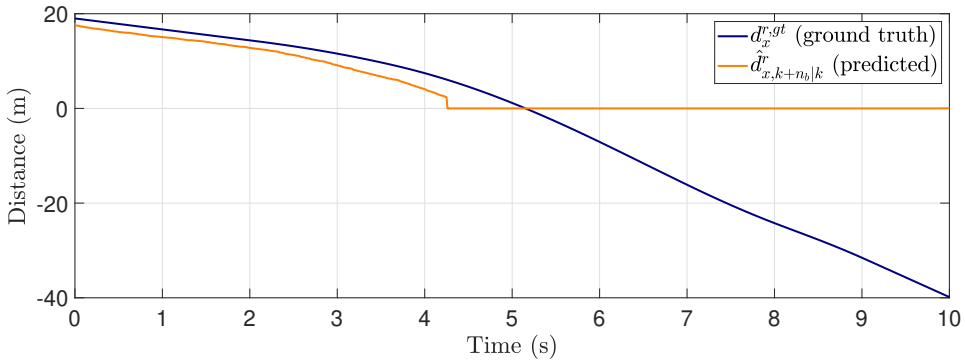

(a) Longitudinal relative distance.

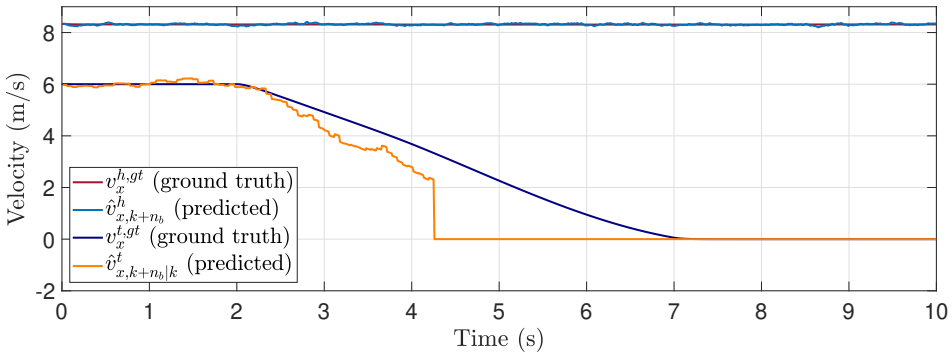

(b) Longitudinal host velocity and longitudinal object velocity.

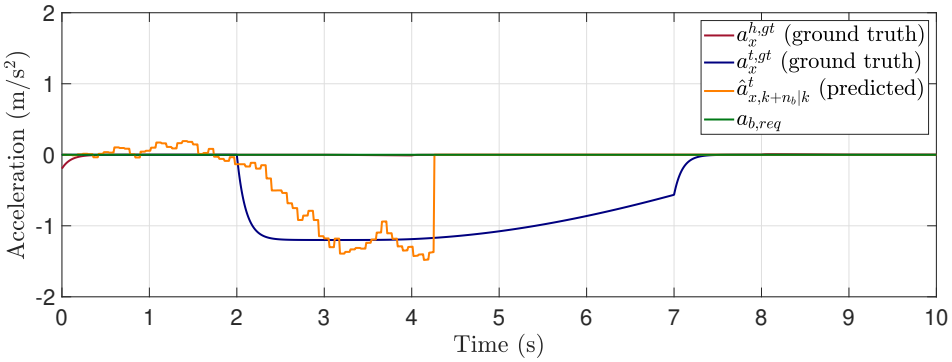

(c) Longitudinal host acceleration, longitudinal object acceleration and the required brake acceleration.

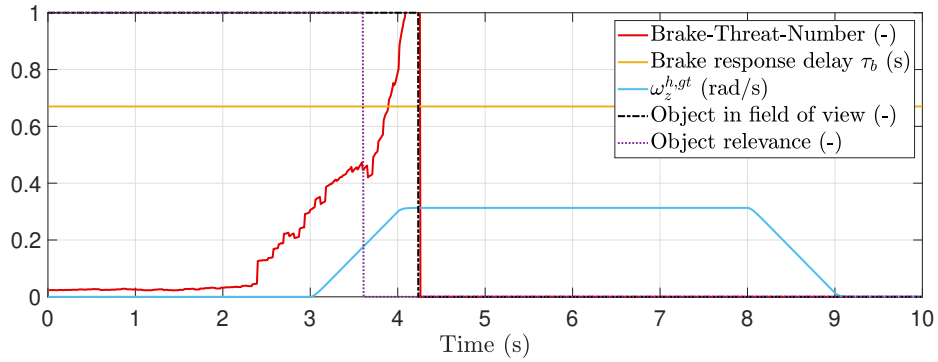

(d) Brake-Threat-Number (BTN) together with the brake response delay of the modelled brake system.

Figure 6.6: Simulation results of the fourth driving scenario turning away.

6.2 Open-loop testing of the AEB system

In this section the results of one of the open-loop tests performed with the Renault Twizy will be discussed. In these tests real sensor measurements are used, which afterwards replace the virtual sensor measurements in the simulation environment to test how the AEB system responds to real sensor measurements. These tests are called open-loop since the required brake acceleration $a_{b,req}$ as determined by the AEB controller is not used by the brake system of the host vehicle. Figure 6.7 gives a schematic overview of the open-loop test performed with the Renault Twizy and discussed in this section. Here, a stack of cardboard boxes (representing an object) is placed right in front of the host vehicle at a distance of approximately 20-25 m. The host vehicle drives towards the object with a constant velocity of approximately 15 km/h, which will not cause any damage to the Renault Twizy. Eventually, the host vehicle collides with the object and the resulting sensor measurements can be used to to test how and when the AEB system would respond when being implemented on the Renault Twizy. Since the object is present right in front of the host vehicle, the object is considered to be relevant and a brake intervention is required to prevent a collision. Furthermore, for the same reason, the measured longitudinal relative distance d_x^r and the measured longitudinal relative velocity v_x^r are set equal to the range and range rate respectively as measured by the radar sensor on the Renault Twizy. Finally, to reduce the noise level of the measured longitudinal velocity v_x^h and acceleration a_x^h, they are filtered using a first-order low-pass filter with a time constant of 0.1 s before being used by the AEB system.

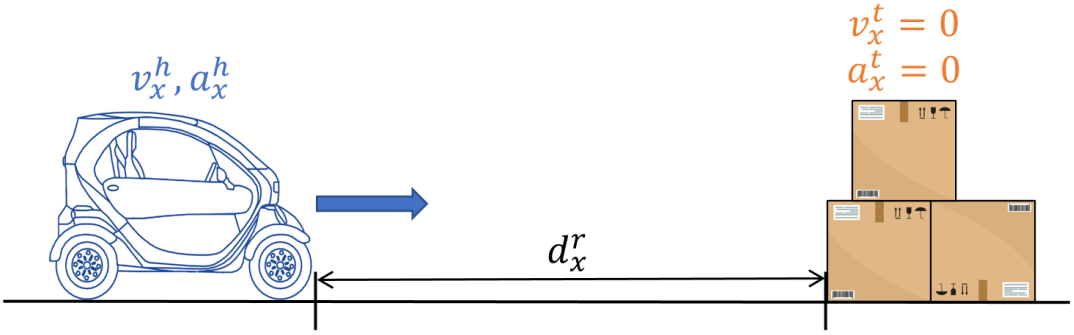

Figure 6.7: Schematic overview of the open-loop test performed with the Renault Twizy.

The results of the open-loop test are given in Figure 6.8, which shows the sensor measurements together with the predicted signals in the current body-fixed frame. As shown in Figures 6.8b and 6.8c, the predicted longitudinal object velocity and acceleration are approximately zero, which is correct since the object is stationary. As shown in Figure 6.8d, the BTN rises as the host vehicle approaches the object and the longitudinal relative distance decreases. At a longitudinal relative distance of approximately 2.5 m, when the BTN exceeds the value of the BTN threshold parameter BTN_{FCW} as given in Table 5.1, the AEB system would be activated when implemented on the host vehicle. However, in the performed test, the host vehicle collides with the object, which is shown in Figure 6.8a where the longitudinal relative distance reaches zero. This can also be seen in Figure 6.8d, where the BTN surpasses a value of 1, meaning a collision with the object cannot be avoided anymore by braking the vehicle.

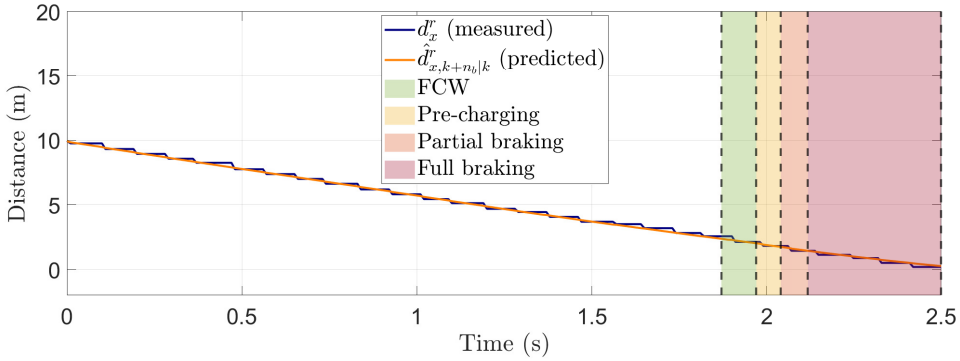

(a) Longitudinal relative distance.

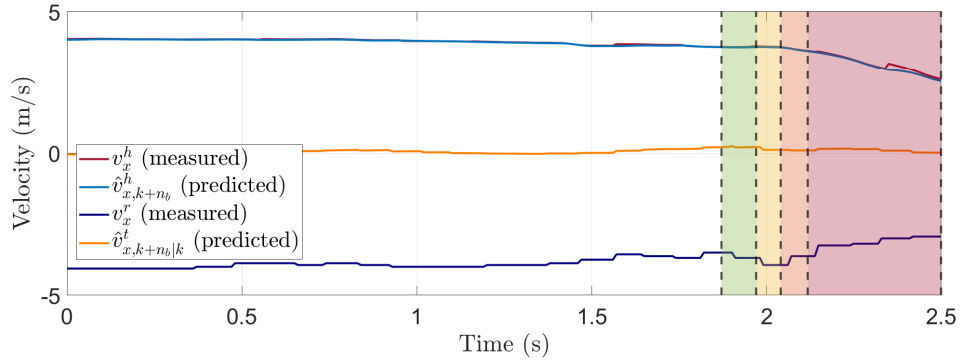

(b) Longitudinal host velocity, longitudinal relative velocity and the longitudinal object velocity.

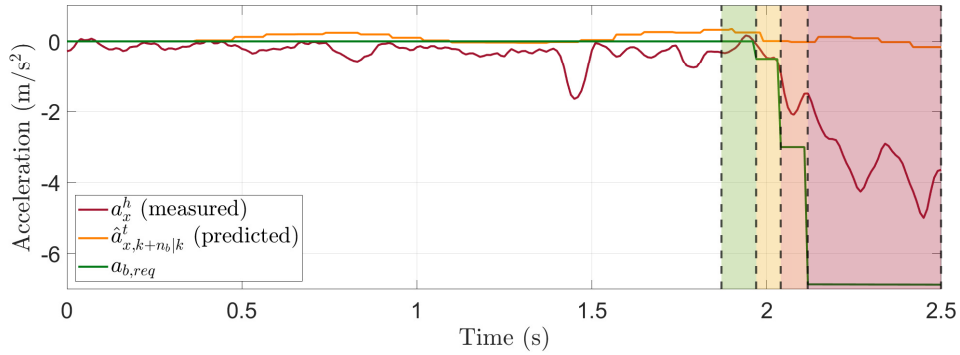

(c) Longitudinal host acceleration, longitudinal object acceleration and the required brake acceleration.

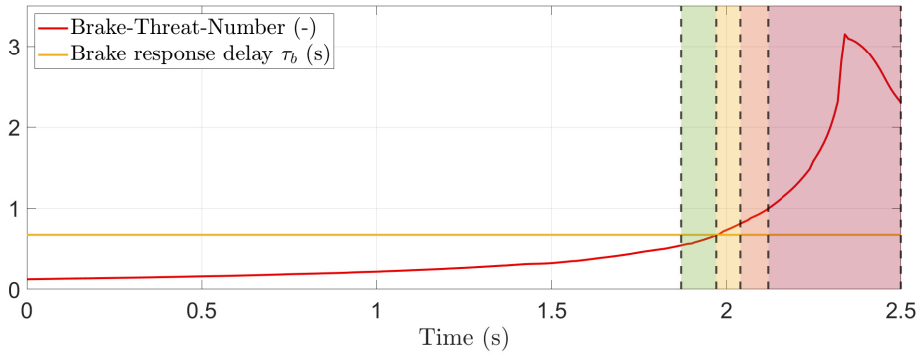

(d) Brake-Threat-Number (BTN) together with the brake response delay of the modelled brake system.

Figure 6.8: Results of the open-loop test performed by driving towards a stationary object.

6.3 Summary

In this chapter, first the performance of the AEB system has been evaluated via simulations for different driving scenarios. For the AEB Vulnerable Road User (VRU) scenario, the object is correctly considered to be relevant for the AEB system, a brake intervention is initiated by the AEB system, and a collision with the object is avoided with a desired safety distance of at least 0.5 m between the host vehicle and the object. Then, for the Car-to-Car Rear moving (CCRm) scenario, the object is again correctly considered to be relevant for the AEB system, a brake intervention by the AEB system is initiated to prevent a collision, which stops once the velocity of the host vehicle becomes smaller than the velocity of the object. For the turning away scenario, a brake intervention by the AEB system is not initiated, since the object is not considered to be relevant anymore once the host vehicle turns away from the object. In addition to these closed-loop tests, open-loop tests are performed with the Renault Twizy to test how the AEB system responds to real sensor measurements. In the open-loop test, a stationary object is placed right in front of the host vehicle and a brake intervention is required to prevent a collision. The results show the AEB system responds well to real sensor measurements and a brake intervention by the AEB system would be initiated when implemented on the host vehicle.

Chapter 7

Conclusions and recommendations

7.1 Conclusions

In this final chapter, the most important conclusions of this research are given as well as recommendations for future research on this topic. The main objective of this research is defined as follows: *"Develop an Automated Emergency Braking (AEB) system for the Renault Twizy used in the i-CAVE research program"*. The AEB system is developed and tested in a simulation environment for different driving scenarios. The sensors used by the AEB sytem are a front facing radar sensor, an Inertial Measurement Unit and an odometer, which are all modelled using realistic operating frequencies and noise levels. Furthermore, the modified brake system of the Renault Twizy is modelled in the simulation environment, which consists of two main parts, being the brake cam actuator followed by the brake cam actuator dynamics. The response delay of the brake system model is determined as a function of the camshaft angle. The motion of the host vehicle and the object is modelled using a single-track vehicle model with three degrees of freedom: the longitudinal, lateral and yaw motion.

The first sub-objective is defined as follows: *"Develop a state estimator to estimate the motion of a detected object from radar sensor measurements and measurements of the Renault Twizy's own motion"*. A linear discrete-time Kalman filter is used to estimate the motion of a detected object from the available sensor measurements. The motion model used in the Kalman filter is the constant acceleration model, which normally describes the relative motion between the host vehicle and the object. However, in this research, the motion model is slightly adapted, since the absolute motion of the object is required. Furthermore, an additional correction step is proposed for the Kalman filter to reduce the state estimation errors when the host vehicle is cornering. Since the radar sensor on the host vehicle has a lower sampling rate than the AEB controller (including the Kalman filter), the state estimates are only updated in case a new measurement becomes available. In between measurements, only the prediction step of the Kalman filter is used to estimate the states. By performing simulations for the most complex driving scenario, the process noise values of the process noise covariance matrix $\mathbf{Q}$ resulting in the lowest cost C are found. For all simulated driving scenarios, the Kalman filter performs well and is able to estimate the states accurately with an acceptable error.

The second sub-objective of this research is defined as follows: *"Determine if a detected object is relevant for the AEB system and present in the driving path of the Renault Twizy"*. To this end, first the paths of both the host vehicle and the object are predicted. The position of the object is predicted by making a n-step a-priori prediction using the last available state estimates from the Kalman filter. The level of uncertainty on the predicted positions of the object is determined from the predicted state estimation covariance. Furthermore, the position of the host vehicle is predicted directly from the available sensor measurements and the level of uncertainty on the

predicted positions is determined from the corresponding sensor measurement noise levels. A new method is proposed to determine if an object is relevant, which uses the predicted positions and the corresponding levels of uncertainty to draw uncertainty ellipses around the predicted positions of the host vehicle and the object. A possible collision between the host vehicle and the object is found if for a certain prediction time t_{pre} the corresponding uncertainty ellipses intersect.

The last sub-objective is defined as follows: *"Estimate the threat level of the current traffic situation and develop a controller in the form of a finite state machine, which uses the estimated threat level to determine which system response should be initiated"*. The AEB controller uses a parameter called the Brake-Threat-Number (BTN) to determine if a brake intervention is needed to avoid a collision with a detected object, which is a measure of the threat level and indicates the effort that is required to avoid a collision with the object. The BTN is defined as the required host acceleration to avoid a collision divided by the minimal achievable host acceleration. Two cases are considered to determine the required host acceleration, in which the object is either stationary or moving in the longitudinal direction of the current body-fixed frame. To compensate for the response delay of the brake system, the threat level is determined using the predicted future motions of the host vehicle and the object, which are predicted over the time spanned by the brake response delay. When activated, the AEB system can operate in four different operating modes, being Forward Collision Warning (FCW), pre-charging of the brakes, partial braking and full braking.

The performance of the AEB system is evaluated via simulations for different driving scenarios. For the AEB Vulnerable Road User (VRU) scenario, the object is correctly considered to be relevant for the AEB system, a brake intervention is initiated by the AEB system, and a collision with the object is avoided with a desired safety distance of at least 0.5 m between the host vehicle and the object. Then, for the Car-to-Car Rear moving (CCRm) scenario, the object is again correctly considered to be relevant for the AEB system, a brake intervention by the AEB system is initiated to prevent a collision, which stops once the velocity of the host vehicle becomes smaller than the velocity of the object. For the turning away scenario, a brake intervention by the AEB system is not initiated, since the object is not considered to be relevant anymore once the host vehicle turns away from the object. In addition to these closed-loop tests, open-loop tests are performed with the Renault Twizy to test how the AEB system responds to real sensor measurements. In the open-loop test, a stationary object is placed right in front of the host vehicle and a brake intervention is required to prevent a collision. The results show the AEB system responds well to real sensor measurements and a brake intervention by the AEB system would be initiated when implemented on the host vehicle.

7.2 Recommendations

This research can be improved or extended as follows:

- Use additional environmental sensors and combine them to obtain more accurate measurements of the objects in front of the host vehicle and to improve the reliability of the AEB system. Furthermore, by placing environmental sensors at different angles, the field of view can be extended. In this way, the AEB system could be made suitable for more complex driving scenarios and crossing vulnerable road users can be detected at an earlier stage.

- The longitudinal velocity of the host vehicle should be estimated in the presence of wheel slip. In this research, the longitudinal velocity is determined from the rotational speed of the rear axle, where it is assumed that the wheels on the rear axle have no wheel slip. However, especially in situations in which an AEB system is activated, this assumption is not valid.

- In this research, sensor biases are neglected and sensor delay is assumed to be neglectable compared to the response delay of the brake system. However, to improve accuracy of the model, these could be added to the simulation environment.

- It is assumed that the host vehicle is driving on a dry road surface and therefore a fixed tire-road friction coefficient is used. However, by dynamically adapting the tire-road friction coefficient to the current road surface, the AEB system can be made robust against changing road surfaces. Furthermore, it is assumed that the host vehicle is driving on a flat road surface. However, by taking into account the road gradient, the AEB system can be made robust against road grade influences.

- To prevent the wheels from blocking when a brake intervention by the AEB system is initiated, which could cause stability and steerability issues, the Renault Twizy should be equipped with an Anti-lock Brake System (ABS).

- A single-track vehicle model is used to model the motion of the host vehicle and the object. However, to increase the accuracy of the model, a multibody vehicle model of the Renault Twizy should be used instead. Furthermore, to improve the accuracy of the AEB system, the physical dimensions of both the host vehicle and the object should be taken into account in the decision process of the AEB system.

- The brake response delay is estimated from the brake system model. However, a more accurate estimation could be made when performing brake tests on the Renault Twizy and by measuring the total response delay of the vehicle.

- A low-pass filter with a time constant of 0.1 s is used to reduce the noise levels on the longitudinal velocity v_x^h and acceleration a_x^h. Using a larger time constant will reduce the noise levels on these signals more, but will also result in a larger phase lag. In this case, the effects of low-pass filtering on the state estimates of the Kalman filter should be taken into account.

- The position of the host vehicle is predicted directly from the available sensor measurements and the level of uncertainty on the predicted positions is determined from the corresponding sensor measurement noise levels, which means the model uncertainty is neglected. However, when estimating the motion of the host vehicle with a state estimator, this model uncertainty is also taken into account when determining the level of uncertainty on the predicted positions of the host vehicle.

- The assumptions and uncertainties introduced throughout this research have a significant effect on determining whether an object is relevant for the AEB system and present in the driving path of the host vehicle. Therefore, a degree of certainty should be added to the proposed method, which indicates the certainty of an object being relevant. This can be

done by determining the probability of a collision, or in other words, the probability of both the host vehicle and the object being present within the overlapping area of the uncertainty ellipses at a certain prediction time t_{pre}.

- Extend the AEB system such that it is able to deal with multiple objects simultaneously and select the most important object (MIO) out of all detected objects.
- The required radar sensor measurements of an object are assumed to be available. However, in reality, before being able to implement the AEB system on the Renault Twizy, the AEB system needs to be combined with an object tracking algorithm.
- The BTN used by the AEB controller is obtained directly from the predicted states of the host vehicle and the object. Due to the uncertainty of the predicted states, the actual BTN lies within a certain range. This range can be determined and used by the AEB controller to either decrease the number of false positives or false negatives. In addition, the effect of all uncertainties on the safety distance d_{safe} could be determined.
- Implement the AEB system on the Renault Twizy and test the system for different driving scenarios.

Bibliography

[1] World Health Organization, "Road traffic injuries," https://www.who.int/news-room/fact-sheets/detail/road-traffic-injuries, 2021, online; accessed: 21-01-2022.

[2] European Parliament, "Road fatality statistics in the EU (infographic)," https://www.europarl.europa.eu/news/en/headlines/society/20190410STO36615/road-fatality-statistics-in-the-eu-infographic, 2021, online; accessed: 21-01-2022.

[3] European Commission, "Study on the feasibility, costs and benefits of retrofitting advanced driver assistance to improve road safety," https://op.europa.eu/nl/publication-detail/-/publication/72659808-7ec1-11ea-aea8-01aa75ed71a1, 2020, online; accessed: 21-01-2022.

[4] European Transport Safety Council, "Road deaths in the European Union – latest data," https://etsc.eu/euroadsafetydata/, 2020, online; accessed: 21-01-2022.

[5] Society of Automotive Engineers, "SAE Levels of Driving Automation Refined for Clarity and International Audience," https://www.sae.org/blog/sae-j3016-update, 2021, online; accessed: 21-01-2022.

[6] Robert Bosch GmbH, *Automotive Handbook 10th Edition*. Wiley, 2018.

[7] B. Fildes, M. Keall, N. Bos, A. Lie, Y. Page, C. Pastor, L. Pennisi, M. Rizzi, P. Thomas, and C. Tingvall, "Effectiveness of low speed autonomous emergency braking in real-world rear-end crashes," *Accident Analysis & Prevention*, vol. 81, pp. 24–29, 2015.

[8] European Transport Safety Council, "AEB systems cut rear-end collisions by 45%," https://etsc.eu/aeb-systems-cut-rear-end-collisions-by-45/, 2020, online; accessed: 21-01-2022.

[9] United Nations Economic Commission for Europe, "Uniform provisions concerning the approval of motor vehicles with regard to the Advanced Emergency Braking Systems (AEBS)," https://unece.org/fileadmin/DAM/trans/main/wp29/wp29regs/2015/R131r1e.pdf, 2014, online; accessed: 21-01-2022.

[10] Euro NCAP, "AEB Car-to-Car," https://www.euroncap.com/en/vehicle-safety/the-ratings-explained/safety-assist/aeb-car-to-car/, 2020, online; accessed: 22-01-2022.

[11] Bosch Mobility Solutions, "Automatic emergency braking on vulnerable road users," https://www.bosch-mobility-solutions.com/en/solutions/assistance-systems/automatic-emergency-braking-on-vulnerable-road-user, 2022, online; accessed: 10-02-2022.

[12] H. Nijmeijer, T. van der Sande, E. Klerks, G. Notten, and J. van der Sar, *i-Cave: The future of moving forward*. MediaToko, 2021.

[13] H. Nijmeijer and T. van der Sande, "I-CAVE," https://i-cave.nl/workpackage-7/, Accessed: 2021-10-20.

[14] H.-K. Lee, S.-G. Shin, and D.-S. Kwon, "Design of emergency braking algorithm for pedestrian protection based on multi-sensor fusion," *International Journal of Automotive Technology*, vol. 18, no. 6, pp. 1067–1076, 2017.

[15] J. Han, O. Heo, M. Park, S. Kee, and M. Sunwoo, "Vehicle distance estimation using a mono-camera for fcw/aeb systems," *International journal of automotive technology*, vol. 17, no. 3, pp. 483–491, 2016.

[16] Y. Bar-Shalom, X. R. Li, and T. Kirubarajan, *Estimation with applications to tracking and navigation: theory algorithms and software*. John Wiley & Sons, 2004.

[17] D. Simon, *Optimal state estimation: Kalman, H infinity, and nonlinear approaches*. John Wiley & Sons, 2006.

[18] A. Mukhtar, L. Xia, and T. B. Tang, "Vehicle detection techniques for collision avoidance systems: A review," *IEEE transactions on intelligent transportation systems*, vol. 16, no. 5, pp. 2318–2338, 2015.

[19] E. A. Wan and R. Van Der Merwe, "The unscented kalman filter for nonlinear estimation," in *Proceedings of the IEEE 2000 Adaptive Systems for Signal Processing, Communications, and Control Symposium (Cat. No. 00EX373)*. Ieee, 2000, pp. 153–158.

[20] X. R. Li and V. P. Jilkov, "Survey of Maneuvering Target Tracking. Part I: Dynamic Models," *IEEE Transactions on Aerospace and Electronic Systems*, vol. 39, no. 4, pp. 1333–1364, 2003.

[21] R. Schubert, E. Richter, and G. Wanielik, "Comparison and evaluation of advanced motion models for vehicle tracking," in *2008 11th international conference on information fusion*. IEEE, 2008, pp. 1–6.

[22] S. Solmaz, G. Nestlinger, and G. Stettinger, "Improvement of lane keeping assistance adas function utilizing a kalman filter prediction of delayed position states," in *2019 IEEE International Conference on Connected Vehicles and Expo (ICCVE)*. IEEE, 2019, pp. 1–8.

[23] R. Schubert, C. Adam, M. Obst, N. Mattern, V. Leonhardt, and G. Wanielik, "Empirical evaluation of vehicular models for ego motion estimation," in *2011 IEEE intelligent vehicles symposium (IV)*. IEEE, 2011, pp. 534–539.

[24] S. Ammoun and F. Nashashibi, "Real time trajectory prediction for collision risk estimation between vehicles," in *2009 IEEE 5th International Conference on Intelligent Computer Communication and Processing*. IEEE, 2009, pp. 417–422.

[25] A. Houenou, P. Bonnifait, V. Cherfaoui, and W. Yao, "Vehicle trajectory prediction based on motion model and maneuver recognition," in *2013 IEEE/RSJ international conference on intelligent robots and systems*. IEEE, 2013, pp. 4363–4369.

[26] G. Xie, H. Gao, L. Qian, B. Huang, K. Li, and J. Wang, "Vehicle trajectory prediction by integrating physics-and maneuver-based approaches using interactive multiple models," *IEEE Transactions on Industrial Electronics*, vol. 65, no. 7, pp. 5999–6008, 2017.

[27] C. Laugier, I. E. Paromtchik, M. Perrollaz, M. Yong, J.-D. Yoder, C. Tay, K. Mekhnacha, and A. Nègre, "Probabilistic analysis of dynamic scenes and collision risks assessment to improve driving safety," *IEEE Intelligent Transportation Systems Magazine*, vol. 3, no. 4, pp. 4–19, 2011.

[28] B. Kim, C. M. Kang, J. Kim, S. H. Lee, C. C. Chung, and J. W. Choi, "Probabilistic vehicle trajectory prediction over occupancy grid map via recurrent neural network," in *2017 IEEE 20th International Conference on Intelligent Transportation Systems (ITSC)*. IEEE, 2017, pp. 399–404.

[29] N. Schneider and D. M. Gavrila, "Pedestrian path prediction with recursive bayesian filters: A comparative study," in *German Conference on Pattern Recognition*. Springer, 2013, pp. 174–183.

[30] J. Wiest, M. Höffken, U. Kreßel, and K. Dietmayer, "Probabilistic trajectory prediction with gaussian mixture models," in *2012 IEEE Intelligent Vehicles Symposium*. IEEE, 2012, pp. 141–146.

[31] J. Hillenbrand, K. Kroschel, and V. Schmid, "Situation assessment algorithm for a collision prevention assistant," in *IEEE Proceedings. Intelligent Vehicles Symposium, 2005.* IEEE, 2005, pp. 459–465.

[32] R. Van Der Horst and J. Hogema, "Time-to-collision and collision avoidance systems," 1993.

[33] E. R. Gelso and J. Sjöberg, "Consistent Threat Assessment Using BTN and TTB Metrics ,," no. January 2017, pp. 74–89, 2017.

[34] I. Koglbauer, J. Holzinger, A. Eichberger, and C. Lex, "Autonomous emergency braking systems adapted to snowy road conditions improve drivers' perceived safety and trust," *Traffic Injury Prevention*, vol. 19, no. 3, pp. 332–337, 2018. [Online]. Available: https://doi.org/10.1080/15389588.2017.1407411

[35] H. Kim, S. Kyungsik, I. Chang, and K. Huh, "Autonomous emergency braking considering road slope and friction coefficient," *International Journal of Automotive Technology*, vol. 19, pp. 1013–1022, 2018.

[36] F. Diederichs, T. Schüttke, and D. Spath, "Driver intention algorithm for pedestrian protection and automated emergency braking systems," in *2015 IEEE 18th International Conference on Intelligent Transportation Systems*. IEEE, 2015, pp. 1049–1054.

[37] J. Jansson, "Collision avoidance theory: With application to automotive collision mitigation," Ph.D. dissertation, Linköping University Electronic Press, 2005.

[38] W. Schinkel, T. van der Sande, and H. Nijmeijer, "State estimation for cooperative lateral vehicle following using vehicle-to-vehicle communication," *Electronics*, vol. 10, no. 6, p. 651, 2021.

[39] Robert Bosch GmbH, "Radar-based driver assistance systems - mid-range radar sensor," 2017. [Online]. Available: https://bosch-mobility-solutions.com

[40] F. N. Hoogeboom, "Safety of automated vehicles: design, implementation, and analysis," 2020, Eindhoven University of Technology.

[41] Bosch Engineering GmbH, "Acceleration sensor mm5.10," 2020. [Online]. Available: https://www.bosch-motorsport.com/content/downloads/Raceparts/en-GB/51546379119226251.html

[42] S. Baaij, "Development and validation of a multibody model of a renault twizy," Ph.D. dissertation, MSc. Thesis, Eindhoven University of Technology, Department of Mechanical . . . , 2019.

[43] J. C. Gerdes and J. K. Hedrick, "Brake system modeling for simulation and control," 1999.

[44] W. S. Levine, *The Control Handbook (three volume set)*. CRC press, 2018.

[45] I. Besselink, "Vehicle Dynamics [4AT000]," 2019, unpublished University Lecture Notes.

[46] N. van de Wouw, "Multibody Dynamics Lecture Notes [4DM10]," 2017, unpublished University Lecture Notes.

[47] R. Rajamani, *Vehicle dynamics and control*. Springer Science & Business Media, 2011.

[48] M. van Zutphen, "Brake system identification and control of a renault twizy," 2019, Eindhoven University of Technology.

[49] Euro NCAP, "Assessment protocol – safety assist," 2020, version 9.0.3. [Online]. Available: https://cdn.euroncap.com/media/58229/euro-ncap-assessment-protocol-sa-v903.pdf

[50] ——, "Assessment protocol – vulnerable road user protection," 2020, version 10.0.3. [Online]. Available: https://cdn.euroncap.com/media/58230/euro-ncap-assessment-protocol-vru-v1003.pdf

[51] T. Cipra and R. Romera, "Kalman filter with outliers and missing observations," *Test*, vol. 6, no. 2, pp. 379–395, 1997.

[52] H. M. Faridani, "Performance of kalman filter with missing measurements," *Automatica*, vol. 22, no. 1, pp. 117–120, 1986.

[53] Y. Wang, B. M. Nguyen, H. Fujimoto, and Y. Hori, "Multirate estimation and control of body slip angle for electric vehicles based on onboard vision system," *IEEE Transactions on Industrial Electronics*, vol. 61, no. 2, pp. 1133–1143, 2013.

[54] M. Kordestani, M. Dehghani, B. Moshiri, and M. Saif, "A new fusion estimation method for multi-rate multi-sensor systems with missing measurements," *IEEE Access*, vol. 8, pp. 47 522–47 532, 2020.

[55] A. Fatehi and B. Huang, "Kalman filtering approach to multi-rate information fusion in the presence of irregular sampling rate and variable measurement delay," *Journal of Process Control*, vol. 53, pp. 15–25, 2017.

[56] G. Strang and E. P. Herman, *Calculus. Volume 1.* OpenStax College, Rice University, 2016.

[57] S. M. Carr, "Critical values of the Chi-square distribution with d degrees of freedom," https://www.mun.ca/biology/scarr/4250_Chi-square_critical_values.html, 2021, online; accessed: 02-02-2022.

Appendix A

Brake cam actuator controller

A.1 PID controller gains

To control the brake motor torque T_{bm} given a required camshaft angle $\delta_{c,req}$, a position controller is used, which consists of a feedforward part and a PID controller. The PID controller can operate in control mode or in tracking mode. In control mode the PID controller operates as a conventional PID controller and is given by

$$P + IT_s \frac{1}{z-1} + D \frac{N}{1 + NT_s \frac{1}{z-1}}, \tag{A.1}$$

where the proportional gain P has a value of 1.3248, the integral gain I has a value of 0, the derivative gain D has a value of 0.1736 and the filter coefficient N is equal to 61.0339 [40].

Appendix B

Performance of the state estimator

B.1 Simulation results

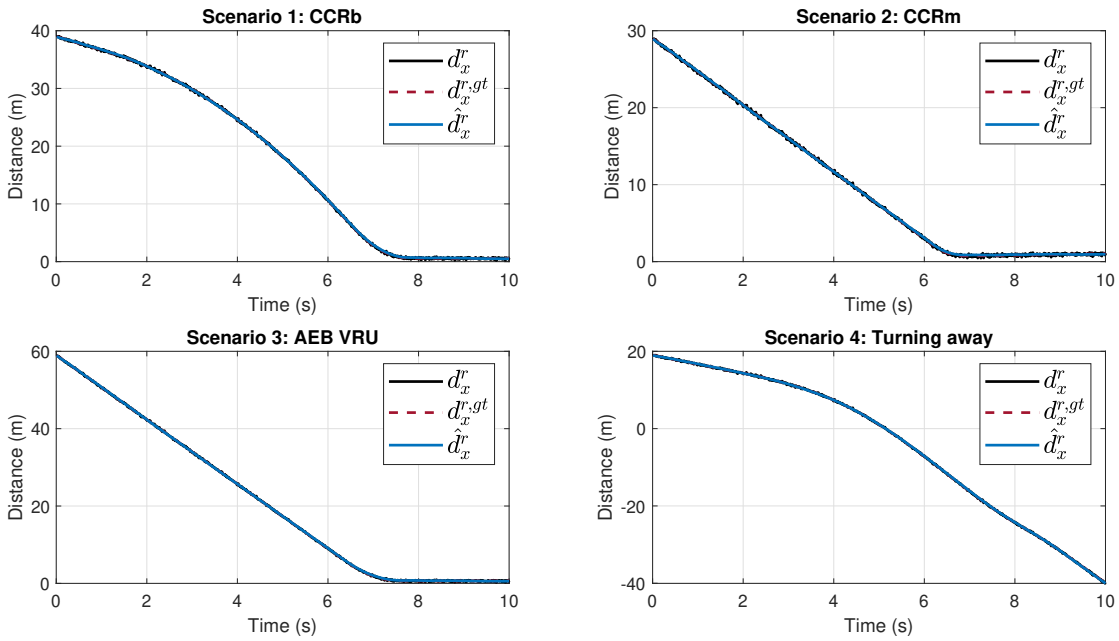

(a) Longitudinal relative distance.

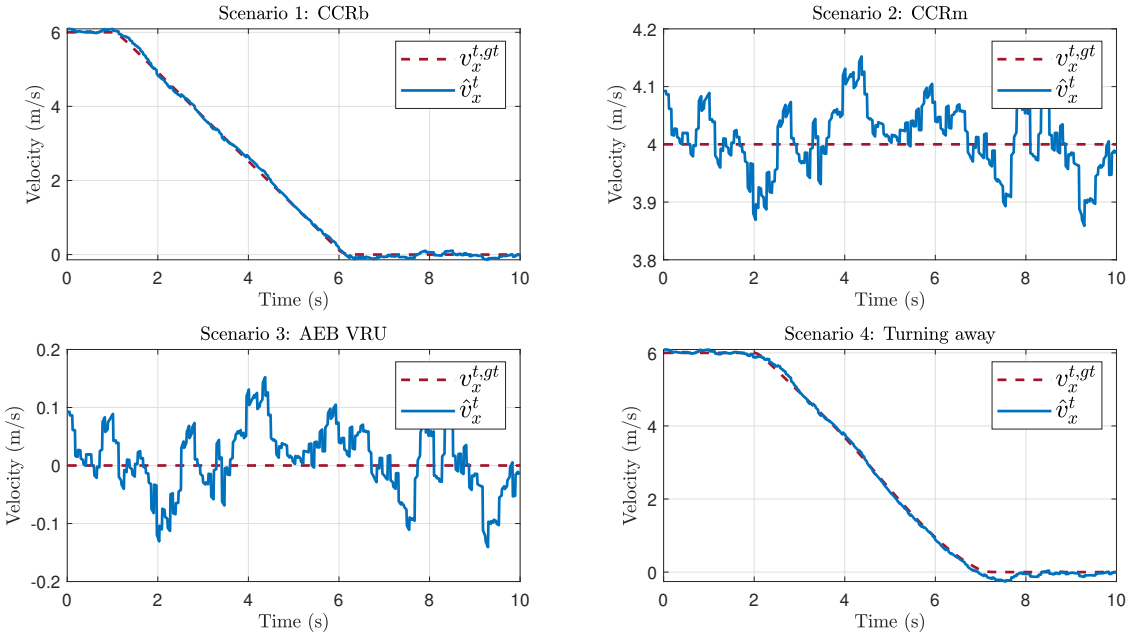

(b) Longitudinal target velocity.

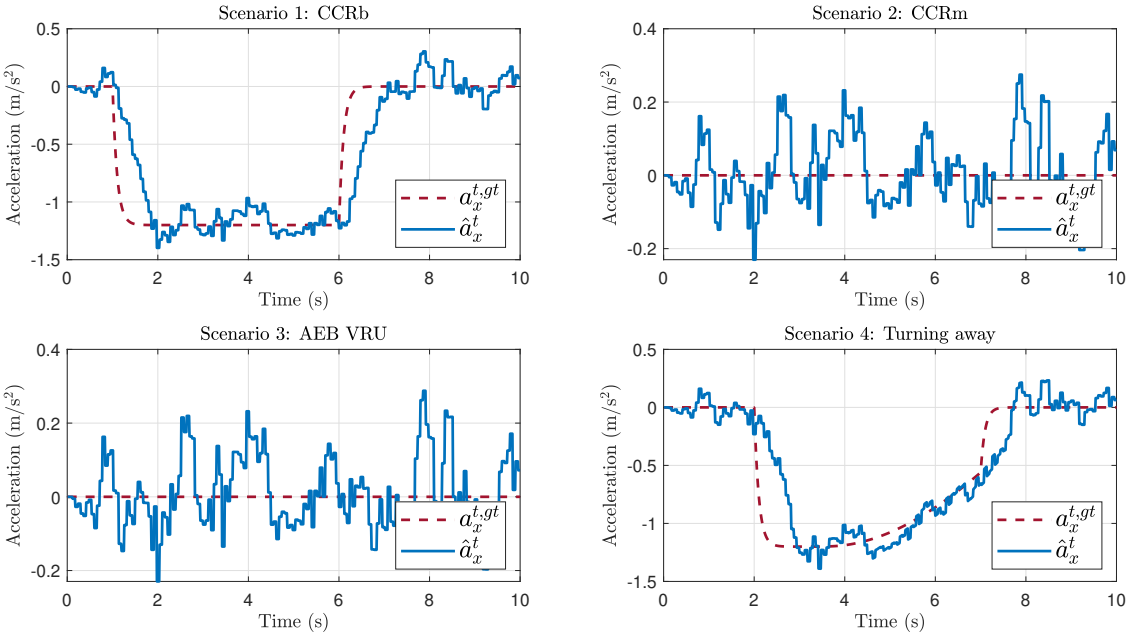

(c) Longitudinal target acceleration.

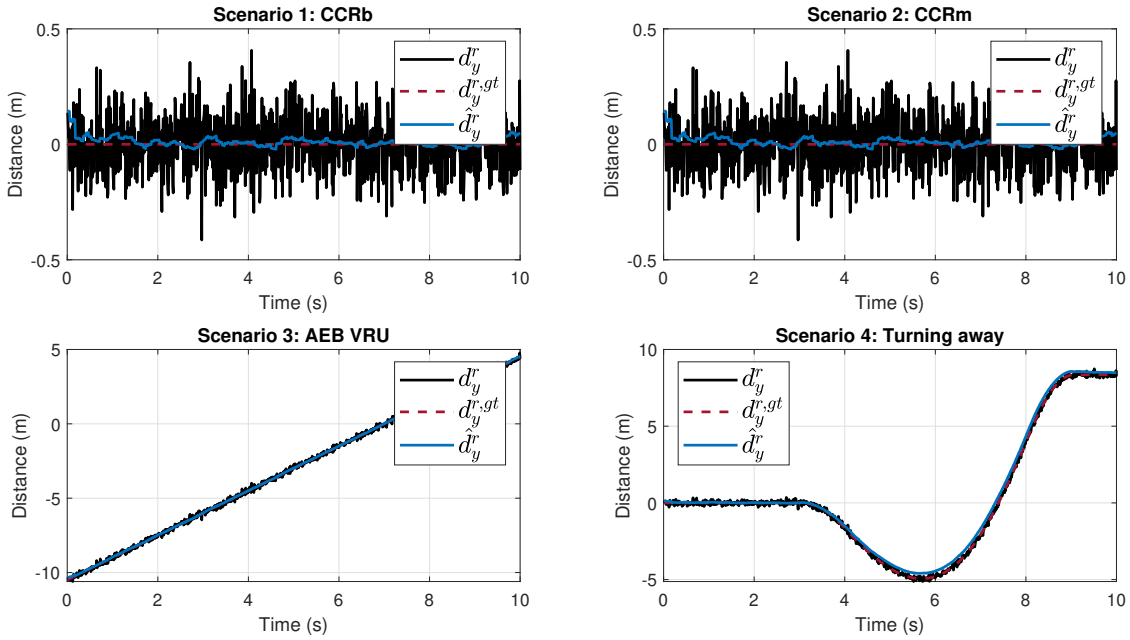

(d) Lateral relative distance.

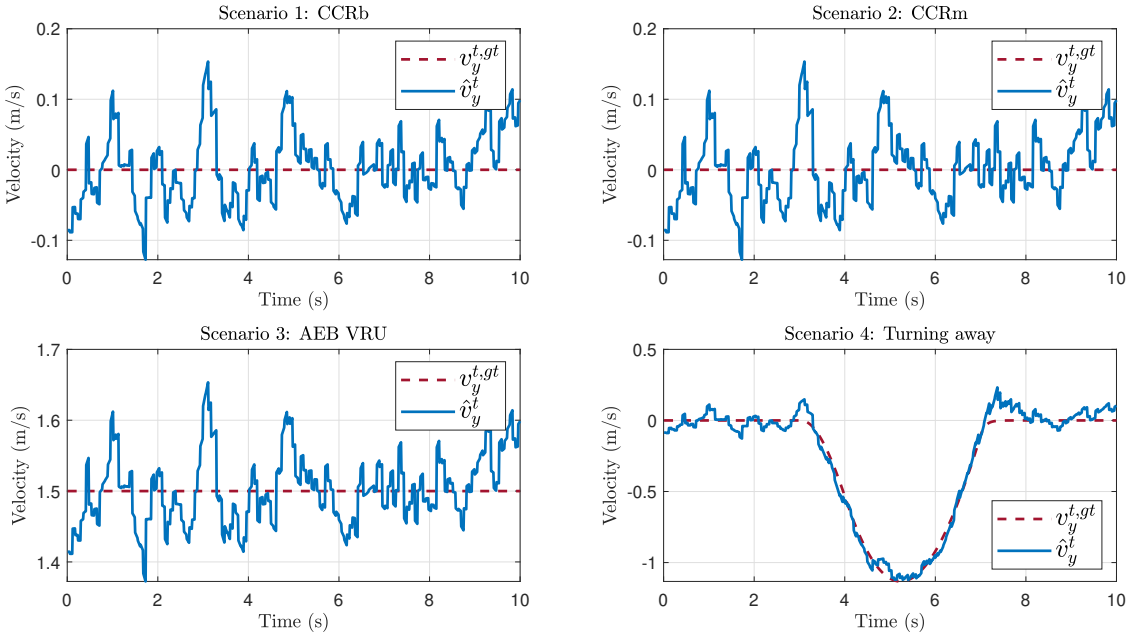

(e) Lateral target velocity.

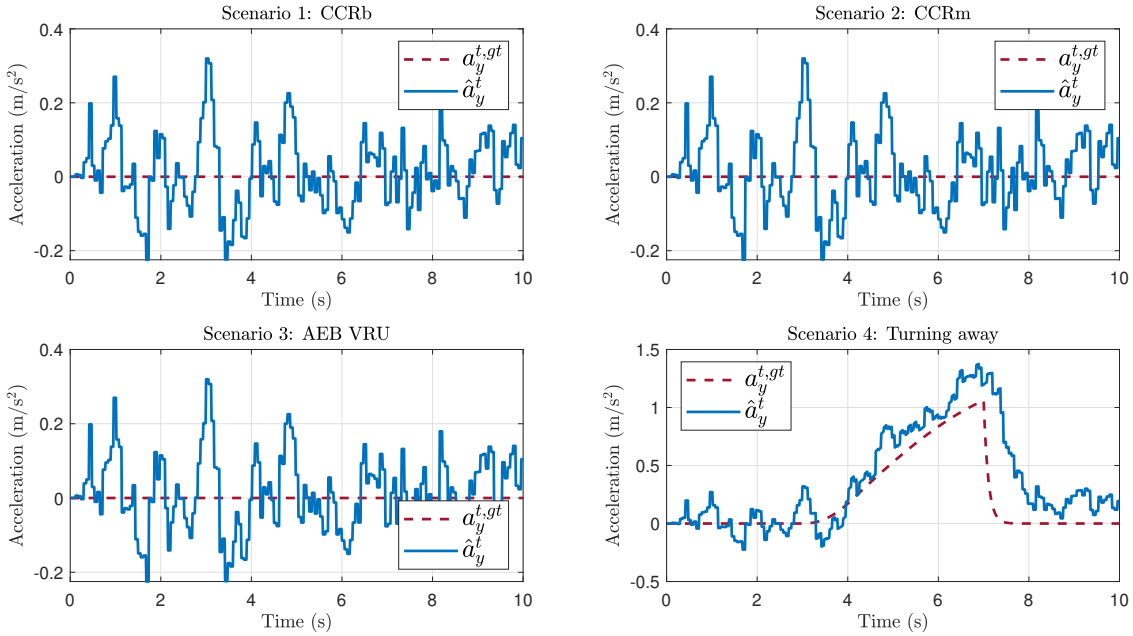

(f) Lateral target acceleration.

Figure B.1: The ground truth and the estimations of all states for different driving scenarios together with the measured longitudinal and lateral relative distance.

Appendix C

Derivation of the required host acceleration

C.1 Derivation of the required host acceleration with a stationary detected object

To derive the required host acceleration, it is assumed that the longitudinal acceleration of both the host vehicle a_x^h and the object a_x^t are constant. Given the current states of the host vehicle and the object, the longitudinal position of the host vehicle and the object along their path at time t is given by

$$\begin{aligned} d_x^h(t) &= d_x^h(0) + v_x^h(0)t + \frac{1}{2}a_x^h(0)t^2 \\ d_x^t(t) &= d_x^t(0) + v_x^t(0)t + \frac{1}{2}a_x^t(0)t^2, \end{aligned} \tag{C.1}$$

and the longitudinal velocity of the host vehicle and the object at time t is given by

$$\begin{aligned} v_x^h(t) &= v_x^h(0) + a_x^h(0)t \\ v_x^t(t) &= v_x^t(0) + a_x^t(0)t, \end{aligned} \tag{C.2}$$

where the current states of the host vehicle and the object are taken at $t = 0$.

Since the longitudinal velocity of the object is zero at the stopping time ($v_x^t(t_{stop}) = 0$), the stopping time can be derived from (C.2) as follows

$$t_{stop} = -\frac{v_x^t(0)}{a_x^t(0)}. \tag{C.3}$$

Solving (C.1) for the stopping time gives the stopping distance of the object, which is given by

$$\begin{aligned} d_{stop}^t &= d_x^t(t_{stop}) - d_x^t(0) = v_x^t(0)t_{stop} + \frac{1}{2}a_x^t(0)t_{stop}^2 \\ &= v_x^t(0)\left(-\frac{v_x^t(0)}{a_x^t(0)}\right) + \frac{1}{2}a_x^t(0)\left(-\frac{v_x^t(0)}{a_x^t(0)}\right)^2 \\ &= -\frac{1}{2}\frac{{v_x^t}^2(0)}{a_x^t(0)}. \end{aligned} \tag{C.4}$$

From the stopping distance of the object d_{stop}^t, the available stopping distance of the host vehicle can be determined as follows

$$d_{stop}^h = d_x^t(0) - d_x^h(0) + d_{stop}^t = d_x^r(0) + d_{stop}^t. \tag{C.5}$$

Finally, using the current velocity of the host vehicle $v_x^h(0)$ and the available stopping distance of the host vehicle d_{stop}^h, the required acceleration of the host vehicle a_{req}^h is determined as follows [33]

$$a_{req}^h = -\frac{1}{2}\frac{{v_x^h}^2(0)}{d_{stop}^h} = -\frac{1}{2}\frac{{v_x^h}^2(0)}{d_x^r(0) + d_{stop}^t}. \tag{C.6}$$

C.2 Derivation of the required host acceleration with a moving detected object

The relative longitudinal distance between the host vehicle and the object at time t can be derived from (C.1) as follows

$$\begin{aligned} d_x^r(t) &= \left(d_x^t(0) - d_x^h(0)\right) + \left(v_x^t(0) - v_x^h(0)\right)t + \frac{1}{2}\left(a_x^t(0) - a_x^h(0)\right)t^2 \\ &= d_x^r(0) + v_x^r(0)t + \frac{1}{2}a_x^r(0)t^2. \end{aligned} \tag{C.7}$$

Furthermore, the relative longitudinal velocity between the host vehicle and the object at time t can be derived from (C.2) as follows

$$\begin{aligned} v_x^r(t) &= \left(v_x^t(0) - v_x^h(0)\right) + \left(a_x^t(0) - a_x^h(0)\right)t \\ &= v_x^r(0) + a_x^r(0)t. \end{aligned} \tag{C.8}$$

In this second case, a collision between the host vehicle and the object is avoided when their velocities are equal at a time instant called Time-to-Touch (t_{TTT}) [33]. At this time instant, the relative longitudinal velocity is zero ($v_x^r(t_{TTT}) = 0$) and the relative longitudinal distance is also zero ($d_x^r(t_{TTT}) = 0$). The Time-to-Touch can be derived from (C.8) as follows

$$t_{TTT} = -\frac{v_x^r(0)}{a_x^r(0)} = -\frac{\left(v_x^t(0) - v_x^h(0)\right)}{\left(a_x^t(0) - a_x^h(0)\right)}. \tag{C.9}$$

Solving (C.7) for the Time-to-Touch gives the required acceleration of the host vehicle a_{req}^h, which is given by

$$a_{req}^h = a_x^t(0) - \frac{\left(v_x^t(0) - v_x^h(0)\right)^2}{2d_x^r(0)}. \tag{C.10}$$

Substituting the required host acceleration a_{req}^h into (C.9), gives the following expression for the Time-to-Touch

$$t_{TTT} = -\frac{v_x^r(0)}{a_x^r(0)} = -\frac{v_x^r(0)}{\frac{(v_x^t(0) - v_x^h(0))^2}{2d_x^r(0)}} = -\frac{2d_x^r(0)}{\left(v_x^t(0) - v_x^h(0)\right)}. \tag{C.11}$$

Now the velocity of both the host vehicle and the object at the Time-to-Touch can be derived by substituting the Time-to-Touch into (C.2) as follows

$$v_x^t(t_{TTT}) = v_x^t(0) + a_x^t(0)t_{TTT}. \tag{C.12}$$

The second case holds if this velocity is positive ($v_x^t(t_{TTT}) > 0$). Otherwise, the first case holds and the required acceleration of the host vehicle a_{req}^h is calculated using (C.6).